Molecular Theory of Vapor Phase Nucleation

Thesis by

Isamu Kusaka

In Partial Fulfillment of the Requirements

for the Degree of

Doctor of Philosophy

Department of Chemical Engineering

California Institute of Technology

Pasadena, California

1998

(Submitted November 26, 1997)

Acknowledgements

I owe a great deal of gratitude to both Professor John H. Seinfeld and Professor Zhen-Gang Wang for their guidance as my research advisors. Among all, the weekly meeting I had with them every Friday has been a major source of motivation and inspiration. Virtually all of the key concepts developed in this thesis were conceived and refined during these meetings. Professor David W. Oxtoby at the University of Chicago kindly allowed me to spend as much time as I needed to complete the work presented in Chapters 4 and 5 of this thesis before I join his group. By the time I start as his postdoc, the delay will amount precisely to 18 months. Without his understanding and encouragement, the work would have been impossible. Professor Richard C. Flagan and Professor George R. Gavalas kindly accepted the responsibility of the thesis committee members. Finally, I would like to express my gratitude to Professor Kazumi Nishioka at University of Tokushima in Japan, who encouraged and helped me to pursue my Ph. D. at Caltech in the first place. He also carefully revealed to me, during 1988–1990 and in the summer of 1992, the subtlety behind the Gibbsian thermodynamics and the Lothe-Pound theory which otherwise would have escaped me.

Pasadena, November, 1997 I. K.

Abstract

An attempt has been made to establish the foundation of molecular level theory of vapor phase nucleation. We have focused on evaluating the reversible work of cluster formation and followed two major trends in this direction, namely, statistical mechanical density functional theory and molecular level simulation.

We applied density functional theory to heterogeneous nucleation onto an ion. Our prime interest is to predict a sign preference of nucleation rate, which has been experimentally observed yet remained inexplicable in the classical framework. The theory indicates that asymmetry in ion-molecule interaction is directly responsible for the sign preference. The predicted sign dependence decreases as the supersaturation is increased. Our results from density functional theory agree well with the existing experimental observations.

Molecular simulation offers an alternative to molecular level approach. A long-standing issue of fundamental importance in cluster simulation is the precise definition of a cluster. Thus far, all attempts of defining a cluster had introduced *ad hoc* criteria to determine unambiguously whether a given molecule in the system belongs to vapor or to a cluster for any instantaneous configuration of molecules. From a careful examination of the context in which a cluster should be introduced into nucleation theory, we conclude that such a criterion is unnecessary. Then, we present a new approach to cluster simulation which is free of any arbitrariness involved in the definition of a cluster. Instead, it preferentially and automatically generates the physical clusters, defined as the density fluctuations that lead to nucleation, and determines their equilibrium distribution in a single simulation. The latter feature permits one to completely bypass the computationally demanding free energy evaluation that is necessary in a conventional simulation. The method is applied first to water using the SPC/E model. We then turn to H_2SO_4/H_2O binary system to obtain a large section of the reversible work surface. The resulting surface is markedly different from that in classical theory and indicates that the rate limiting step of stable particle formation in this system is the binary collision of the sulfuric acid hydrates.

Contents

Chapter 1 Introduction

When a bulk homogeneous phase is brought to a condition of two phase coexistence, the free energy density of this phase becomes equal to that of the coexisting phase. However, the free energy barrier that separates these two phases is practically infinite for a macroscopic system and a formation of the new phase cannot take place unless the barrier is lowered considerably by an external agency such as the container wall or impurities. In the absence of such agencies, one must reduce the free energy barrier by lowering the free energy density of the new phase.

Near the coexistence, the parent phase remains metastable, separated from the more stable new phase by a finite free energy barrier. Thus, relaxation of this metastable state, i.e., the phase transition, is an activated process that must take place through spontaneous fluctuations. If the system is far from the critical point and the free energy barrier is not vanishingly small, these fluctuations are spatially distant from each other, and hence statistically uncorrelated. Then, the limit of metastability of the parent phase is marked by formation of a single spatially localized fluctuation, called a critical nucleus, which is in unstable equilibrium with respect to further growth and hence can serve as an embryo of the new phase. In this work, we limit ourselves to the phase transition far from the critical point. Hence, the word nucleation refers to the formation of this critical nucleus.

The subject of nucleation is important in a variety of contexts, such as atmospheric science, material processing, and cryopreservation. Also, the phenomenon of nucleation is crucial for the understanding of the dynamics of the first-order phase transition.

One of the quantities of major interest in nucleation theory is the rate of nucleation J per unit volume and unit time. Since nucleation is an activated process, this rate assumes a general form:

$$J = J_0 e^{-\beta W^{rev}}, \tag{1.1}$$

where $\beta = (k_B T)^{-1}$ with k_B being the Boltzmann constant and T denoting the absolute temperature, W^{rev} is the reversible work to form a critical nucleus in the metastable parent phase, and J_0 is a frequency factor. In this chapter, we briefly review some important

progresses made thus far in evaluating W^{rev} and J_0. In doing so, we focus on the most thoroughly studied case of vapor to liquid nucleation. Vapor phase nucleation is the simplest of all first-order phase transitions, allowing the most accurate quantitative predictions to be made. Thus, the theory of vapor phase nucleation is subject to the most thorough experimental verifications. A thorough understanding of the underlying concepts developed for vapor phase nucleation is the prerequisite in developing a theory of nucleation in other far less understood cases such as solidification from melt and cavitation in liquid.

Since excellent reviews[1–3] already exist on the classical theory, we shall focus on some of the basic issues and try to provide a new perspective to classical theory. For the sake of simplicity, the following exposition will be limited to a single component system. We stress that the expression of W^{rev} can be readily generalized to a multicomponent system and that the expression of J_0 for a binary system was derived as early as 1950 by Reiss.[4]

1.1 The Classical Theory

The first quantitative theory of nucleation was developed through a successive effort by Gibbs, Volmer and Weber, Becker and Döring, Frenkel, and Zeldovich. The theory has found its final form early this century and is commonly referred to as the classical theory. Despite its shortcomings, which we shall discuss later, the classical theory is presently the only practical approach in predicting nucleation rates.

1.1.1 Reversible work of cluster formation

An expression for W^{rev} was first derived by Gibbs[5] in the framework of his theory of capillarity. Under a condition typical of vapor phase nucleation, the number of molecules contained in a critical nucleus is of the order of 100. In such a microscopic droplet, the thickness of the vapor-liquid interface is comparable to the size of the droplet itself and no bulk liquid behavior is expected to hold. Nonetheless, Gibbs was able to show that, as far as thermodynamic properties of the droplet is concerned, there is an exact correspondence between the droplet and a highly idealized system obtained by replacing the interface of finite thickness with a membrane without thickness or rigidity and having a tension γ and by assuming that the parent phase and the nucleating phase separated by this membrane both behave as if they are a part of the corresponding bulk phases.

When an intensive state of the vapor phase is specified, the thermodynamic properties of a critical nucleus, including the reversible work W^{rev}, are uniquely determined by the condition that the nucleus is in equilibrium with the surrounding vapor. If both the parent phase and the nucleating phase are isotropic, as in the present case, Gibbs' formula is summarized by the following set of equations:[5,6]

$$\phi(T, p^v) = \mu(T, p^l) \tag{1.2}$$

$$p^l - p^v = \frac{2\gamma}{R} \tag{1.3}$$

$$W^{rev} = -\frac{4\pi}{3} R^3 (p^l - p^v) + 4\pi R^2 \gamma, \tag{1.4}$$

where p^v and ϕ respectively denote pressure and the chemical potential in the vapor phase. Similarly for p^l and μ in the liquid phase. γ is the surface tension and R is the radius of the surface of tension. Equations (1.2) and (1.3), along with the uniformity of temperature, *can* be interpreted as the conditions of equilibrium for the idealized system mentioned above. For a given intensive state of the vapor phase specified by (T, p^v), Eq. (1.2) determines p^l. Equation (1.3) along with the knowledge of γ, then determines R and Eq. (1.4) finally yields the the reversible work. We stress that, unless the droplet is large enough, no bulk behavior is observed even at its center and that p^l, for example, cannot be identified with a mechanical pressure observed in the droplet.

The validity of the method of Gibbs rests on the fact that, when a cluster possesses a high degrees of symmetry, one can take as a system a part of the cluster and the surrounding vapor in such a way that its internal energy and entropy are well-defined and various thermodynamic quantities of this system can be classified into extensive and intensive variables despite the microscopic nature of the cluster. This being the case, the thermodynamics of the system thus defined is *isomorphic* with that of a macroscopic system. Namely, the presence of an interface in the former simply introduces a term γA ($A = 4\pi R^2$) in place of the $-pV$ term in the latter.

A major difficulty in applying the formula arises from the fact that the surface tension γ is a function of R, while experimental measurements of the quantity provides its value only for a bulk interface, corresponding to the limit of $R \to \infty$. We denote γ in this limit by γ_∞. For vapor phase nucleation of water, for example, 10% decrease in γ results in the increase in J by a factor of 10^6 under a typical condition. To illustrate the magnitude of the R

dependence of γ, let us apply Eqs. (1.2)-(1.4) for a case of vanishingly small W^{rev}, which is realized when the free energy density of the liquid phase is sufficiently decreased. As W^{rev} vanishes, either γ or R must approach zero to satisfy Eq. (1.4), while the L.H.S. of Eq. (1.3) remains finite, indicating that γ and R vanish simultaneously with W^{rev}. Conversely, under the usual approximation $\gamma \approx \gamma_\infty$, adopted in lack of the precise knowledge of γ, the nucleation barrier is considerably overestimated near the spinodal where W^{rev} becomes negligible.

The radius dependence of the surface tension was studied by Tolman[7–9] and Koenig,[10] who derived the following differential equation:

$$\frac{\partial \log \gamma}{\partial q} = -\frac{2\delta(1 + \delta q + \frac{1}{3}\delta^2 q^2)}{1 + 2\delta q(1 + \delta q + \frac{1}{3}\delta^2 q^2)}, \tag{1.5}$$

where $q = 1/R$ and δ is a distance between the surface of tension and an auxiliary dividing surface. The precise determination of δ, which is again a function of R, requires a detailed description of the interfacial region. Thus, the difficulty regarding the precise value of γ is not resolved but simply transfered to determining δ.

1.1.2 Equilibrium cluster size distribution

The frequency factor J_0 reflects the dynamical nature of nucleation process, and its evaluation requires a concrete model. The model currently in use dates back to Frenkel[11,12] and Band,[13,14] who proposed that the metastable vapor phase can be regarded as a gas mixture of clusters of various sizes, such as monomer, dimer, trimer, and so on. As we shall see in Sec. 1.1.6, a quantity of central importance in the rate expression is the equilibrium cluster size distribution, the average number of clusters of different sizes per unit volume. Our purpose here is to determine this distribution $c(n)$ as a function of the cluster size n. Along the way, we introduce the capillarity approximation that is used exclusively in the classical nucleation theory.

In the classical picture of Frenkel and Band, a cluster of size n, hereafter referred to as the n-cluster, can be regarded as a product of the following reaction

$$n\ \mathrm{X} \rightleftharpoons \mathrm{X}_n, \tag{1.6}$$

where X denote the constituent molecule of which clusters are made. At equilibrium, we have

$$n\phi_1(T, p^v, \{c\}) = \phi_n(T, p^v, \{c\}) \tag{1.7}$$

where ϕ_n is the chemical potential of the n-cluster, which is regarded as one of the molecular species. In the notation employed here, a 1-cluster is identified with a monomer. We have assumed the most general situation in which the chemical potential ϕ_n depends on T, p^v, and the number densities c of all sizes of clusters as collectively denoted by $\{c\}$. If the vapor phase is regarded as an *ideal* gas mixture of clusters, $\phi_n(T, p^v, \{c\})$ is given by

$$\phi_n(T, p^v, \{c\}) = \phi_n^0(T, p^v) + k_B T \log \frac{c(n)}{c_{tot}}, \tag{1.8}$$

where c_{tot} is the total number density of clusters of all sizes:

$$c_{tot} = \sum_{n=1}^{n_{cut}} c(n), \tag{1.9}$$

where n_{cut} is the size of the largest cluster permitted in the system. This rather artificial constraint is necessary to constrain the system to a metastable state; recall that the critical nucleus of size n^* is in unstable equilibrium with the surrounding vapor and would grow indefinitely unless n is bounded from above. Under a condition typical of vapor phase nucleation, $c(n^*)$ is many orders of magnitude smaller than $c(1)$ and thermodynamic properties of the metastable vapor is determined mainly by $c(1)$. Thus, n_{cut} is commonly chosen to slightly exceed n^* while ensuring that $c(n_{cut})$ is negligible. As long as these conditions are met, the arbitrariness in choosing n_{cut} has no quantitative consequence.

By setting $c(n) = c_{tot}$ in Eq. (1.8), we see that $\phi_n^0(T, p^v)$ is the chemical potential of pure system composed only of the n-clusters at temperature T and pressure $p^v = k_B T c_{tot}$. In classical theory, one assumes that

$$\phi_n^0(T, p^v) \approx n\mu(T, p^v) + \gamma_\infty A(n), \tag{1.10}$$

where $A(n)$ is the surface area of the n-cluster usually approximated by

$$A(n) \approx 4\pi \left(\frac{3nv^l}{4\pi} \right)^{2/3} \tag{1.11}$$

with v^l denoting the molecular volume in bulk liquid. In other words, the n-cluster is regarded as a spherical droplet with uniform density $(v^l)^{-1}$. Using Eq. (1.10) in Eq. (1.7), we obtain

$$c(n) = c_{tot} e^{-\beta \Delta G(n)}, \tag{1.12}$$

where we have defined

$$\Delta G(n) \equiv n \left[\mu(T, p^v) - \phi_1(T, p^v, \{c\}) \right] + \gamma_\infty A(n). \tag{1.13}$$

Unless clustering of molecules leads to a significant depletion of monomers, as in the case of associative molecules,[15] molecular species in the vapor is dominated by monomers. Thus, we may introduce a further approximations

$$n^v \equiv c(1) \approx c_{tot} \tag{1.14}$$

and rewrite Eq. (1.12) as

$$c(n) = n^v e^{-\beta \Delta G(n)}, \tag{1.15}$$

which along with Eq. (1.13) constitutes the capillarity approximation.

With the ideal gas approximation we have adopted,

$$\phi_1(T, p^v, \{c\}) = \phi_1^0(T) + k_B T \log p_1^v \tag{1.16}$$

and

$$\mu(T, p^v) = \phi_1^0(T) + k_B T \log p_1^{v,eq}, \tag{1.17}$$

where $\phi_1(T)$ is the chemical potential of a monomer in the vapor at unit pressure. p_1^v and $p_1^{v,eq}$ are the partial pressures of monomers in the vapor phase in the metastable state and at saturation, respectively. Further noting that

$$p_1^v = k_B T n^v \tag{1.18}$$

and

$$p_1^{v,eq} = k_B T n^{v,eq}, \tag{1.19}$$

where $n^{v,eq}$ is the number density of monomers in the vapor at saturation, we obtain

$$\Delta G(n) \equiv -k_B T n \log \frac{n^v}{n^{v,eq}} + \gamma_\infty A(n). \tag{1.20}$$

As long as the monomer is the dominant species, we can approximate n^v by the net number density of molecules:

$$n^v \approx \sum_{n=1}^{n_{cut}} n c(n). \tag{1.21}$$

Thus, all quantities in Eq. (1.20) can be readily obtained.

1.1.3 Gibbs' formula and the capillarity approximation

We briefly comment on the relation between Gibbs' formula summarized in Eqs. (1.2)–(1.4) and the capillarity approximation.

First, it can be shown that $\Delta G(n)$ given by Eq. (1.13) is an approximate form of W^{rev} given by Eq. (1.4). Recall the Gibbs-Duhem relation at constant T:

$$v^l dp = d\mu, \tag{1.22}$$

which can be integrated assuming the incompressibility of the bulk liquid phase to yield

$$\begin{aligned} v^l(p^l - p^v) &= \mu(T, p^l) - \mu(T, p^v) \\ &= \phi(T, p^v) - \mu(T, p^v), \end{aligned} \tag{1.23}$$

where we have used Eq. (1.2). With the additional approximations

$$\gamma(T, p^v) \approx \gamma_\infty(T, p^v) \tag{1.24}$$

and

$$\frac{4\pi}{3} R^3 \approx n v_l(T, p^v), \tag{1.25}$$

Eq. (1.13) follows from Eq. (1.4). This implies that Eq. (1.13) is inapplicable for nucleation of compressible fluid as in the case of cavitation.

Second, note that Gibbs' formula is applicable only for a critical nucleus. Consequently, its approximate version Eq. (1.13) is subject to the same limitation, while in practice,

Eq. (1.13) is used for clusters of all sizes. When Gibbs' formula is extended to include clusters other than the critical ($n = n^*$),[16,17] one finds that an additional term proportional to $n - n^*$ arises in Eq. (1.13). The neglect of this additional term leads to a much debated problem of thermodynamic inconsistency in the case of a binary system.[18–21] As we shall see in Sec. 1.1.6, however, the nucleation rate J is determined by the values of $\Delta G(n)$ at and near $n = n^*$. Thus, from a practical point of view, such correction to $\Delta G(n)$ as just mentioned is rather unimportant.

1.1.4 Law of mass action

At first glance, the capillarity approximation seems inconsistent with the law of mass action since Eqs. (1.15) and (1.20) indicate that

$$c(n) \sim (n^v)^{n+1}. \tag{1.26}$$

Here, we shall examine the implication of the capillarity approximation in the light of the law of mass action, which states that

$$\frac{c(n)}{(n^v)^n} = \frac{q_n/V}{(q_1/V)^n}, \tag{1.27}$$

where V is the volume of the vapor and q_n is the partition function of the n-cluster. Assuming a simple spherical molecule for simplicity, q_n is given by

$$q_n \equiv \frac{1}{\Lambda^{3n} n!} \int d\mathbf{r}^n e^{-\beta U_n}, \tag{1.28}$$

where Λ is the thermal wavelength and U_n is the interaction potential of n molecules whose coordinates are collectively denoted by $\mathbf{r}^n$. Equation (1.28) indicates that

$$q_1 = \frac{V}{\Lambda^3}. \tag{1.29}$$

Also, noting that

$$n^v = \frac{e^{\beta\phi}}{\Lambda^3} \tag{1.30}$$

for an ideal gas, we obtain from Eq. (1.27)

$$c(n) = n^v \exp\left\{-\beta\left[-k_BT\log q_n - n\phi + k_BT\log(n^vV)\right]\right\}. \tag{1.31}$$

Comparing Eq. (1.31) with Eqs. (1.13) and (1.15), we find

$$-k_BT\log\frac{q_n}{n^vV} = n\mu + \gamma_\infty A(n) \tag{1.32}$$

Note that the L.H.S of Eq. (1.32) is the Helmholtz free energy of a cluster confined in the volume $(n^v)^{-1}$. Thus, the capillarity approximation implies that this free energy is given in terms of the chemical potential of the bulk liquid and the bulk surface tension.

Lothe and Pound[22–26] pointed out that the validity of Eq. (1.32) is rather questionable and that a proper consideration is lacking in the capillarity approximation of the contribution to the free energy of a cluster arising from its translational and rotational degrees of freedom as a whole. A proper correction to Eq. (1.32) is confronted with the difficulty due to the fact that the expression $n\mu + \gamma_\infty A(n)$ presumably reflects all of the $3n$ mechanical degrees of freedom and hence that the contribution is already *partially* accounted for in the capillarity approximation. According to Lothe and Pound, when the capillarity approximation is corrected to *fully* rather than *partially* include the contribution from translational and the rotational degrees of freedom of the cluster, the correction amount to a decrease in ΔG by as much as $40k_BT$ under a condition typical of water nucleation.

1.1.5 Fluctuation picture and reaction picture

In the point of view employed by Gibbs, a cluster is regarded as a density fluctuation in a uniform vapor. Thus, the reversible work of cluster formation in this fluctuation picture represents the excess in free energy over its value for the uniform vapor due to the presence of the cluster. In fact, W^{rev} becomes zero at $R = 0$. In the capillarity approximation, which is an approximate version of the Gibbs' formula as discussed in Sec. 1.1.3, $\Delta G(n)$ becomes zero at $n = 0$. On the other hand, in the point of view of Frenkel and Band discussed at the beginning of Sec. 1.1.2, a cluster is regarded as a product of the reaction Eq. (1.6). In this reaction picture, $\Delta G(n)$ would have to be zero at $n = 1$. Thus, the use of Eq. (1.13) in this picture, as is done in classical theory, is in principle inconsistent.

It may prove fruitful to elucidate the relation between these two pictures. In fact, both the fluctuation picture and the reaction picture appear quite reasonable in the case of vapor to liquid nucleation. Hence, we expect that the rate theory appropriate for the fluctuation picture and that for the reaction picture will yield a consistent description of the nucleation phenomenon. We shall, however, stick to the classical theory and employ the capillarity approximation in our exposition of the rate theory given in Sec. 1.1.6, even though the latter is formulated exclusively in the language of the reaction picture.

1.1.6 Rate theory

Since monomers are dominant over other sizes of clusters under a condition typical of vapor phase nucleation, we may assume that a cluster changes its size either by acquiring or loosing a monomer. In a single component system, this model leads to the following equation for the number density $f(n,t)$ of n-cluster at a given instant t:

$$\begin{aligned}\frac{\partial f(n,t)}{\partial t} &= K^+(n-1)f(n-1,t) - K^-(n)f(n,t) \\ &\quad -K^+(n)f(n,t) + K^-(n+1)f(n+1,t) \\ &= J(n-1 \to n) - J(n \to n+1),\end{aligned} \tag{1.33}$$

where $K^+(n)$ and $K^-(n)$ denote the rates for an n-cluster to acquire a monomer and lose a monomer, respectively. The expression

$$J(n-1 \to n) = K^+(n-1)f(n-1,t) - K^-(n)f(n,t) \tag{1.34}$$

is the net rate at which an $(n-1)$-cluster becomes an n-cluster. In writing Eq. (1.33), we assumed that $K^+(n)$ and $K^-(n)$ are both independent of time. The assumption does not hold for the growth process, for example, where a significant depletion of monomers causes $K^+(n)$ to decrease with time.

Expressions for $K^+(n)$ and $K^-(n)$ are necessary to solve Eq. (1.33). A reasonable approximation for $K^+(n)$ is suggested by kinetic theory of gas as

$$K^+(n) \approx \frac{p}{\sqrt{2\pi m k_B T}} A(n), \tag{1.35}$$

where m is the mass of a monomer and $A(n)$ is the surface area of the n-cluster and is usually approximated by

$$A(n) \approx 4\pi R^2 \tag{1.36}$$

with R calculated from Eq. (1.25). The evaporation rate $K^-(n)$ is, to a good approximation, an intrinsic property of the cluster, of which we have no detailed knowledge. To circumvent this difficulty, one assumes that the principle of detailed balance is valid in the vapor phase constrained in the metastable equilibrium:

$$K^+(n)c(n) = K^-(n+1)c(n+1), \tag{1.37}$$

Strictly speaking, this is an assumption since the principle of detailed balance is only *sufficient* but not necessary for equilibrium. Using Eq. (1.37) in Eq. (1.34) we obtain

$$J(n-1 \to n) = K^+(n-1)c(n-1)\left\{\frac{f(n-1,t)}{c(n-1)} - \frac{f(n,t)}{c(n)}\right\}, \tag{1.38}$$

which can be used in Eq. (1.33) to obtain

$$\begin{aligned}\frac{\partial f(n,t)}{\partial t} &= K^+(n-1)c(n-1)\left\{\frac{f(n-1,t)}{c(n-1)} - \frac{f(n,t)}{c(n)}\right\} \\ &\quad -K^+(n)c(n)\left\{\frac{f(n,t)}{c(n)} - \frac{f(n+1,t)}{c(n+1)}\right\}.\end{aligned} \tag{1.39}$$

Equation (1.39) can be solved numerically with proper initial and boundary conditions.

Here, we focus on the steady state solution of Eq. (1.39) since the solution can be obtained analytically and further reduced to a general form of Eq. (1.1) with a reasonable approximation. A steady state is realized by removing a critical nucleus from the system as soon as it is formed and introducing the same amount of molecules into the system in the form of monomers. The steady state approximation is relevant, for example, if large clusters are removed from the system by gravity and no appreciable depletion of monomer concentration is observed. In the steady state, we have

$$\frac{\partial f(n,t)}{\partial t} = 0 \tag{1.40}$$

for any n. Eq. (1.33) then indicates that $J(n \to n+1)$ is a constant independent of n and

that the constant is the steady state nucleation rate J_{ss}:

$$J_{ss} = K^+(n)c(n)\left\{\frac{f(n)}{c(n)} - \frac{f(n+1)}{c(n+1)}\right\}. \tag{1.41}$$

Dividing Eq. (1.41) by $K^+(n)c(n)$ and taking the sum over n, we obtain

$$J_{ss}\sum_{n=1}^{n_{cut}} \frac{1}{K^+(n)c(n)} = \frac{f(1)}{c(1)} - \frac{f(n_{cut}+1)}{c(n_{cut}+1)}. \tag{1.42}$$

If nucleation does not lead to a significant depletion of monomer concentration, we may set

$$\frac{f(1)}{c(1)} = 1. \tag{1.43}$$

Moreover, since a cluster with its size greater than n^* are constantly removed from the system,

$$\frac{f(n_{cut}+1)}{c(n_{cut}+1)} = 0. \tag{1.44}$$

Using Eqs. (1.43) and (1.44) in Eq. (1.42), we obtain

$$J_{ss} = \left[\sum_{n=1}^{n_{cut}} \frac{1}{K^+(n)c(n)}\right]^{-1}. \tag{1.45}$$

It is worth noting that the nucleation rate is given in terms of the equilibrium property $c(n)$ even though nucleation is a dynamical process. Further approximation is necessary to reduce Eq. (1.45) to a general form of Eq. (1.1). Note that $c(n)$ has a sharp minimum at $n = n^*$, while $K^+(n)$ varies relatively slowly. Thus, we can approximate the latter by $K^+(n^*)$ to obtain

$$\begin{aligned} J_{ss} &\approx K^+(n^*)\left[\sum_{n=1}^{n_{cut}} \frac{1}{c(n)}\right]^{-1} \\ &= n^v K^+(n^*)\left[\sum_{n=1}^{n_{cut}} e^{\beta\Delta G(n)}\right]^{-1} \end{aligned} \tag{1.46}$$

where we have used Eq. (1.15). Replacing the sum over n by integration from $n = -\infty$ to

$n = \infty$ and expanding $\Delta G(n)$ around n^* where $\Delta G(n)$ is maximum, we obtain

$$\begin{aligned} J_{ss} &\approx n^v K^+(n^*) \left\{ \int_{-\infty}^{\infty} dn \exp\left[\beta \Delta G(n^*) + \frac{\beta}{2} \frac{\partial^2 \Delta G(n)}{\partial n^2} (n - n^*)^2 \right] \right\}^{-1} \\ &= n^v K^+(n^*) \sqrt{-\frac{\beta}{2\pi} \frac{\partial^2 \Delta G(n)}{\partial n^2}} e^{-\beta \Delta G(n^*)}, \end{aligned} \tag{1.47}$$

which has a general form of Eq. (1.1). Using Eq. (1.20), we see that

$$J_{ss} \sim \left(\frac{n^v}{n^{v,eq}} \right)^{n^*}, \tag{1.48}$$

i.e., the nucleation rate depends strongly on the supersaturation $S \equiv n^v / n^{v,eq}$. This indicates that one can identify, in experiment, the critical supersaturation, the value of S beyond which the nucleation rate becomes noticeable.

1.1.7 Current status of classical theory

As mentioned earlier, classical theory is used in virtually all practical situations. This predominant use of the theory is quite understandable. First of all, classical theory predicts the nucleation rate J using parameters that are widely available, such as $n^{v,eq}$, v^l, and γ_∞. Secondly, classical theory is quite successful in predicting the critical supersaturation.

In Sec. 1.1.4, we pointed out that the Lothe-Pound theory predicts the value of ΔG lower than the classical prediction by as much as $40 k_B T$,[22–26] which translates to a correction factor of the order of 10^{17} in nucleation rate. This enormous correction factor destroyed the apparent agreement between the experiment and the theory regarding the value of the critical supersaturation and triggered numerous work on both experimental and theoretical fronts. The new experiments revealed that some substances such as water follows classical theory while others such as ammonia follows the Lothe-Pound theory.[26] On the theoretical fronts, numerous papers have appeared claiming to disprove the Lothe-Pound theory.[27–31] However, these works are based entirely on the misinterpretation of the original theory and merely brought confusion. As a result, it has become a major trend to simply dismiss the theory and no satisfactory resolution of the problem exists to date. The Lothe-Pound theory is conceptually, if not quantitatively, relevant to all kinds of nucleation, as long as the free energy of a cluster is evaluated using bulk thermodynamic quantities as is done in

Eq. (1.10).

Recently, measurements on the rate of nucleation itself have become available, revealing that classical theory is systematically in error predicting too low a rate at low temperature and too high a rate at high temperature. Thus, attempts have been made to "improve" the capillarity approximation by adding various correction factors to $\Delta G(n)$ or by assuming a certain functional form of $\Delta G(n)$ based on an *ad hoc* self-consistency requirement. Such attempts, however, are quite unsatisfactory since they usually result in only a minor correction to the predicted nucleation rate. More importantly, the theory of capillarity, as summarized by Eqs. (1.2)–(1.4), is already closed as it is, except for the Lothe-Pound factor, thereby precluding any *ad hoc* attempt to improve it.

1.2 Molecular Level Approach

To overcome the shortcomings of classical theory from a fundamental point of view, there has been a great interest in capturing the molecular level details of nucleation. There are two major trends in this direction, namely statistical density functional theory and molecular level simulation. Since these approaches are explained in detail and applied to investigate particular systems in the following chapters, we shall limit the review given here to minimum.

1.2.1 Density functional theory

Statistical mechanical density functional theory[32] was first applied to homogeneous nucleation by Oxtoby and Evans.[33] In this approach, the grand potential ($-pV$ in a uniform system) of the system is written as a functional of spatially varying order parameters. Then, the stationarity condition of the grand potential determines the order parameters for the critical nucleus and the corresponding grand potential follows from the functional. When a cluster possesses a high degree of symmetry and the intermolecular potential is relatively simple, this approach is computationally far less demanding compared to simulation, allowing one to investigate a much wider range of the parameter space. Thus, one usually employs model potentials that capture the essential features of the molecules under consideration. When the results are compared against predictions from classical theory, which uses bulk thermodynamic quantities obtained from the same theoretical framework, one can

isolate the deviations from the classical predictions arising from the molecular level details. Although the approach is more approximate compared to molecular simulation, the theory is extremely powerful in addressing the deviations in a semi-quantitative manner and has been employed to investigate several interesting systems[34–42] for which no simulation has been performed. The theory was recently applied to a ternary system.[43]

In Chapters 2 and 3, we apply density functional theory to study heterogeneous nucleation onto an ion. The phenomenon of ion-induced nucleation plays an important role in atmospheric condensation, particularly in the ionosphere. Also, a possibility is suggested recently of developing highly sensitive detection methods that take advantage of this phenomenon.[44–46]

1.2.2 Molecular simulation

A typical value of the free energy barrier of nucleation ($\Delta G(n^*)$) ranges from $10k_BT$ to $100k_BT$. Hence the concentration of a critical nucleus is 10^{-5} to 10^{-44} times that of monomer. Also, the time scale required for a cluster to change its size by either acquiring or losing a single monomer is about 10^3 times longer than the characteristic time scale of vibrations of molecules in the cluster. Therefore, a direct molecular simulation of a nucleation event requires that simulation be performed with prohibitively large number of molecules for a very long period of time. Thus, conventional molecular level simulation relies on the reaction picture of Frenkel[11,12] and Band[13,14] discussed in Sec. 1.1.2 and focuses on evaluating the free energy of the clusters of various sizes using Eq. (1.28). In principle, simulation can be applied regardless of the complexity of the intermolecular interaction. However, the free energy of a cluster is usually evaluated by integrating its internal energy obtained at different temperatures from separate simulations.[47] This aspect renders the approach computationally demanding and, as a result, virtually all of the simulations are limited to a single component system with simple interaction potentials.

In calculating the partition function q_n defined by Eq. (1.28), the integration must be taken over all possible configurations of molecules consistent with the condition that the n molecules form a cluster. This leads to a long-standing issue of a precise definition of the cluster, which must be specified before any simulation is performed. All of the existing methods, therefore, introduce *a priori* criteria to unambiguously determine, for any instantaneous configuration of molecules, whether or not a given molecule belongs to the cluster

or vapor. It is by no means obvious, however, that the clusters thus defined are identical to those actually participating in a nucleation event. Thus, in a series of papers, Reiss *et al.*[48–53] made an attempt to identify the physical clusters, defined as density fluctuations that lead to nucleation. In addition to the concept of the physical cluster, we note the importance of the "observational situation"[54,55] to which clusters are subject. Since a typical cluster consists of only about 100 molecules, the very concept of cluster implicitly assumes a situation where our measurement is sensitive to the behavior of individual molecules. Thus, statistical mechanical quantities associated with the clusters, such as their equilibrium distribution, cannot be defined without specifying precisely how these quantities are measured. To understand this, recall that it is the insensitivity of a macroscopic measurement to the microscopic details that permits us to define statistical mechanical quantities of a macroscopic system without any reference to the exact experimental setup.[54,55] It follows that the cluster cannot be defined independent of the actual nucleation process and how we describe the process in our theoretical framework.

In Chapter 4, we challenge this problem of a cluster definition by employing the fluctuation picture of Gibbs. First, we examine the context in which a cluster should be introduced into nucleation theory and conclude that an *a priori* criterion as mentioned above is unnecessary. Then, we present a new approach to cluster simulation which is free of any arbitrariness involved in the definition of a cluster. Instead, it preferentially and automatically generates the physical clusters and determines their equilibrium distribution in a single simulation. The latter feature permits one to completely bypass the computationally demanding free energy evaluation that is necessary in a conventional simulation. The method is applied first to water using the SPC/E model in Chapter 4. We then turn to H_2SO_4/H_2O binary system in Chapter 5.

Chapter 2 Ion-Induced Nucleation: A Density Functional Approach

Density functional theory is applied to ion-induced nucleation of dipolar molecules. The predicted reversible work shows a sign preference, resulting in a difference in the nucleation rate by a factor of 10 to 10^2, for realistic values of model parameters. The sign effect is found to decrease systematically as the supersaturation is increased. The asymmetry of a molecule is shown to be directly responsible for the sign preference in ion-induced nucleation.

2.1 Introduction

The presence of ions has been shown to greatly enhance the rate of nucleation of liquid drops in a supersaturated vapor.[56–62] The phenomenon of ion-induced nucleation plays an important role in atmospheric condensation, particularly in the ionosphere. While both positive and negative ions increase the nucleation rate, a variety of substances exhibit a dependence of the nucleation rate on the sign of the ion.[56–62] No theory currently exists that is capable of predicting this sign dependence.

One of the key quantities in estimating a nucleation rate is the reversible work to form a critical nucleus from a metastable state. Unlike the case of homogeneous nucleation, the metastable state relevant here is identified as the one with a vapor-solvated ion. The earliest attempt to calculate the reversible work of ion-induced nucleation is due to Thomson,[63] based on the theory of capillarity, where a nucleus, either critical or metastable, is represented as a bulk liquid enclosed by an interface of zero thickness with an ion placed at the center. The reversible work is then given in terms of the thermodynamic quantities such as the surface tension, dielectric constants of the bulk phases, etc. The reversible work depends on q^2, where q is the ion charge, and has no dependence on the sign of q.

Physically, the dependence of the ion-induced nucleation rate of a substance on the sign of the ion charge must arise from some asymmetry in the molecular interactions. Such asymmetry should, in principle, manifest itself in a sign dependence of the relevant thermodynamic quantities such as the surface tension. Several attempts have been made to

incorporate molecular characteristics within the framework of the capillarity theory,[59,64,65] where a certain structure in the interfacial region is inevitably assumed. A somewhat different approach was taken by Rusanov and Kuni,[66–68] in which the surface tension is related to the ion charge and the distance between two dividing surfaces located in the interfacial region. The reversible work predicted by the theory shows extreme sensitivity to this distance,[69] a slight change of which results in a reversal of the sign preference in the nucleation rate. It has also been noted[69] that, except for its inability to explain the sign effect, the best predictions of the reversible work, when compared with experimental data, come from the original Thomson's equation.

Clearly, even a qualitative description of ion-induced nucleation requires a theory based on a statistical mechanical treatment, which assumes an intermolecular potential as the fundamental information required to evaluate the relevant thermodynamic potentials. One of such approaches is to directly evaluate the partition function of a nucleus by Monte Carlo simulation. Recently, major progress has been made in this direction for homogeneous nucleation by Reiss and co-workers.[48–53] An alternative, and computationally less demanding, approach is to use density functional theory. The theory was first applied to homogeneous nucleation in a one-component system by Oxtoby and Evans.[33] In this theory, the grand potential Ω (equal to $-pV$ for a uniform system) is written as a functional of order parameters such as the average number density of molecules. The critical nucleus is obtained from the stationarity condition of the grand potential with respect to the density profile. Recently, the theory has also been applied to binary homogeneous nucleation.[35]

In this work, we present a density functional theory for ion-induced nucleation of dipolar molecules. Asymmetry is introduced into a molecule by placing a dipole moment at some fixed distance from its center. As a result of the asymmetric nature of the molecules and their interactions with the ion, the reversible work acquires a dependence on the ion charge.

The outline of this paper is as follows. In Sec. 2.2, we first briefly review some of the important results from the general framework of density functional theory, and then develop a density functional for the grand potential in terms of two order parameters, the number density of molecules and the average dipole moment. Bulk properties are derived from the density functional. Sec. 2.3 describes the solution methods to determine the equilibrium profiles. The reversible work of nucleation is obtained from the equilibrium profiles and reported in Sec. 2.4. Finally, some concluding remarks are given with a brief discussion in

Sec. 2.5.

2.2 Density Functional Theory

2.2.1 The model and some general results

Let us consider a system of spherical molecules each of which has a dipole of moment p_0 located at some fixed distance a from its center. For simplicity, the dipole moment is assumed to be pointing in the radial direction with respect to the center of the molecule, as shown in Fig. 2.1. Suppose that the interaction potential $\phi\,(1,2)$ between one molecule

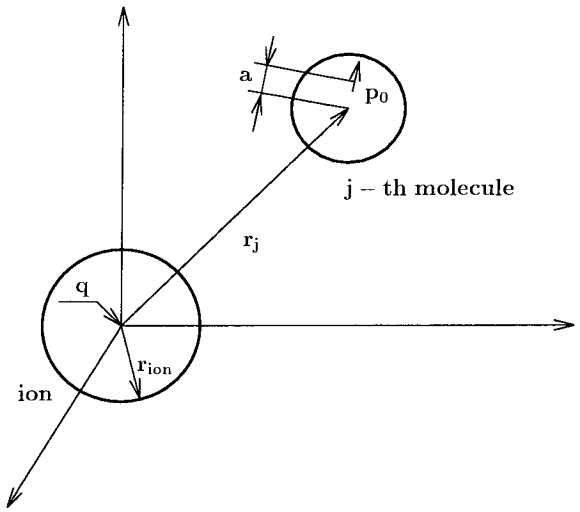

Figure 2.1: Model of a dipolar molecule and an ion. The molecule has a dipole moment p_0 pointing outward with respect to its center at a distance a from the center. An ion is represented as a point charge placed at the center of a hard sphere of radius r_{ion}.

at $\mathbf{r}_1$ with orientation $\hat{R}_1$ and the other at $\mathbf{r}_2$ with orientation $\hat{R}_2$ can be written as

$$\phi\,(1,2) = \phi^d\,(r_{12}) + \phi^{att}\,(r_{12}) + \phi^p\,(1,2), \tag{2.1}$$

where $r_{12} = |\mathbf{r}_2 - \mathbf{r}_1|$. We use the notation j to represent both the translational and orientational coordinates of molecule j. $\phi^d(r_{12})$ is the hard sphere potential given by

$$\phi^d(r_{12}) = \begin{cases} +\infty & \text{if } r_{12} < d \\ 0 & \text{otherwise.} \end{cases} \tag{2.2}$$

$\phi^{att}(r_{12})$ is the perturbative attractive potential whose explicit form is chosen to be

$$\phi^{att}(r_{12}) = -\epsilon \left(\frac{d}{r_{12}}\right)^6, \tag{2.3}$$

where ϵ is a positive constant. $\phi^p(1,2)$ is the dipole-dipole interaction between molecules 1 and 2, and is given by

$$\phi^p(1,2) = \frac{{p_0}^2}{{u_{12}}^3}\left[\hat{R}_1 \cdot \hat{R}_2 - 3(\hat{R}_1 \cdot \hat{u}_{12})(\hat{R}_2 \cdot \hat{u}_{12})\right], \tag{2.4}$$

where $\mathbf{u}_j = \mathbf{r}_j + a\hat{R}_j$, $u_{12} = |\mathbf{u}_2 - \mathbf{u}_1|$, and $\hat{u}_{12} = (\mathbf{u}_2 - \mathbf{u}_1)/u_{12}$. To avoid complications due to possible overlap of two dipoles, we choose a to be smaller than $d/2$.

Consider an open system, for which the grand potential Ω is the proper thermodynamic potential. In density functional theory, Ω of the system is given as a functional of order parameters such as the position-orientation distribution function $\rho(\mathbf{r}, \hat{R})$ defined by

$$\rho(\mathbf{r}, \hat{R}) \equiv \left\langle \sum_{j=1}^{N} \delta(\mathbf{r} - \mathbf{r}_j)\, \delta(\hat{R} - \hat{R}_j) \right\rangle. \tag{2.5}$$

Later, we shall use the particle density distribution function

$$n(\mathbf{r}) \equiv \left\langle \sum_{j=1}^{N} \delta(\mathbf{r} - \mathbf{r}_j) \right\rangle \tag{2.6}$$

and the orientation distribution function

$$m(\mathbf{r}, \hat{R}) \equiv \rho(\mathbf{r}, \hat{R})/n(\mathbf{r}). \tag{2.7}$$

From the definition Eqs. (2.5) - (2.7), it follows that

$$n(\mathbf{r}) = \int d\hat{R}\, \rho(\mathbf{r}, \hat{R}) \tag{2.8}$$

and

$$\int d\hat{R}\, m(\mathbf{r}, \hat{R}) = 1. \tag{2.9}$$

In terms of $\rho(\mathbf{r}, \hat{R})$, Ω is given exactly by[32]

$$\begin{aligned} \Omega[\rho] &= F_r[\rho] - \int d1\, \rho(1)\, [\mu - v(1)] \\ &\quad + \frac{1}{2} \iint d1\, d2\, \rho(1)\, \rho(2) \int_0^1 d\lambda\, g(1,2;\lambda)\, [\phi(1,2) - \phi_r(1,2)], \end{aligned} \tag{2.10}$$

where $F_r[\rho]$ is the intrinsic Helmholtz free energy of the reference system in which molecules interact via potential $\phi_r(1,2)$. μ is the chemical potential of the system. $v(\mathbf{r}, \hat{R})$ is the external potential, which arises from the ion-molecule interaction in our study of ion-induced nucleation. $g(1,2;\lambda)$ is the pair correlation function of the system with intermolecular potential,

$$\phi_\lambda(1,2) = \phi_r(1,2) + \lambda\, [\phi(1,2) - \phi_r(1,2)]. \tag{2.11}$$

We take a fluid of hard spheres as the reference system, for which $F_r[\rho]$ can be decomposed into the ideal gas contribution,

$$F^{ideal}[\rho] = k_B T \int d1\, \rho(1) \left\{ \log \left[\Lambda^3\, \rho(1) \right] - 1 \right\} \tag{2.12}$$

and the excess free energy $F^{exc}[\rho]$ due to the hard sphere exclusion. k_B is the Boltzmann constant, T is temperature, and Λ is de Broglie's thermal wavelength. Following the previous work on homogeneous nucleation by Oxtoby and Evans,[33] we introduce the local density approximation, under which

$$F^{exc}[\rho] \approx \int d\mathbf{r}_1\, f^{exc}(n(\mathbf{r}_1)). \tag{2.13}$$

To approximate the excess free energy density $f^{exc}(n(\mathbf{r}))$ per unit volume of the reference system of density n, Carnahan-Starling's formula[70,71] is employed:

$$f^{exc}(n) = k_B T n\, \frac{y(4-3y)}{(1-y)^2}, \tag{2.14}$$

where $y \equiv (\pi/6)\, d^3\, n$. Because little is known about the pair-correlation functions of in-

homogeneous fluids in which molecules assume orientational degrees of freedom, some approximation is required. Following Oxtoby and Evans,[33] we employ the approximation:

$$g(1,2;\lambda) \approx H(r_{12}-d), \tag{2.15}$$

where H is the Heaviside step function and independent of λ. It follows that

$$\begin{aligned}\Omega[\rho] &= k_BT\int d1\,\rho(1)\left\{\log\left[\Lambda^3\,\rho(1)\right]-1\right\}+\int d\mathbf{r}_1\,f^{exc}(n(\mathbf{r}_1)) \\ &\quad -\int d1\,\rho(1)\,[\mu-v(1)] \\ &\quad +\frac{1}{2}\iint d1\,d2\,\rho(1)\,\rho(2)H(r_{12}-d)[\,\phi^{att}\,(r_{12})+\phi^{p}\,(1,2)\,].\end{aligned} \tag{2.16}$$

The equilibrium distribution for $\rho(\mathbf{r},\hat{R})$ is determined by the stationarity condition of the grand potential:

$$\frac{\delta\Omega}{\delta\rho(1)}=0. \tag{2.17}$$

From Eqs. (2.16) and (2.17), we obtain

$$\begin{aligned}&k_BT\,\log\left[\Lambda^3\,\rho(1)\right]+\mu^{exc}(n(\mathbf{r}_1))-[\,\mu-v(1)\,] \\ &\quad+\int d2\,\rho(2)H(r_{12}-d)[\,\phi^{att}\,(r_{12})+\phi^{p}\,(1,2)\,] \;=\; 0,\end{aligned} \tag{2.18}$$

where we have defined $\mu^{exc}(n)\equiv\partial f^{exc}/\partial n$. The solution of Eq. (2.18) can be used in Eq. (2.16) to evaluate Ω of the system.

In our study of ion-induced nucleation, an ion is taken as a point charge placed at the center of a hard sphere, which itself is supposed to be fixed at the center of a cluster. The ion-molecule interaction can be treated as an external potential, which is composed of the hard core repulsive potential and

$$-p_0\hat{R}\cdot\mathbf{E}(\mathbf{u}), \tag{2.19}$$

where $\mathbf{E}$ is the electric field due to the ion. It will be readily observed from Eqs. (2.16), (2.18), and (2.19) that flipping the dipole moment embodied in each molecule and simultaneously reversing the direction of the electric field (by changing the sign of the ion charge) leaves $\rho(\mathbf{r},\hat{R})$ and Ω unchanged. However, for a given direction of the dipole moments, both $\rho(\mathbf{r},\hat{R})$ and Ω change when the sign of the ion charge is changed.

2.2.2 Approximate formulae

The solution of the full distribution function $\rho(\mathbf{r}, \hat{R})$ requires inordinate computer time and memory. To reduce the computational task, we make a further mean field approximation, where the orientational degrees of freedom $\hat{R}$ is replaced by an order parameter $\mathbf{p}(\mathbf{r})$ defined by

$$\mathbf{p}(\mathbf{r}) \equiv \int d\hat{R}\, m(\mathbf{r}, \hat{R})\hat{R}. \tag{2.20}$$

As a result of interactions with other molecules and the external field, the molecule at $\mathbf{r}$ orients itself in various directions with a certain probability $m(\mathbf{r}, \hat{R})$. On average, however, the molecule can be described as having a dipole moment $\mathbf{p}(\mathbf{r})$. For a specified functional form of $\mathbf{p}(\mathbf{r})$, the distribution function $m(\mathbf{r}, \hat{R})$ consistent with this $\mathbf{p}(\mathbf{r})$ is not unique. Therefore, some approximation must be employed to introduce $\mathbf{p}(\mathbf{r})$ instead of $m(\mathbf{r}, \hat{R})$.

Without any loss of generality, Eq. (2.7) may be introduced into Eq. (2.16):

$$\begin{aligned}
\Omega[n(\mathbf{r}), m(\mathbf{r}, \hat{R})] \;=\; & k_B T \int d1\, n(\mathbf{r}_1) m(1) \log m(1) \\
& + \int d\mathbf{r}_1\, f_d(n(\mathbf{r}_1)) - \int d1\, n(\mathbf{r}_1) m(1)[\mu - v(1)] \\
& + \frac{1}{2} \iint d\mathbf{r}_1\, d\mathbf{r}_2\, n(\mathbf{r}_1) n(\mathbf{r}_2) H(r_{12} - d) \phi^{att}(r_{12}) \\
& + \frac{1}{2} \iint d1\, d2\, n(\mathbf{r}_1) n(\mathbf{r}_2) m(1) m(2) H(r_{12} - d) \phi^{p}(1, 2),
\end{aligned} \tag{2.21}$$

where $f_d(n)$ is the Helmholtz free energy density per unit volume of the reference system, and is given by

$$f_d(n) = k_B T n \left[\log(\Lambda^3 n) - 1 \right] + f^{exc}(n). \tag{2.22}$$

In the first term of Eq. (2.21), the quantity

$$-k_B \int d\hat{R}\, m(\mathbf{r}, \hat{R}) \log m(\mathbf{r}, \hat{R}) \tag{2.23}$$

represents the entropy of a molecule at $\mathbf{r}$ associated with its orientational degrees of freedom. In order to express this quantity in terms of $\mathbf{p}(\mathbf{r})$, we choose a particular $m(\mathbf{r}, \hat{R})$ as an

ansatz. In our mean field approximation, we take

$$m(\mathbf{r}, \hat{R}) = \frac{1}{Z} \exp\left(\frac{p_0 \hat{R} \cdot \mathbf{E}_0}{k_B T}\right), \tag{2.24}$$

the orientation distribution function of a molecule in an auxiliary uniform electric field $\mathbf{E}_0$. Z is the normalization constant determined by Eq. (2.9):

$$\begin{aligned} Z &= \int d\hat{R} \exp\left(\frac{p_0 \hat{R} \cdot \mathbf{E}_0}{k_B T}\right) \\ &= \frac{4\pi k_B T}{p_0 E_0} \sinh\left(\frac{p_0 E_0}{k_B T}\right). \end{aligned} \tag{2.25}$$

Namely, for every point $\mathbf{r}$ in the system, we assign $m(\mathbf{r}, \hat{R})$ which would be obtained if the molecule were subject to the uniform external field $\mathbf{E}_0$ and there were no interaction among molecules. The auxiliary electric field $\mathbf{E}_0$ to be imposed on the molecule is determined so that it yields the specified $\mathbf{p}(\mathbf{r})$ given by Eq. (2.20):

$$p(\mathbf{r}) = -\frac{1}{x} + \coth x, \tag{2.26}$$

where $x \equiv p_0 E_0 / k_B T$ and $\mathbf{p}(\mathbf{r})$ and $\mathbf{E}_0$ are parallel to each other. For the ansatz of $m(\mathbf{r}, \hat{R})$ employed here,

$$-\int d\hat{R}\, m(\mathbf{r}, \hat{R}) \log m(\mathbf{r}, \hat{R}) = \log\left(\frac{4\pi}{x} \sinh x\right) - x p(\mathbf{r}), \tag{2.27}$$

which, along with Eq. (2.26), serves as a parametric representation of the orientational entropy (divided by k_B) of a molecule. It is more convenient, however, to represent this quantity as a function of $\mathbf{p}(\mathbf{r})$ only. For this purpose, the R.H.S. of Eq. (2.26) and the logarithmic term in Eq. (2.27) are expanded in power series of x. Inverting the former series for $p(\mathbf{r})$ and substituting the resulting series in the latter, one finds

$$\begin{aligned} & -\int d\hat{R}\, m(\mathbf{r}, \hat{R}) \log m(\mathbf{r}, \hat{R}) \\ = \; & \log 4\pi - \frac{3}{2} p(\mathbf{r})^2 - \frac{9}{20} p(\mathbf{r})^4 - \frac{99}{350} p(\mathbf{r})^6 - \frac{1539}{7000} p(\mathbf{r})^8 + O(p^{10}). \end{aligned} \tag{2.28}$$

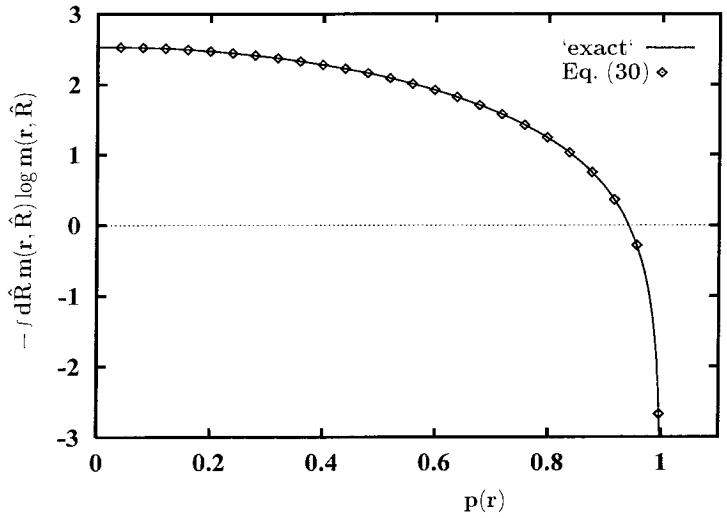

Figure 2.2: Orientational entropy per molecule (divided by k_B). The Padé approximation, Eq. (30), is compared with the 'exact' result using the parametric representation, Eqs. (26) and (27).

From the parametric representation Eqs. (2.26) and (2.27), it can be shown that

$$-\int d\hat{R}\, m(\mathbf{r},\hat{R}) \log m(\mathbf{r},\hat{R}) \sim \log[1-p(\mathbf{r})^2] \quad \text{as } p(\mathbf{r})^2 \to 1. \tag{2.29}$$

To recapture such limiting behavior, we employ the Padé approximation, by which the R.H.S. of Eq. (2.28) is resummed as

$$\begin{aligned} & -\int d\hat{R}\, m(\mathbf{r},\hat{R}) \log m(\mathbf{r},\hat{R}) \\ \approx\ & \log 4\pi + \log[1-p(\mathbf{r})^2] - \frac{1}{2}p(\mathbf{r})^2 + \frac{1}{20}p(\mathbf{r})^4 + \frac{53}{1050}p(\mathbf{r})^6 + \frac{211}{7000}p(\mathbf{r})^8 \\ \equiv\ & s^{ort}(p(\mathbf{r})), \end{aligned} \tag{2.30}$$

where the coefficients of $p(\mathbf{r})^{2k}$ are determined so as to ensure the matching of two expressions at the small $p(\mathbf{r})$ limit. In Fig. 2.2, Eq. (2.30) is compared with the 'exact' result using parametric representation given by Eqs. (2.26) and (2.27). As is seen from Fig. 2.2, the two representations are indistinguishable.

The remainder of the terms in Eq.(2.21) can be treated similarly. To further simplify

the equation, we have expanded $v(1)$ and $\phi^p(1,2)$ around $a = 0$. Retaining the terms up to $O(a/d)$, we obtain

$$\begin{aligned}
&\Omega[n(\mathbf{r}), \mathbf{p}(\mathbf{r})] = \\
&\quad -k_B T \int d\mathbf{r}_1\, n(\mathbf{r}_1) s^{ort}(p(\mathbf{r}_1)) + \int d\mathbf{r}_1\, f_d(n(\mathbf{r}_1)) \\
&\quad - \int d\mathbf{r}_1\, n(\mathbf{r}_1) \left\{ \mu + p_0 p_\alpha(\mathbf{r_1}) \left[E_\alpha(\mathbf{r}_1) + \frac{3}{5}\, a\, \left.\frac{\partial E_\alpha}{\partial x_\beta}\right|_{\mathbf{r}=\mathbf{r}_1} p_\beta(\mathbf{r}_1) \right] \right\} \\
&\quad + \frac{1}{2} \iint d\mathbf{r}_1\, d\mathbf{r}_2\, n(\mathbf{r}_1)\, n(\mathbf{r}_2) H(r_{12} - d) \phi^{att}(r_{12}) \\
&\quad + \frac{1}{2} \iint d\mathbf{r}_1\, d\mathbf{r}_2\, n(\mathbf{r}_1)\, n(\mathbf{r}_2) H(r_{12} - d) \\
&\qquad \times \left\{ \Phi^p_{\alpha\beta}(\mathbf{r}_{12}) + \frac{3}{5}\, a\, \left.\frac{\partial \Phi^p_{\alpha\beta}}{\partial x_\gamma}\right|_{\mathbf{r}=\mathbf{r}_{12}} [p_\gamma(\mathbf{r}_2) - p_\gamma(\mathbf{r}_1)] \right\} p_\alpha(\mathbf{r}_1)\, p_\beta(\mathbf{r}_2),
\end{aligned} \tag{2.31}$$

where, for clarity, we use tensor notation to represent electrostatic terms. $\Phi^p_{\alpha\beta}(\mathbf{r})$ is defined by

$$\Phi^p_{\alpha\beta}(\mathbf{r}) = {p_0}^2 \left[\frac{\delta_{\alpha\beta}}{r^3} - \frac{3 x_\alpha x_\beta}{r^5} \right], \tag{2.32}$$

and x_α is the α-th component of $\mathbf{r}$ in Cartesian coordinate system. In arriving at Eq. (2.31) we have used the following relation:

$$\int d\hat{R}\, m(\mathbf{r}, \hat{R})\, \hat{R}_\alpha\, \hat{R}_\beta = \left[\frac{1}{3} - \frac{1}{5}\, p(\mathbf{r})^2 \right] \delta_{\alpha\beta} + \frac{3}{5}\, p_\alpha(\mathbf{r})\, p_\beta(\mathbf{r}) + O(p^4) \tag{2.33}$$

by employing the ansatz for $m(\mathbf{r}, \hat{R})$ given by Eq. (2.24). As before, the stationarity condition of Ω determines the equilibrium profiles for $n(\mathbf{r})$ and $\mathbf{p}(\mathbf{r})$:

$$\frac{\delta \Omega}{\delta n(\mathbf{r}_1)} = 0 \quad \text{and} \quad \frac{\delta \Omega}{\delta \mathbf{p}(\mathbf{r}_1)} = \mathbf{0}, \tag{2.34}$$

subject to boundary conditions imposed by the hard core interaction with an ion. Written explicitly,

$$\begin{aligned}
0 \;=\; & -k_B T s^{ort}(p(\mathbf{r}_1)) + \mu_d(n(\mathbf{r}_1)) \\
& - \left\{ \mu + p_0 p_\alpha(\mathbf{r_1}) \left[E_\alpha(\mathbf{r}_1) + \frac{3}{5}\, a\, \left.\frac{\partial E_\alpha}{\partial x_\beta}\right|_{\mathbf{r}=\mathbf{r}_1} p_\beta(\mathbf{r}_1) \right] \right\}
\end{aligned}$$

$$+\int d\mathbf{r}_2\, n(\mathbf{r}_2) H(r_{12}-d)\phi^{att}(r_{12})$$
$$+\int d\mathbf{r}_2\, n(\mathbf{r}_2) H(r_{12}-d)$$
$$\times\left\{\Phi^p_{\alpha\beta}(\mathbf{r}_{12})+\frac{3}{5}a\left.\frac{\partial\Phi^p_{\alpha\beta}}{\partial x_\gamma}\right|_{\mathbf{r}=\mathbf{r}_{12}}[p_\gamma(\mathbf{r}_2)-p_\gamma(\mathbf{r}_1)]\right\}p_\alpha(\mathbf{r}_1)\,p_\beta(\mathbf{r}_2) \tag{2.35}$$

and

$$0 = -k_BT\frac{ds^{ort}}{dp(\mathbf{r}_1)}\frac{p_\alpha(\mathbf{r}_1)}{p(\mathbf{r}_1)} - p_0\left[E_\alpha(\mathbf{r_1})+\frac{6}{5}a\left.\frac{\partial E_\alpha}{\partial x_\beta}\right|_{\mathbf{r}=\mathbf{r}_1}p_\beta(\mathbf{r}_1)\right]$$
$$+\int d\mathbf{r}_2\, n(\mathbf{r}_2) H(r_{12}-d)$$
$$\times\left\{\Phi^p_{\alpha\beta}(\mathbf{r}_{12})+\frac{3}{5}a\left.\frac{\partial\Phi^p_{\alpha\beta}}{\partial x_\gamma}\right|_{\mathbf{r}=\mathbf{r}_{12}}[p_\gamma(\mathbf{r}_2)-2p_\gamma(\mathbf{r}_1)]\right\}p_\beta(\mathbf{r}_2), \tag{2.36}$$

where use has been made of the fact that both $\partial E_\alpha/\partial x_\beta$ and $\partial\Phi^p_{\alpha\beta}/\partial x_\gamma$ are invariant with respect to any exchange of indices and that $\Phi^p_{\alpha\beta}(-\mathbf{r}) = \Phi^p_{\alpha\beta}(\mathbf{r})$ while $\partial\Phi^p_{\alpha\beta}/\partial x_\gamma|_{\mathbf{r}=\mathbf{r}_{12}} = -\partial\Phi^p_{\alpha\beta}/\partial x_\gamma|_{\mathbf{r}=\mathbf{r}_{21}}$. We have defined $\mu_d(n) \equiv \partial f_d/\partial n$.

In our study of ion-induced nucleation, the system is spherically symmetric about the center of an ion. Taking this as the origin, the electric field is given by

$$E_\alpha(\mathbf{r}) = q\,\frac{x_\alpha}{r^3}, \tag{2.37}$$

where q is the ion charge. For the particular choice of $\phi^{att}(r_{12})$ in Eq. (2.3), integrations with respect to the polar and azimuthal angles in Eqs. (2.31), (2.35), and (2.36) become analytically tractable, reducing the dimensionality of the integrals to two for Eq. (2.31), and one for Eqs.(2.35) and (2.36). We may now discretize the domain of $\mathbf{r}$. It can be shown that the terms arising from the dipole-dipole interaction become identically zero unless r_1 and r_2 satisfy

$$\begin{aligned}(r_1,r_2) \;&\in\; \{r_{ion}+d/2 \le r_1 \le r_{ion}+3d/2 \text{ and } r_{ion}+d/2 \le r_2 \le r_1+d\}\\ &\text{or}\quad \{r_{ion}+3d/2 \le r_1 \le r_o \text{ and } r_1-d \le r_2 \le r_1+d\},\end{aligned} \tag{2.38}$$

where r_0 is the radius of the system boundary. The condition (2.38) results from the volume exclusion represented by $H(r_{12}-d)$. The contribution due to the dipole-dipole interaction is then expected to be small, and neglected as a first approximation. The validity of this approximation will be examined in Sec. 2.4. The grand potential now becomes

$$\begin{aligned}\Omega[n(r),p(r)] = & \\ & -4\pi k_B T \int {r_1}^2\, dr_1 n(r_1) s^{ort}(p(r_1)) + 4\pi \int {r_1}^2\, dr_1\, f_d(n(r_1)) \\ & -4\pi \int {r_1}^2\, dr_1\, n(r_1) \left\{ \mu + p_0 q \frac{p(r_1)}{{r_1}^2} \left[1 - \frac{6}{5} \frac{a}{r_1} p(r_1) \right] \right\} \\ & +4\pi \int {r_1}^2\, dr_1\, n(r_1) \left\{ \pi \int {r_2}^2\, dr_2\, n(r_2) \int_{-1}^{c(r_1,r_2)} d(\cos\theta)\, \phi^{att}(r_{12}) \right\}.\end{aligned} \tag{2.39}$$

Note that

$$\phi^{att}(r_{12}) = \epsilon d^6 \frac{d}{d(\cos\theta)} \left[-\frac{1}{4 r_1 r_2} \frac{1}{({r_1}^2 + {r_2}^2 - 2 r_1 r_2 \cos\theta)^2} \right]. \tag{2.40}$$

$c(r_1, r_2)$ is unity except when r_1 and r_2 satisfy the condition (2.38), in which case

$$c(r_1, r_2) = \frac{{r_1}^2 + {r_2}^2 - d^2}{2 r_1 r_2}. \tag{2.41}$$

The sign preference of the grand potential is clearly seen in Eq. (2.39). Consider a system in equilibrium and suppose that the sign of the charge q is reversed. If a were zero, the system would establish a new equilibrium state by simply reversing the sign of $p(r)$ without changing its magnitude or $n(r)$, since the grand potential is invariant with respect to simultaneous reversal of q and $p(r)$. However, for any nonzero value of a, Ω is no longer invariant and the system has to modify both $n(r)$ and the magnitude of $p(r)$ as well as its sign to establish a new equilibrium state, which in general affects the value of Ω. The equilibrium profiles for $n(r)$ and $p(r)$ are determined by

$$\begin{aligned} 0 \;=\; & -k_B T s^{ort}(p(r_1)) + \mu_d(n(r_1)) - \left\{ \mu + p_0 q \frac{p(r_1)}{{r_1}^2} \left[1 - \frac{6}{5} \frac{a}{r_1} p(r_1) \right] \right\} \\ & +2\pi \int {r_2}^2\, dr_2\, n(r_2) \int_{-1}^{c(r_1,r_2)} d(\cos\theta)\, \phi^{att}(r_{12}) \end{aligned} \tag{2.42}$$

and

$$0 = -k_B T \frac{ds^{ort}}{dp(r_1)} - \frac{p_0 q}{{r_1}^2} \left[1 - \frac{12}{5} \frac{a}{r_1} p(r_1) \right]. \tag{2.43}$$

Note that Eq. (2.43) is now independent of $n(r)$ as a result of ignoring the dipole-dipole interaction.

2.2.3 Bulk properties

In the absence of the external field, the thermodynamic properties of a homogeneous system can be easily derived from Eq. (2.16). Since such a system is isotropic as well, we may set $\rho(\mathbf{r}, \hat{R}) = n/4\pi$ in Eq. (2.16), from which the Helmholtz free energy density per unit volume of the system of density n is obtained:

$$\begin{aligned} f(T,n) &= -p + \mu n \\ &= -k_B T n \log 4\pi + f_d(n) - \frac{\alpha}{8\pi} n^2. \end{aligned} \tag{2.44}$$

Note that $\Omega = -pV$ for a homogeneous system. α is defined here by

$$\begin{aligned} \alpha &\equiv -\frac{1}{4\pi V} \iint d1\, d2\, H(r_{12} - d) \left[\phi^{att}(r_{12}) + \phi^p(1,2) \right] \\ &= -4\pi \int d\mathbf{r}_{12}\, H(r_{12} - d) \phi^{att}(r_{12}), \end{aligned} \tag{2.45}$$

where we have used the fact that the integral of $\phi^p(1,2)$ is zero. For the particular choice of $\phi^{att}(r_{12})$ given by Eq. (2.3), one has

$$\alpha = \frac{(4\pi)^2}{3} \epsilon d^3. \tag{2.46}$$

Eq. (2.44) is a fundamental equation of the isotropic system, from which by well known thermodynamic relations, one obtains

$$\mu(T,n) = -k_B T \log 4\pi + \mu_d(n) - \frac{\alpha}{4\pi} n; \tag{2.47}$$

$$p(T,n) = n\mu_d(n) - f_d(T,n) - \frac{\alpha}{8\pi} n^2. \tag{2.48}$$

Eq. (2.47) is identical with Eq. (2.18) applied to the isotropic system at $v(\mathbf{r}, \hat{R}) = 0$. These results could also have been obtained by setting $\mathbf{E} = \mathbf{0}$ and $\mathbf{p} = \mathbf{0}$ in Eq. (2.31).

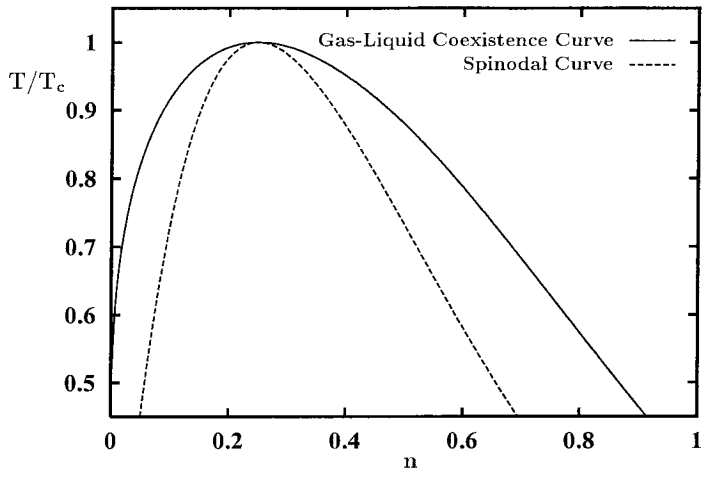

Figure 2.3: The gas-liquid coexistence curve and the spinodal curve calculated for the system composed of the dipole molecules. Density is normalized by d^{-3}.

At a given temperature, the coexisting bulk densities are determined by

$$\begin{aligned} \mu_l(T, n_l^{eq}) &= \mu_v(T, n_v^{eq}); \\ p_l(T, n_l^{eq}) &= p_v(T, n_v^{eq}), \end{aligned} \tag{2.49}$$

where the subscripts $_l$ and $_v$ refer to liquid and vapor, respectively. The spinodal curve which divides the metastable and unstable regions in $T - n$ phase diagram is obtained by

$$\frac{\partial p}{\partial n} = 0. \tag{2.50}$$

The critical point is located in the phase diagram by Eq. (2.50) and

$$\frac{\partial^2 p}{\partial n^2} = 0, \tag{2.51}$$

with a numerical solution

$$\begin{aligned} y_c &= \frac{\pi}{6} d^3 n_c \\ &\approx 0.13044; \\ \frac{1}{k_B T_c} &\approx 14.135 \left(\frac{\pi^2 d^3}{\alpha} \right) \\ &= 2.6503 \left(\frac{1}{\epsilon} \right). \end{aligned} \tag{2.52}$$

The $T - n$ phase diagram is shown in Fig. 2.3.

2.3 Solution Method for the Equilibrium Profiles

Given T/T_c and supersaturation S, defined as the ratio of the metastable vapor pressure and the equilibrium vapor pressure, we can calculate, via Eqs. (2.47)-(2.49), the chemical potential μ of the system and the densities of the bulk liquid n_l and vapor n_v at that chemical potential. As mentioned in Sec. 2.2.2, Eq. (2.43) is independent of $n(r)$ and can be easily solved numerically. The solution is substituted in Eq. (2.42), which is now an integral equation for $n(r)$ only and can be solved by iteration. In the case of homogeneous nucleation, the equation to determine the density profile $n(r)$ has two solutions. One is that of a metastable vapor, namely $n(r) = n_v$. The other is that of a critical nucleus, which corresponds to a saddle point in functional space. When an ion is present in the vapor, the metastable profile exhibits solvation of the ion. This metastable nucleus was obtained by starting from the initial guess $n(r) = n_v$. Iteration can be repeated until the quantity

$$\Delta \equiv \int d\mathbf{r} \left| \frac{\delta \Omega}{\delta n(\mathbf{r})} \right| \tag{2.53}$$

becomes sufficiently small. The iteration process applicable to a critical nucleus is described in detail by Oxtoby and Evans.[33] As the initial guess, we take the step function:

$$n(r) = \begin{cases} n_l & r \leq R \\ n_v & \text{otherwise.} \end{cases} \tag{2.54}$$

If R is too small, the nucleus shrinks as the iteration proceeds, while it grows if R is too large. Starting from several values of R, it is possible to find R^* such that the nucleus

neither shrinks nor grows as the iteration is repeated. Our solution method differs from that proposed by Oxtoby and Evans[33] in some details. Instead of monitoring the behavior of Ω as a function of iteration number, we monitored Δ. R^* was identified with that which yields, after some steps of iteration, $n(r)$ that minimizes Δ. Then, this $n(r)$ was used as the initial guess in solving Eq. (2.42) more accurately by the Newton-Raphson method, which was repeatedly applied until Δ becomes sufficiently small.

Finally, the boundary of the system is taken to be a sphere, the radius of which is sufficiently large so that $n(r)$ attains its limiting value n_v there. As a result of the long ranged nature of the monopole-dipole interaction, $p(r)$ may not reach its limiting value of zero even at r_0. The truncation error thus introduced, however, exactly cancels out when the difference is taken, as in the case of the reversible work calculation, between two states with the same value of n_v.

2.4 Results and their Implications

It is advantageous to normalize the equations by model parameters: d for the length scale; $k_B T_c$ for the energy scale. When the dipole-dipole interaction is ignored, the dipole moment p_0 and the charge q of an ion can be lumped together to form a single dimensionless parameter:

$$\chi \equiv \frac{p_0 q}{d^2 k_B T_c}, \tag{2.55}$$

which is the ratio between the monopole-dipole interaction energy at separation d, the diameter of a molecule, and the thermal energy at the bulk critical point. $\chi > 0$ corresponds to nucleation either around a positive ion of molecules each with dipole pointing outward from its center, or around a negative ion of molecules each with dipole pointing toward its center.

Typical values of χ are of the order of 10. When $p_0 = 1\text{D(Debye)}$, $d = 3\text{Å}$, $T_c = 10^3\text{K}$, and $q = e$, where $-e$ is the charge of an electron, $\chi \approx 3.9$. Our choice of parameters is $|\chi| = 5$, $a = 0.1d$, and the ionic radius $r_{ion} = d$. Later, the effect of the values of these parameters on the reversible work of nucleation will be examined.

The absolute value of the average dipole moment distribution $p(r)$ is shown in Fig. 2.4. The sign of $p(r)$ is the same as that of χ. Near the ion, dipoles tend to line up with the

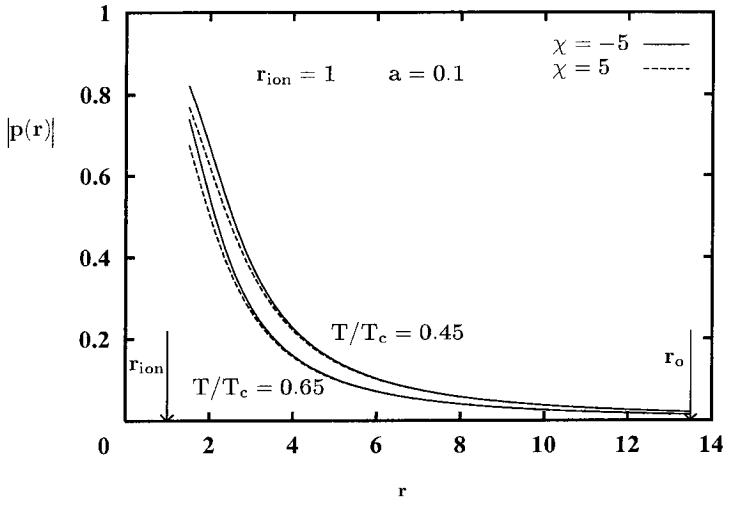

Figure 2.4: The magnitude of an average dipole moment distribution at two different temperatures. r_0 is the radius of the system boundary. Distance is normalized by d.

electric field, showing r^{-2} decay for larger distance, as it should. What is not shown in the figure is the case of $\chi = 0$, when Eq. (2.43) has a trivial solution $p(r) \equiv 0$. Figure 2.4 shows that at a given distance r from the ion, the magnitude of the average dipole moment is always larger when $\chi < 0$. This is readily understood as follows. Suppose for a moment that the dipole moment is placed outward with respect to the center of each molecule. The dipole moment in a molecule at r tends to point toward a negative ion, thereby decreasing its distance from the ion, while it will point away from a positive ion, increasing its distance from the ion. For a given value of $|\chi|$ and at the fixed ion-molecule distance, the monopole-dipole interaction is therefore stronger when $\chi < 0$ than when $\chi > 0$. As seen from Eq. (2.43), T/T_c affects $p(r)$ through the parameter $\chi(T/T_c)^{-1}$. Increasing T/T_c has the same effect as decreasing χ, as shown in Fig. 2.4. Stated differently, the entropic contribution becomes more important at higher T/T_c, and the system prefers a less ordered state.

The number density distribution $n(r)$ is obtained from Eq. (2.42). Figure 2.5 shows the solution at $T/T_c = 0.65$ and supersaturation $S = 3$. Density profile for the case of $\chi < 0$ is shown in Fig. 2.6 at the same temperature for several values of supersaturation. Figs. 2.7 and 2.8 show similar results at $T/T_c = 0.45$.

As mentioned in Sec. 2.3, a metastable profile shows solvation of the ion. The exception is the case of $\chi = 0$, corresponding to nucleation on a neutral particle, for which the profile

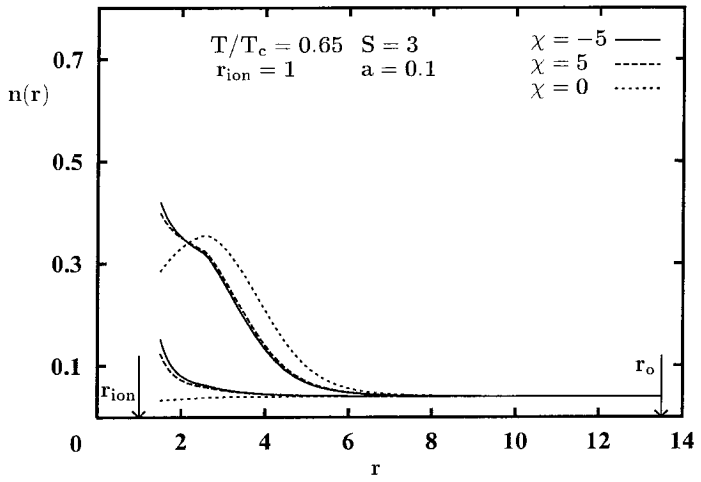

Figure 2.5: Equilibrium density profiles at $T/T_c = 0.65$ and $S = 3$. The profiles with smaller values of $n(r)$ correspond to the metastable nuclei, while those with larger values o $n(r)$ represent the critical nuclei. r_0 is the radius of the system boundary. Distance is normalized by d.

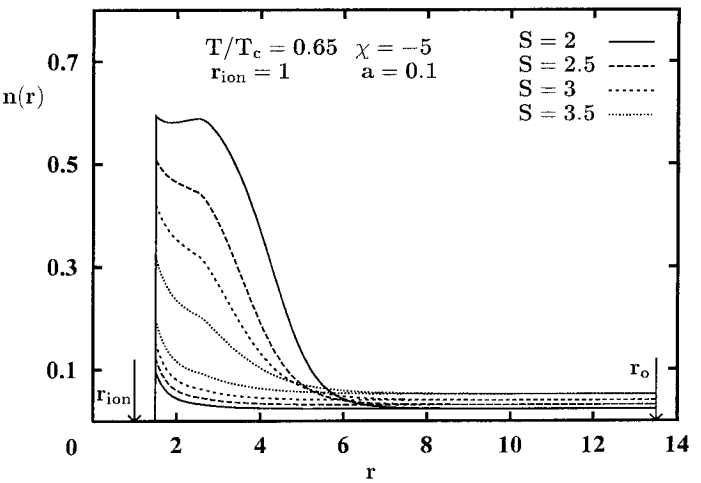

Figure 2.6: Variation of the density profile with the supersaturation S. $T/T_c = 0.65$.

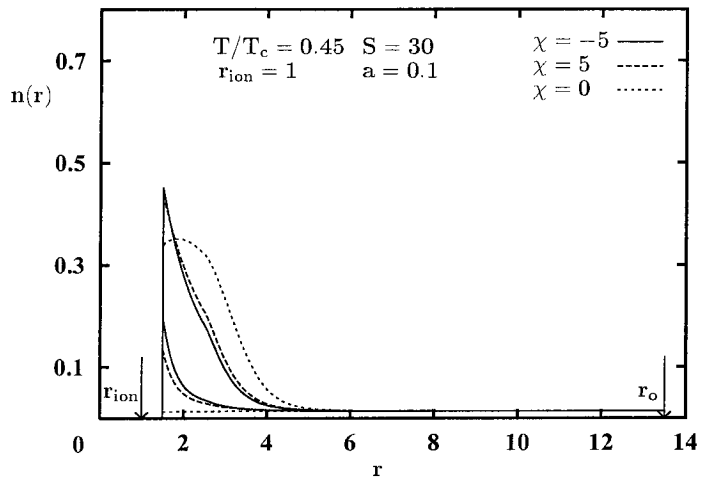

Figure 2.7: Same as (a), but for $T/T_c = 0.45$ and $S = 30$.

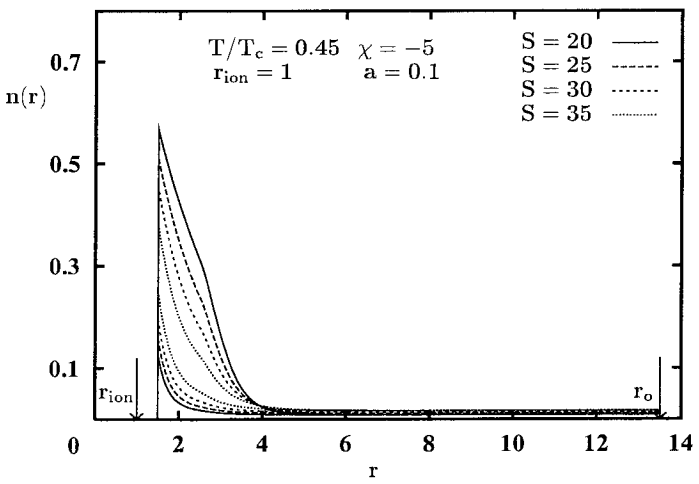

Figure 2.8: Same as (b), but for $T/T_c = 0.45$.

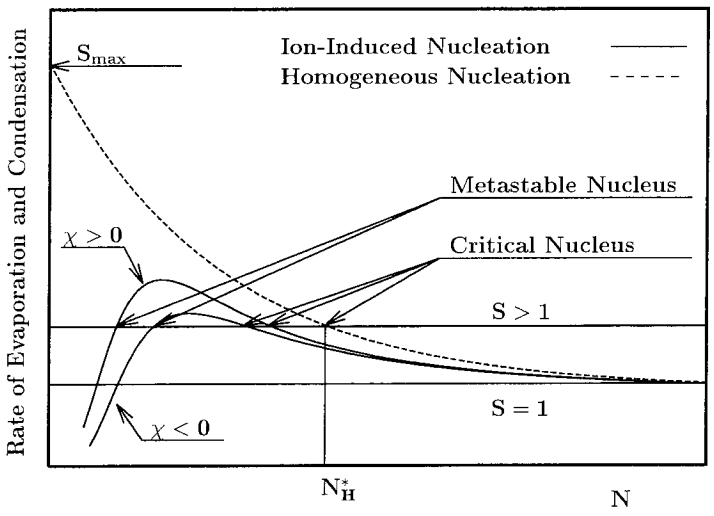

Figure 2.9: A schematic picture of the rate of evaporation (represented by the curves) and condensation (represented by the horizontal lines) of molecules per unit area of the nucleus. The abscissa represents the number of molecules in the nucleus.

shows a decrease in density near the particle. This volume exclusion effect is a result of the repulsive hard core interaction between the particle of radius r_{ion} and the molecules. Although the effect exists for other cases as well, it is often overwhelmed by the attractive interaction between the monopole and the dipoles. The general feature to be observed is that at a given supersaturation S, the metastable nucleus with $\chi < 0$ is always larger than that with $\chi > 0$, while the opposite is true for the critical nuclei. Also, the metastable nucleus grows as S increases, while the critical nucleus shrinks. To qualitatively understand such features, it is helpful to take a molecular point of view. An equilibrium nucleus is then characterized as the one for which the rate of evaporation of molecules (per unit time unit area) and that of condensation is balanced. The qualitative behavior of these rates is shown schematically in Fig. 2.9, where we denote by N the number of molecules within a nucleus. At a given temperature, the physical state of the nucleus and therefore the rate of evaporation are independent of the vapor pressure. While N is relatively small, the intermolecular interaction energy per molecule increases (in its magnitude) as N increases. Thus the rate is a monotonically decreasing function of N and approaches the bulk liquid value equal to the condensation rate at saturation ($S = 1$) as N approaches infinity. The condensation rate, on the other hand, is independent of N and is proportional to the vapor

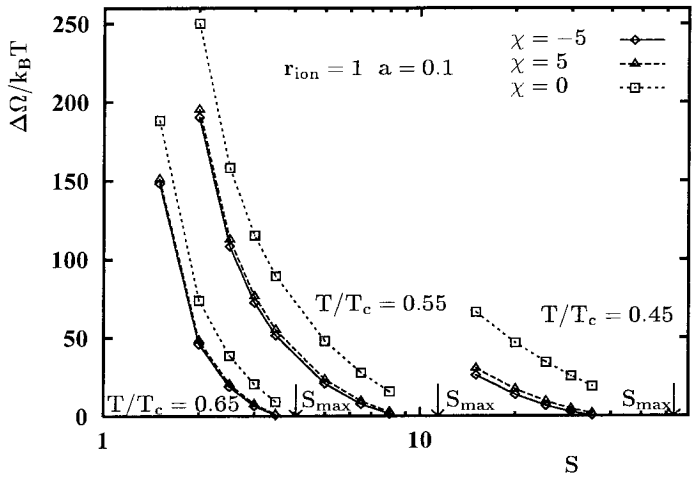

Figure 2.10: The reversible work of nucleation. Three values of S_{max} represent the supersaturation at the stability limit. From the left, they correspond to the value at $T/T_c = 0.65$, at $T/T_c = 0.55$, and at $T/T_c = 0.45$, respectively.

pressure or S. As shown in Fig. 2.9, those two rates are equal when $N = N_H^*$, and N_H^* decreases as S increases, approaching order of one at the spinodal (denoted by S_{max}), where an infinitesimal fluctuation in density promotes phase transition.

When an ion is introduced in a nucleus, it attracts molecules via the monopole-dipole interaction, thereby decreasing the evaporation rate. Since the electric field decays as r^{-2}, the decrease should be most significant for small N and becomes negligible as N approaches infinity. As mentioned in connection with Fig. 4, this attraction is stronger when $\chi < 0$ than when $\chi > 0$, which yields the curves for $\chi > 0$ and $\chi < 0$ in Fig. 2.9. When the attraction between an ion and molecules is sufficiently large, the condensation rate balances the evaporation rate even when $S \leq 1$, which corresponds to vapor solvation of the ion. From Fig. 2.9, it is clear that at a given supersaturation S, a metastable nucleus is larger if $\chi < 0$, while the opposite is true for a critical nucleus. Figure 2.9 also shows that as S increases, a metastable nucleus grows while a critical nucleus shrinks, and that two nuclei coincide, meaning that the system reaches its stability limit, at the supersaturation lower than S_{max}. A similar figure is employed by Castleman et al.[72] in explaining the existence of a metastable nucleus and the instability of the system at a supersaturation lower than S_{max}.

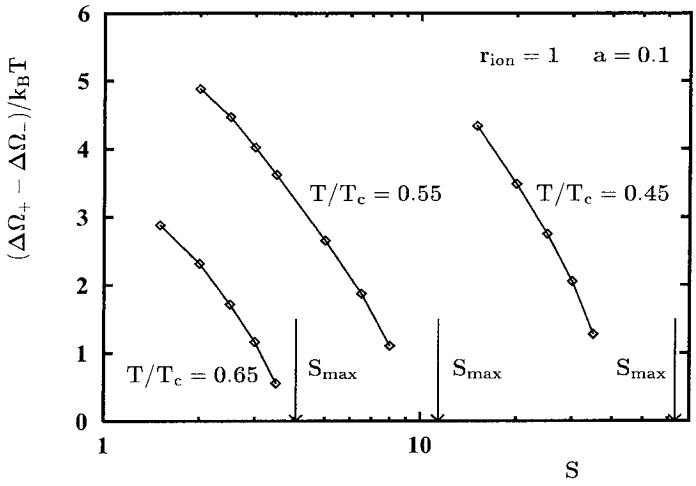

Figure 2.11: The difference in the reversible work reported in Fig. 2.10 between the case of $\chi > 0$ and that with $\chi < 0$.

Figure 2.10 shows the reversible work $\Delta\Omega/k_BT$ of nucleation as a function of supersaturation. The reversible work relevant here is that is required to form a critical nucleus from the metastable one. Figure 2.10 shows that the reversible work decreases as S is increased, and that if $\chi \neq 0$ it approaches zero before S_{max} is reached, which is consistent with the qualitative prediction of Fig. 2.9. Figure 2.11 shows the difference between the reversible work $\Delta\Omega_+/k_BT$ of nucleation with $\chi > 0$ and that $(\Delta\Omega_-/k_BT)$ with $\chi < 0$. Figure 2.11 clearly shows the preference for the case of $\chi < 0$, influencing the nucleation rate by a factor of 10 to 10^2. The observed preference can be understood along the line of discussion given in connection with the average dipole distribution $p(r)$. Figure 2.11 also shows a monotonic decrease in $\Delta\Omega_+ - \Delta\Omega_-$ with increasing S. To understand its implication, let us rearrange this quantity as follows:

$$\begin{aligned} & \Delta\Omega_+ - \Delta\Omega_- \\ = \; & (\Omega_+^{critical} - \Omega_-^{critical}) - (\Omega_+^{metastable} - \Omega_-^{metastable}). \end{aligned} \tag{2.56}$$

For an equilibrium distribution of $p(r)$ and $n(r)$, one may combine Eq. (2.42) with Eq. (2.39) to eliminate the double integral. Expanding the resulting expression for Ω_+ around $\bar{n} \equiv$

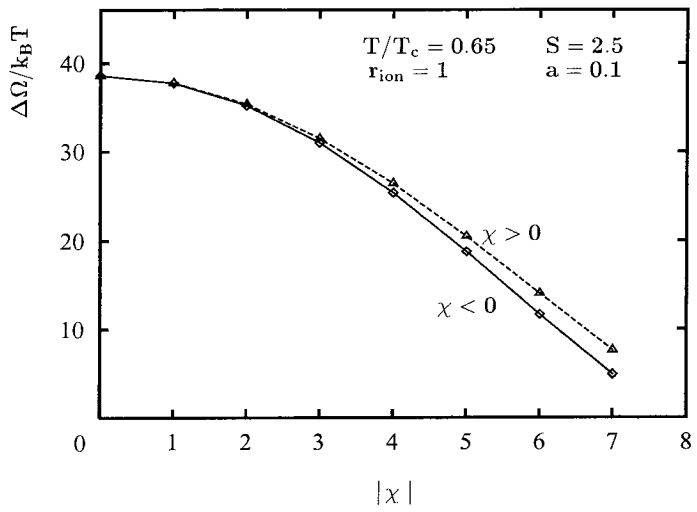

Figure 2.12: Effect of the value of χ on the reversible work.

$(n_+ + n_-)/2$ and $\bar{p} \equiv (p_+ - p_-)/2$, and that for Ω_- around $\bar{n}$ and $-\bar{p}$, one finds

$$\begin{aligned} \Omega_+ - \Omega_- \approx & \frac{6}{5}\, a\, |p_0\, q| \int d\mathbf{r}\, \frac{\bar{n}\, \bar{p}^{\,2}}{r^3} \\ & + \int d\mathbf{r}\, \left[h_1(\bar{n}, \bar{p})\, (n_+ - n_-) + \bar{n}\, h_2(\bar{p})\, (p_+ + p_-) \right], \end{aligned} \tag{2.57}$$

where h_1 and h_2 are certain functions. Noting that $p(r)$ is independent of $n(r)$ and retaining only the leading term,

$$\Delta\Omega_+ - \Delta\Omega_- \approx \frac{6}{5}\, a\, |p_o\, q| \int d\mathbf{r}\, \frac{\bar{p}^{\,2}}{r^3}\, (\bar{n}^{critical} - \bar{n}^{metastable}). \tag{2.58}$$

It is clear that this quantity decreases monotonically as S is increased.

The dependence of the reversible work on the values of model parameters is shown in Figs. 2.12-2.14. Figure 2.12 shows that the presence of the electric field always decreases the reversible work of nucleation of dipolar molecules. Figure 2.13 shows that the increase in r_{ion} results in the increase of the reversible work as well as in the decrease in sign dependence. This is expected since the increase in r_{ion} causes the increase in the monopole-dipole separation. However, as seen from Fig. 2.14, it is the asymmetric nature of molecules that is directly responsible for the sign dependence of the reversible work. Figure 2.14 shows that the reversible work for the case of $\chi > 0$ increases as a is increased, while it decreases

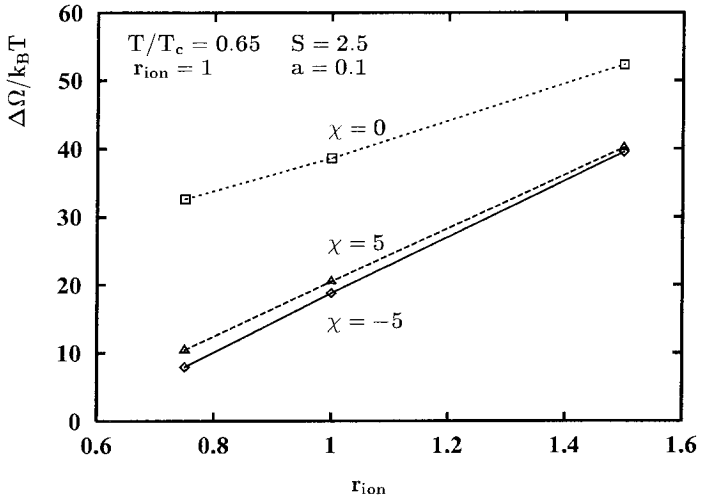

Figure 2.13: Dependence of the reversible work on the size of an ion. Distance is normalized by d.

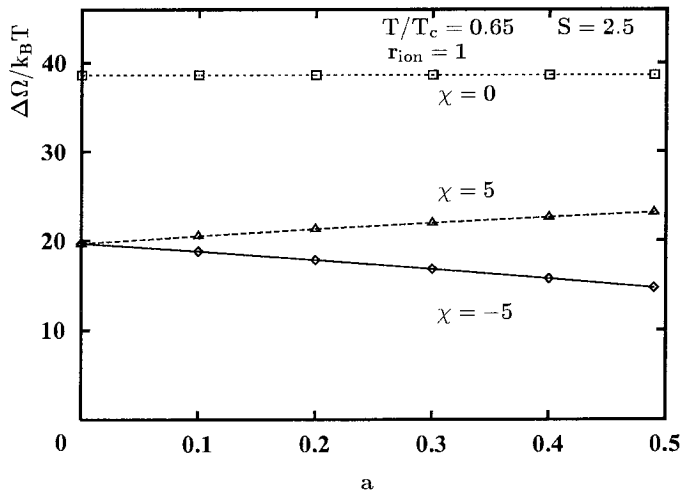

Figure 2.14: Effect of asymmetry of a molecule upon the sign preference of the reversible work of ion-induced nucleation. Distance is normalized by d.

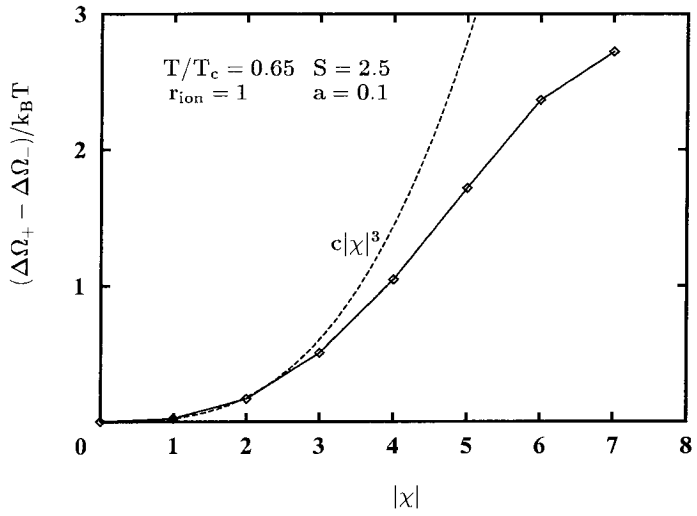

Figure 2.15: Dependence of the sign effect of the reversible work on $|\chi|$. The value of the coefficient c is determined to match the computed value of $(\Delta\Omega_+ - \Delta\Omega_-)/k_BT$ at $|\chi| = 1$.

if $\chi < 0$. Such a trend can be readily understood by noting that a larger value of a implies larger monopole-dipole separation if $\chi > 0$ and smaller separation if $\chi < 0$ for a given ion-molecule separation. Eq. (2.26) shows that, in the weak electric field limit, $p \sim p_0\, q$. From Eqs. (2.55) and (2.58), one finds

$$\Delta\Omega_+ - \Delta\Omega_- \sim a\,|\chi|^3. \tag{2.59}$$

Such dependence on $|\chi|$ and a is clearly seen in Figs. 2.15 and 2.16.

In our calculation, the dipole-dipole interaction has been ignored for computational convenience. To examine the validity of this approximation, we calculated its contribution to the grand potential of the system. As a self-consistency check, we use the equilibrium profile $p(r)$ and $n(r)$ obtained by neglecting the dipole-dipole interaction. In Eq. (2.31), when the integrations with respect to $\mathbf{r}_2$ are carried out,

$$\omega^{att}(\mathbf{r}_1) = \frac{1}{2}\int d\mathbf{r}_2\, n(\mathbf{r}_2) H(r_{12} - d)\, \phi^{att}(r_{12}) \tag{2.60}$$

and

$$\omega^{p}(\mathbf{r}_1) \;=\; \frac{1}{2}\int d\mathbf{r}_2\, n(\mathbf{r}_2) H(r_{12} - d)$$

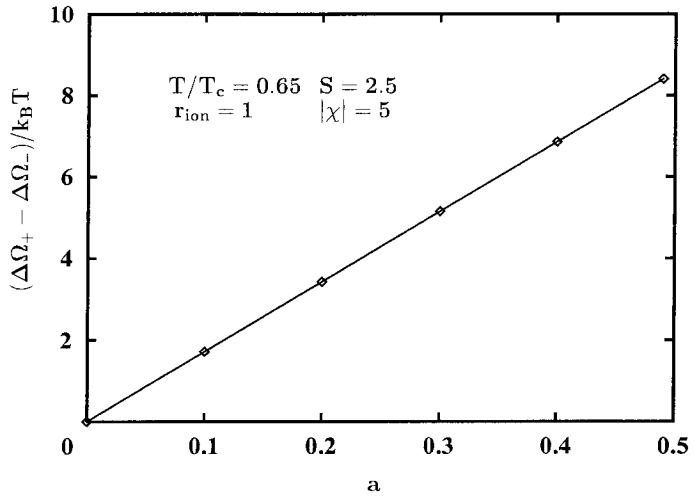

Figure 2.16: Dependence of the sign effect of the reversible work on a. Distance is normalized by d.

$$\times \left\{ \Phi^p_{\alpha\beta}(\mathbf{r}_{12}) + \frac{3}{5} a \left. \frac{\partial \Phi^p_{\alpha\beta}}{\partial x_\gamma} \right|_{\mathbf{r}=\mathbf{r}_{12}} [p_\gamma(\mathbf{r}_2) - p_\gamma(\mathbf{r}_1)] \right\} p_\alpha(\mathbf{r}_1)\, p_\beta(\mathbf{r}_2) \tag{2.61}$$

can be, respectively, regarded as the contributions to the free energy per molecule due to the intermolecular interactions $\phi^{att}(r_{12})$ and $\phi^p(1,2)$. Figure 2.17 shows these quantities as functions of r_1. ω^p can be shown to scale as $\chi p_0/qd$. When $p_0 = 1\text{D}$, $d = 3\text{Å}$, and $q = e$, we have $p_0/qd \approx 0.07$. In Fig. 2.17, we have chosen $p_0/qd = 0.1$. The contribution due to $\phi^p(1,2)$ is, in fact, quite small compared to that from $\phi^{att}(r_{12})$, justifying our approximations of ignoring the dipole-dipole interactions.

2.5 Discussion and Conclusion

In this paper, we have shown that the sign preference in ion-induced nucleation can be explained in terms of the asymmetric nature of the molecular interactions. Consistent treatment of such molecular characteristics is achieved by means of a statistical mechanical density functional theory, by which the grand potential is given in terms of two order parameters, the number density $n(r)$ of molecules and the average dipole moment distribution $p(r)$. When the intensive state of the supersaturated vapor is specified, the stationarity

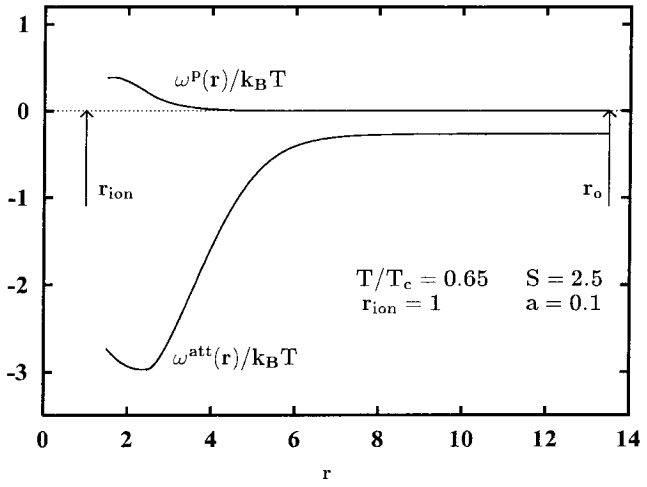

Figure 2.17: The free energy densities resulting from the dipole-dipole interaction (ω^p) and that due to ϕ^{att} (denoted by ω^{att}). r_0 is the radius of the system boundary. Distance is normalized by d.

condition of the grand potential uniquely determines a critical nucleus and a metastable nucleus for given values of model parameters. The calculated reversible work shows a preference toward the case of $\chi < 0$, influencing the nucleation rate by a factor of 10 to 10^2 for some realistic values of the model parameters employed in this paper.

In the present work, ions are assumed to be the only source of the electric field within the system. A uniform electric field is often applied, however, to selectively introduce ions with a particular sign. Rabeony and Mirabel[60] were the first to draw attention to the effect of a uniform electric field on the rate of nucleation. They reported a decrease in the number of nucleation events as the applied field was increased. A similar decrease was reported by Katz et al.,[73] though they clearly demonstrated that the nucleation rate, which was identified as the number of nucleation events divided by the time during which ions stay in the nucleation zone, was independent of the applied field. On the other hand, an increase in the nucleation events was reported by He and Hopke[74] and El-Shall and Kane.[44] Although a thermal diffusion cloud chamber was used in all of these experiments, the disagreement among them seems to arise from the different techniques of introducing ions into the nucleation zone.

In the experiments reported by Rabeony and Mirabel,[60] a sign effect is observed only

in the presence of this uniform field. However, Okuyama et al.[61,62] observed an apparent sign effect in the absence of the field. Their figure 9 indicates that the sign preference in the nucleation rate becomes less significant as supersaturation increases, in agreement with our prediction. (See Fig. 2.11). Such dependence of the sign preference on supersaturation is also reported by El-Shall and Kane.[44]

In trying to make quantitative comparisons with experiment, we note the following points. First, model parameters such as ϵ and d are easily determined from the critical point data, assuming that the substance is well described by the law of corresponding states with two parameters. The dipole moment p_0 can be either related to the bulk dielectric constants or found in a handbook. The value of a that plays such an important role in producing the sign effect, however, is not available in general.

Secondly, ions present in the experiments are often complex molecules such as $H^+(H_2O)_n$ rather than ionized atoms. Then, the ion itself must be treated by means of statistical mechanics. Also, an ion would interact with the condensing molecules via a van der Waals type interaction as well. The latter can be treated in the current theory by simply replacing Eq. (2.19) by the appropriate expression.

We have characterized an ion by its charge and radius, and the ion-molecule interaction is assumed to be purely electrostatic. Such an idealization is acceptable for those ions that have the same electronic structure as that of noble gases.[75,76] On the other hand, one would not expect the present theory to be applicable to a system where the chemical nature of the interaction between the ion and molecules plays an important role.[77] If, however, the effect on the grand potential due to such chemical characteristics is insensitive to the size of a nucleus, it will cancel out on calculating the reversible work of nucleation. In fact, Katz et al.[73] found that, within the accuracy of their experiment, the nucleation rate dependence on the ion characteristics is insignificant. It is therefore interesting to examine the validity of the current theory against the experimental data, assuming that values of all the model parameters are known.

We have avoided the explicit consideration of the fluctuation of an ion within the nucleus by taking the position of the point charge as the origin. Implicit in our calculation is the assumption that the system is, on average, spherically symmetric around the ion. More rigorously, one could treat the system as a binary in which the ion is the second component with extremely low concentration.

Our calculations at this stage are largely qualitative both in the model representation of the system and in the theoretical treatment. Further improvement on both fronts can be envisaged. For example, the model can incorporate the polarizability of molecules, non-spherical charge distribution in an ion, etc. Also, a better treatment of the pair distribution function than that of Eq. (2.15) will undoubtedly give a better description of the structure of the fluid near the ion or interface. Nevertheless, it is clear that some of the most important characteristics of ion-induced nucleation have been captured in the present theory, which forms a basis for explaining this well known phenomenon that has hitherto remained inexplicable within the classical framework.

Acknowledgments[41]

This work was supported by National Science Foundation grant ATM-9307603.

Chapter 3 Ion-Induced Nucleation: II. Polarizable Multipolar Molecules

Density functional theory is applied to ion-induced nucleation of polarizable multipolar molecules. The asymmetric nature of the ion-molecule interaction is shown to cause the sign preference in ion-induced nucleation. When the ion-molecule interaction is weak, the observed sign preference is consistent with that of the bare ion-molecule interaction potential and decreases with increasing supersaturation. However, as the ion-molecule interaction becomes stronger, the sign preference in the reversible work exhibits some non-trivial behavior. For molecular parameters applicable for CS_2 and CH_4, the predicted values of the reversible work of nucleation depend on the sign of the ion charge, yielding a difference in the nucleation rate by factors of 10 to 10^2 and 10 to 10^5, respectively.

3.1 Introduction

In ion-induced-nucleation ions act as sites for vapor molecule cluster formation, thereby enhancing the ease with which clusters can form in a supersaturated vapor over that in the absence of ions.[56–60,62,74] Despite the long recognition of the phenomenon of ion-induced nucleation, a detailed understanding of the physics of the interaction between neutral vapor molecules and ions that leads to an enhanced rate of nucleation in the presence of ions has been lacking. A question basic to the process is — whether one can predict on fundamental grounds how the rate of nucleation will, for a particular vapor molecule, depend on the sign and properties of the ion. While both positive and negative ions increase the nucleation rate, most substances exhibit a preference for one ion polarity over the other. For some substances, however, even a qualitative agreement among experiments on the sign preference for nucleation is lacking.[69] Definite conclusion on the sign preference for some substances still awaits for further investigations.[73]

Physically, the dependence of the ion-induced nucleation rate of a substance on the sign of the ion charge must arise from some sort of asymmetry in the molecular interactions. Such asymmetry should, in principle, manifest itself in a sign dependence of the relevant

thermodynamic quantities such as the surface tension. Several attempts have been made to incorporate molecular characteristics within the framework of the capillarity theory.[59,64–68]

These theories were critically reviewed by Rabeony and Mirabel,[69] who concluded that only Rusanov and Kuni's model[66–68] could correctly predict the sign preference for a few substances, although the predicted sign effect was shown to be extremely sensitive to a parameter in the theory that cannot be evaluated within the classical framework. It has also been noted[69] that, except for its inability to explain the sign effect, the best predictions of the reversible work, when compared with experimental data, come from Thomson's original equation.[63] Most importantly, these theories all apply for polar materials and are incapable of predicting a sign preference for non-polar substances. The failure of these approaches merely points to the need for consistent treatment of the molecular characteristics in evaluating the free energy by means of statistical mechanics.

In the previous work,[41] we applied a statistical mechanical density functional theory to ion-induced nucleation of dipolar molecules. Asymmetry was introduced into the ion-molecule interaction by means of a permanent dipole moment placed at a distance a off the center of a molecule. It was concluded that this asymmetry in the ion-molecule interaction is directly responsible for the sign preference in ion-induced nucleation.

This paper is intended to propose an alternative mechanism, applicable for both polar and non-polar substances, through which a sign preference in the rate of nucleation arises. In particular, we present a density functional theory for ion-induced nucleation of polarizable multipolar molecules. For a fixed orientation of a molecule, the ion-molecule interaction through the molecular polarizability is independent of the sign of the ion charge, while that through the permanent multipole moments is not. As a result of this asymmetry, the reversible work acquires a dependence on the sign of the ion charge.

The outline of this paper is as follows. In Sec. 3.2, we first introduce our model representation of a molecule, and then construct a density functional for the grand potential in terms of two order parameters, the particle number density and the re-scaled ion charge. The latter is related in a simple way to a locally defined dielectric constant. Bulk properties are derived from the density functional. Section 3.3 describes the solution methods for determining the equilibrium profiles. The reversible work of nucleation is obtained from the equilibrium profiles and reported in Sec. 3.4. Finally, some concluding remarks are given with a brief discussion in Sec. 3.5.

3.2 Density Functional Theory

3.2.1 The model and the intermolecular potential

Let us consider a system of spherical molecules each of which has, at its center, electric permanent multipole moments, polarizability, and hyperpolarizabilities. We assume that a molecule is in its ground state under the influence of the external electric field and suppose that the interaction potential $\phi(1,2)$ between one molecule at $\mathbf{r}_1$ with orientation $\hat{R}_1$ and the other at $\mathbf{r}_2$ with orientation $\hat{R}_2$ can be written as

$$\phi(1,2) = \phi^d(r_{12}) + \phi^{att}(r_{12}) + \phi^{mp}(1,2), \tag{3.1}$$

where $r_{12} = |\mathbf{r}_2 - \mathbf{r}_1|$. We use the notation j to represent both the translational and orientational coordinates of molecule j. $\phi^d(r_{12})$ and $\phi^{att}(r_{12})$ form the isotropic part of the interaction potential $\phi(1,2)$. $\phi^d(r_{12})$ is the hard sphere potential given by

$$\phi^d(r_{12}) = \begin{cases} +\infty & \text{if } r_{12} < d \\ 0 & \text{otherwise.} \end{cases} \tag{3.2}$$

$\phi^{att}(r_{12})$ is the perturbative attractive potential whose explicit form is chosen to be

$$\phi^{att}(r_{12}) = -\epsilon^{att}\left(\frac{d}{r_{12}}\right)^6, \tag{3.3}$$

where ϵ^{att} is a positive constant.

In this model, the anisotropic part of $\phi(1,2)$ arises from the orientational dependence of the interaction potential between multipole moments on the molecule 1 and those on the molecule 2. Care must be taken, however, to correctly incorporate the effect of the molecular polarizability. To determine the explicit form of this anisotropic interaction potential $\phi^{mp}(1,2)$, we first consider the electrostatic energy $U(1)$, in the external electric field $F_\alpha(\mathbf{r})$, of a neutral molecule 1 in a fixed position and orientation. In this external field, the molecule acquires the induced multipole moments, which along with its permanent multipole moments constitute the total multipole moments. Thus[78,79]

$$U(1) = U^{pol}(1) - \mu_\alpha^{(T)}(1)F_\alpha(\mathbf{r}_1) - \frac{1}{3}\Theta_{\alpha\beta}^{(T)}(1)F_{\alpha\beta}(\mathbf{r}_1)$$

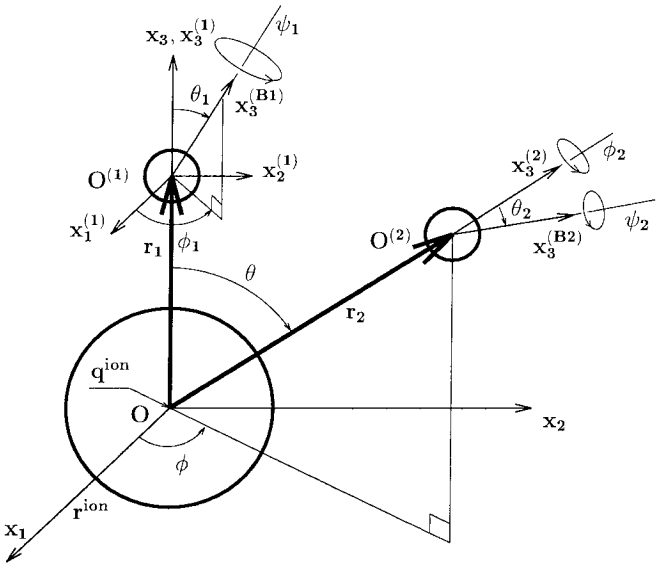

Figure 3.1: Model of a molecule and an ion. The origin of the laboratory coordinate system $O - x_1x_2x_3$ is taken at the center of the ion, where a point charge q^{ion} is located. $O^{(1)} - x_1^{(1)}x_2^{(1)}x_3^{(1)}$ is the local coordinate system whose origin coincides with the center of the molecule 1, and $x_3^{(1)}$-axis is parallel to x_3-axis. $(\phi_1, \theta_1, \psi_1)$ is the Euler angle of the body fixed coordinate system $O^{(B1)} - x_1^{(B1)}x_2^{(B1)}x_3^{(B1)}$.

$$-\frac{1}{15}\Omega^{(T)}_{\alpha\beta\gamma}(1)F_{\alpha\beta\gamma}(\mathbf{r}_1) - \frac{1}{105}\Phi^{(T)}_{\alpha\beta\gamma\delta}(1)F_{\alpha\beta\gamma\delta}(\mathbf{r}_1) + h.o. \tag{3.4}$$

where tensor notation is employed and

$$U^{pol}(1) \equiv \frac{1}{2}\alpha_{\alpha\beta}(1)F_\alpha(\mathbf{r}_1)F_\beta(\mathbf{r}_1) + \frac{1}{3}A_{\alpha,\beta\gamma}(1)F_\alpha(\mathbf{r}_1)F_{\beta\gamma}(\mathbf{r}_1) \tag{3.5}$$

is the work required to polarize the molecule. $\alpha_{\alpha\beta}$ and $A_{\gamma,\alpha\beta}$ are, respectively, polarizability and hyperpolarizability and are symmetric in α and β. Also, $A_{\gamma,\alpha\alpha} \equiv 0$.[78,79] Other terms in Eq. (3.4) are the electrostatic interaction energy between the resulting total multipole moments on the molecule 1 and the external electric field. $\mu^{(T)}_\alpha(1)$, $\Theta^{(T)}_{\alpha\beta}(1)$, $\Omega^{(T)}_{\alpha\beta\gamma}(1)$, and $\Phi^{(T)}_{\alpha\beta\gamma\delta}(1)$ are, respectively, the total electric dipole, quadrupole, octopole, and hexadecapole moments, of the molecule 1 expressed in a laboratory coordinate system $O - x_1x_2x_3$. (See Fig. 3.1.) In Eqs. (3.4) and (3.5),

$$
\begin{aligned}
F_{\alpha\beta}(\mathbf{r}_1) &\equiv \left.\frac{\partial F_\alpha}{\partial x_\beta}\right|_{\mathbf{r}=\mathbf{r}_1} \\
F_{\alpha\beta\gamma}(\mathbf{r}_1) &\equiv \left.\frac{\partial F_\alpha}{\partial x_\beta \partial x_\gamma}\right|_{\mathbf{r}=\mathbf{r}_1} \\
F_{\alpha\beta\gamma\delta}(\mathbf{r}_1) &\equiv \left.\frac{\partial F_\alpha}{\partial x_\beta \partial x_\gamma \partial x_\delta}\right|_{\mathbf{r}=\mathbf{r}_1}
\end{aligned} \tag{3.6}
$$

are the spatial gradients of $F_\alpha(\mathbf{r})$ evaluated at the center of the molecule 1. x_α is the α component of $\mathbf{r}$. When the electric field $F_\alpha(\mathbf{r})$ is due only to a point charge, *h.o.* in Eq. (3.4) represents the terms $O(R^{-6})$ or smaller, where R temporarily denotes the distance between the point charge and a molecule. In Appendix A, the total multipole moments are related to the polarizabilities and the permanent multipole moments.

In our study of ion-induced nucleation, we may decompose F_α into F_α^{ion} due to an ion and $F_\alpha^{(j)}$ due to total multipole moments on the molecule j. Thus

$$
U(1) = U^{pol}(1) + U^{ion}(1) + \sum_{j\neq 1} U^{mp}(1,j), \tag{3.7}
$$

where

$$
\begin{aligned}
U^{ion}(1) &= -\mu_\alpha^{(T)}(1) F_\alpha^{ion}(\mathbf{r}_1) - \frac{1}{3}\Theta_{\alpha\beta}^{(T)}(1) F_{\alpha\beta}^{ion}(\mathbf{r}_1) \\
&\quad -\frac{1}{15}\Omega_{\alpha\beta\gamma}^{(T)}(1) F_{\alpha\beta\gamma}^{ion}(\mathbf{r}_1) - \frac{1}{105}\Phi_{\alpha\beta\gamma\delta}^{(T)}(1) F_{\alpha\beta\gamma\delta}^{ion}(\mathbf{r}_1) + h.o.
\end{aligned} \tag{3.8}
$$

and

$$
\begin{aligned}
U^{mp}(1,2) &= -\mu_\alpha^{(T)}(1) F_\alpha^{(2)}(\mathbf{r}_1) - \frac{1}{3}\Theta_{\alpha\beta}^{(T)}(1) F_{\alpha\beta}^{(2)}(\mathbf{r}_1) \\
&\quad -\frac{1}{15}\Omega_{\alpha\beta\gamma}^{(T)}(1) F_{\alpha\beta\gamma}^{(2)}(\mathbf{r}_1) - \frac{1}{105}\Phi_{\alpha\beta\gamma\delta}^{(T)}(1) F_{\alpha\beta\gamma\delta}^{(2)}(\mathbf{r}_1) + h.o.
\end{aligned} \tag{3.9}
$$

Then, $U^{pol}(1) + U^{ion}(1)$ can be regarded as an external potential of the molecule 1 and $U^{mp}(1,2)$ can be identified with $\phi^{mp}(1,2)$. The explicit expression for $U^{mp}(1,2)$ is given in Appendix B with its derivation. In what follows, it is enough to note that $U^{mp}(1,2)$ is a sum of terms proportional to a product of a total multipole moment of the molecule 1 and that of the molecule 2 and is symmetric in 1 and 2.

It should be noted here that the separation implied by Eq. (3.7) is only formal at this

stage. In fact, neither $U^{pol}(1)$ nor $U^{ion}(1)$ is a one body potential since $F_\alpha(\mathbf{r}_1)$ and the total multipole moments at the molecule 1 depend on the electric field due to other molecules as well as on $F_\alpha^{ion}(\mathbf{r}_1)$.

3.2.2 Construction of the functional

Consider an open system, for which the grand potential Ω is the proper thermodynamic potential. In density functional theory, Ω of the system is given as a functional of order parameters such as the position-orientation distribution function $\rho(\mathbf{r}, \hat{R})$ defined by

$$\rho(\mathbf{r}, \hat{R}) \equiv \left\langle \sum_{j=1}^{N} \delta(\mathbf{r} - \mathbf{r}_j)\, \delta(\hat{R} - \hat{R}_j) \right\rangle. \tag{3.10}$$

Within the framework of mean field theory and under the local density approximation, Ω is given in terms of $\rho(\mathbf{r}, \hat{R})$ by[32,41]

$$\begin{aligned} \Omega[\rho] &= k_B T \int d1\, \rho(1) \left\{ \log \left[\Lambda^3 \rho(1) \right] - 1 \right\} + \int d\mathbf{r}_1\, f^{exc}(n(\mathbf{r}_1)) \\ &\quad - \int d1\, \rho(1)\, [\mu - v(1)] \\ &\quad + \frac{1}{2} \iint d1\, d2\, \rho(1)\, \rho(2) H(r_{12} - d) [\phi^{att}(r_{12}) + \phi^{mp}(1,2)], \end{aligned} \tag{3.11}$$

where k_B is the Boltzmann constant, T is temperature, Λ is de Broglie's thermal wavelength, and μ is the chemical potential of the system. $f^{exc}(n(\mathbf{r}))$ is the excess Helmholtz free energy per unit volume, arising from hard sphere exclusion, over the free energy density of an ideal gas. Employing the Carnahan-Starling equation,[70,71]

$$\begin{aligned} f^{exc}(n) &= k_B T n \frac{y(4-3y)}{(1-y)^2}, \\ y &\equiv (\pi/6)\, d^3\, n. \end{aligned} \tag{3.12}$$

H is the Heaviside step function approximating the hard-core exclusion between a pair of molecules.

In Eq. (3.11), $v(1)$ is an external field. We take an ion as a point charge q^{ion} placed at the center of a hard sphere of radius r^{ion}, which itself is fixed at the center of a molecular cluster. Then the ion-molecule interaction can be treated as an external potential $v(1)$, which is composed of the hard core repulsive potential and $U^{pol}(1) + U^{ion}(1)$. As shown in

Fig. 3.1, we take the origin of the coordinate system $O - x_1x_2x_3$ at the center of the ion, and choose the x_3-axis parallel to $\mathbf{r}_1$. Then

$$F_\alpha^{ion}(\mathbf{r}) = q^{ion}\,\frac{x_\alpha}{r^3}, \tag{3.13}$$

which is substituted into Eq. (3.8) to obtain

$$\begin{aligned} U^{ion}(1) &= q^{ion}\left\{-\frac{1}{{r_1}^2}\,\mu_3^{(T)}(1) + \frac{1}{{r_1}^3}\,\Theta_{33}^{(T)}(1) - \frac{1}{{r_1}^4}\,\Omega_{333}^{(T)}(1) + \frac{1}{{r_1}^5}\,\Phi_{3333}^{(T)}(1)\right\} \\ &\equiv q^{ion}u^T(1). \end{aligned} \tag{3.14}$$

We leave the detailed derivation of Eq. (3.14) to Appendix C.

3.2.3 Approximate formulae

The equilibrium distribution for $\rho(\mathbf{r}, \hat{R})$ is determined by the stationarity condition of the grand potential Ω:

$$\frac{\delta\Omega}{\delta\rho} = 0. \tag{3.15}$$

Because of the implicit dependence of $U^{pol}(1)$ and $U^{ion}(1)$ on $\rho(\mathbf{r}, \hat{R})$, the functional derivative in Eq. (3.15) cannot be readily performed. To circumvent this difficulty, we shall introduce further approximations.

In this work, a molecule is represented as a polarizable hard sphere of radius $d/2$ with attractive potential and permanent multipole moments grafted on it. Consider the electric field $F_\alpha(\mathbf{r})$ inside the molecule 1, fixed at $\mathbf{r}_1$, as a result of the ion and other molecules, which constitute charge distribution exterior to this hard sphere of radius $d/2$. Note that $F_\alpha(\mathbf{r})$ depends parametrically on r_1 which determines the boundary of the charge distribution. Because of the axial symmetry of the system around $\mathbf{r}_1$, $F_\alpha(\mathbf{r})$ is given in terms of some function f_1 as

$$F_\alpha(\mathbf{r}; r_1) = f_1(\theta; r_1)\,\frac{x_\alpha}{r^3}, \tag{3.16}$$

where θ is the angle between $\mathbf{r}$ and $\mathbf{r}_1$. In arriving at Eq. (3.16), we made use of the fact that $F_\alpha(\mathbf{r})$ is divergenceless inside the hard sphere. As an approximation, we ignore the θ

dependence of f_1 and denote it by $q^{eff}(r_1)$. Then,

$$F_\alpha(\mathbf{r}; r_1) = q^{eff}(r_1)\,\frac{x_\alpha}{r^3}, \tag{3.17}$$

which is the electric field we would have in the absence of any molecule as a result of a point charge $q^{eff}(r_1)$ at the origin. In other words, under the approximation we have introduced, the effect of the intermolecular interaction represented by $\phi^{mp}(1,2)$ is to simply re-scale the ion charge q^{ion} to $q^{eff}(r_1)$. Equation (3.17) gives the electric field produced by the ion and other molecules inside the hard sphere representing the molecule 1, in contrast to the electric displacement given by Eq. (3.13). Their ratio can be interpreted as a locally defined dielectric constant $\varepsilon(r_1)$:

$$\varepsilon(r_1) = \frac{q^{ion}}{q^{eff}(r_1)}. \tag{3.18}$$

Using the explicit form of $F_\alpha(\mathbf{r})$ given by Eq. (3.17), we may rewrite Eqs. (3.4) and (3.5) as

$$U(1) = U^{pol}(1) + q^{eff}(r_1)u^T(1) \tag{3.19}$$

and

$$\begin{aligned} U^{pol}(1) &= \frac{1}{2}\,q^{eff}(r_1)^2\left(\frac{1}{{r_1}^4}\,\alpha_{33}(1) - \frac{2}{{r_1}^5}\,A_{3,33}(1)\right) \\ &\equiv \frac{1}{2}\,q^{eff}(r_1)^2 u^{pol}(1), \end{aligned} \tag{3.20}$$

respectively. It should be noted here that the field gradients in Eqs. (3.4) and (3.5) are evaluated at the center of the molecule 1 for the fixed position of that molecule. Operationally, we take the spatial derivatives of the field $F_\alpha(\mathbf{r}; r_1)$ with respect to $\mathbf{r}$ for fixed $\mathbf{r}_1$ and evaluate them at $\mathbf{r}_1$. As mentioned in Sec. 3.2.1, the total multipole moments can be expressed in terms of the permanent multipole moments and the polarizabilities, thus we may rewrite $u^T(1)$ defined in Eq. (3.14) as

$$\begin{aligned} u^T(1) &= -q^{eff}(r_1)\,u^{pol}(1) \\ &\quad -\frac{1}{{r_1}^2}\,\mu_3^{(P)}(1) + \frac{1}{{r_1}^3}\,\Theta_{33}^{(P)}(1) - \frac{1}{{r_1}^4}\,\Omega_{333}^{(P)}(1) + \frac{1}{{r_1}^5}\,\Phi_{3333}^{(P)}(1) \\ &\equiv -q^{eff}(r_1)\,u^{pol}(1) + u^P(1). \end{aligned} \tag{3.21}$$

The detailed derivation of Eqs. (3.19)-(3.21) is given in Appendix C. We use the superscript (P) for the tensor components of the permanent multipole moments. Inspection of Eqs. (3.14), (3.20), and (3.21) reveals that $U^{pol}(1)$ and $U^{ion}(1)$ now depend only on r_1 and the orientation of the molecule 1. Thus, we have reduced the many body potential $U^{pol}(1)$ and $U^{ion}(1)$ to the corresponding effective one body potentials.

$q^{eff}(r)$ introduced above has yet to be determined. It is therefore natural to rewrite the functional for Ω so that $q^{eff}(r)$ serves as an order parameter. We first assume that $\rho(\mathbf{r}, \hat{R})$ is separable:

$$\rho(\mathbf{r}, \hat{R}) = n(\mathbf{r}) m(\mathbf{r}, \hat{R}) \tag{3.22}$$

where

$$n(\mathbf{r}) \equiv \left\langle \sum_{j=1}^{N} \delta(\mathbf{r} - \mathbf{r}_j) \right\rangle \tag{3.23}$$

is the particle number density distribution function and $m(\mathbf{r}, \hat{R})$ is the orientational distribution function at position $\mathbf{r}$. From Eqs. (3.10), (3.22), and (3.23), it follows that

$$n(\mathbf{r}) = \int d\hat{R}\, \rho(\mathbf{r}, \hat{R}) \tag{3.24}$$

and

$$\int d\hat{R}\, m(\mathbf{r}, \hat{R}) = 1. \tag{3.25}$$

When Eq. (3.22) is introduced, Eq. (3.11) becomes

$$\begin{aligned} \Omega[n, m] \;=\; & k_B T \int d1\, n(r_1) m(1) \log m(1) \\ & + \int d\mathbf{r}_1\, f^d(n(r_1)) - \int d1\, n(r_1) m(1) [\mu - v(1)] \\ & + \frac{1}{2} \iint d\mathbf{r}_1\, d\mathbf{r}_2\, n(r_1) n(r_2) H(r_{12} - d) \phi^{att}(r_{12}) \\ & + \frac{1}{2} \iint d1\, d2\, n(r_1) n(r_2) m(1) m(2) H(r_{12} - d) \phi^{mp}(1, 2), \end{aligned} \tag{3.26}$$

where $f^d(n)$ is the Helmholtz free energy density per unit volume of the hard sphere fluid, and is given by

$$f^d(n) = k_B T n \left[\log(\Lambda^3 n) - 1 \right] + f^{exc}(n). \tag{3.27}$$

Since $U(1)$ obtained in Eq. (3.19) is now a one body potential, we make an ansatz:

$$m(1) = \frac{1}{Z_R(r_1)} \exp\left\{-\frac{U(1)}{k_B T}\right\}, \tag{3.28}$$

which is the orientational distribution, in an external field $U(1)$, of a molecule that is otherwise isolated. $Z_R(r_1)$ is a normalization constant required by Eq. (3.25)

$$Z_R(r_1) = \int d\hat{R} \exp\left\{-\frac{U(1)}{k_B T}\right\}. \tag{3.29}$$

Equation (3.28) shows that we can introduce $U(1)$ as a new order parameter in place of $m(1)$. An alternative, yet physically more transparent, choice is $q^{eff}(r_1)$, which is related to the local dielectric constant $\varepsilon(r_1)$ through Eq. (3.18). For arbitrary functions $G_a(1)$ and $G_b(1,2)$, we define their angular averages by

$$\langle G_a(1)\rangle_{\hat{R}_1} \equiv \int d\hat{R}_1\, m(1)\, G_a(1) \tag{3.30}$$

and

$$\langle G_b(1,2)\rangle_{\hat{R}_1\hat{R}_2} \equiv \iint d\hat{R}_1\, d\hat{R}_2\, m(1)\, m(2)\, G_b(1,2), \tag{3.31}$$

respectively. Using Eqs. (3.14), (3.19), and (3.28), we rewrite Eq. (3.26) as follows:

$$\begin{aligned}
\Omega[n, q^{eff}] \;=\; & \int d\mathbf{r}_1\, f^d(n(r_1)) - \int d\mathbf{r}_1\, n(r_1)\,\{\,\mu + k_B T \log[\,Z_R(r_1)\,]\,\} \\
& + \int d\mathbf{r}_1\, n(r_1)\left[\, q^{ion} - q^{eff}(r_1)\,\right]\left\langle u^T(1)\right\rangle_{\hat{R}_1} \\
& + \frac{1}{2}\iint d\mathbf{r}_1\, d\mathbf{r}_2\, n(r_1) n(r_2) H(r_{12} - d)\phi^{att}(r_{12}) \\
& + \frac{1}{2}\iint d\mathbf{r}_1\, d\mathbf{r}_2\, n(r_1) n(r_2) H(r_{12} - d)\,\langle \phi^{mp}(1,2)\rangle_{\hat{R}_1\hat{R}_2}\,.
\end{aligned} \tag{3.32}$$

We have replaced $v(1)$ by $U^{pol}(1) + U^{ion}(1)$. The hard core repulsion of the ion imposes the boundary condition

$$n(r) = 0 \qquad (\text{if} \quad r < r^{ion} + \frac{d}{2}). \tag{3.33}$$

As before, the stationarity condition of Ω determines the equilibrium profile for $n(r)$ and

$q^{eff}(r)$:

$$\frac{\delta\Omega}{\delta n} = 0 \quad \text{and} \quad \frac{\delta\Omega}{\delta q^{eff}} = 0. \tag{3.34}$$

Noting that $q^{eff}(r_1)$ dependence of Ω is explicit in the third term of Eq. (3.32) and also implicit in $Z_R(r_1)$ and the angular averages indicated by $< \cdots >_{\hat{R}_1}$ and $< \cdots >_{\hat{R}_1\hat{R}_2}$, Eq. (3.34) becomes

$$\begin{aligned} 0 \;=\; & \mu^d(n(r_1)) - \{\,\mu + k_BT \log[\,Z_R(r_1)\,]\,\} \\ & + \Big[\, q^{ion} - q^{eff}(r_1) \,\Big] \Big\langle u^T(1) \Big\rangle_{\hat{R}_1} \\ & + \int d\mathbf{r}_2\, n(r_2) H(r_{12} - d) \phi^{att}(r_{12}) \\ & + \int d\mathbf{r}_2\, n(r_2) H(r_{12} - d) \left\langle \phi^{mp}(1,2) \right\rangle_{\hat{R}_1\hat{R}_2} \end{aligned} \tag{3.35}$$

and

$$\begin{aligned} 0 \;=\; & \Big[\, q^{eff}(r_1) - q^{ion} \,\Big] \left\{ \left[\Big\langle u^T(1)^2 \Big\rangle_{\hat{R}_1} - \Big\langle u^T(1) \Big\rangle^2_{\hat{R}_1} \right] + k_BT \Big\langle u^{pol}(1) \Big\rangle_{\hat{R}_1} \right\} \\ & - \int d\mathbf{r}_2\, n(r_2) H(r_{12} - d) \left\{ \left[\Big\langle \phi^{mp}(1,2) u^T(1) \Big\rangle_{\hat{R}_1\hat{R}_2} - \langle \phi^{mp}(1,2) \rangle_{\hat{R}_1\hat{R}_2} \Big\langle u^T(1) \Big\rangle_{\hat{R}_1} \right] \right. \\ & \left. - k_BT \left\langle \frac{\partial \phi^{mp}(1,2)}{\partial q^{eff}(r_1)} \right\rangle_{\hat{R}_1\hat{R}_2} \right\}, \end{aligned} \tag{3.36}$$

where $\mu^d(n) \equiv \partial f^d / \partial n$. The derivation of Eq. (3.36) is rather lengthy and is given in Appendix D.

Equations (3.32), (3.35), and (3.36) constitute the central result at this stage. Briefly, first we solve Eqs. (3.35) and (3.36) to obtain the equilibrium profiles of $n(r)$ and $q^{eff}(r)$ in $r > r^{ion} + \frac{d}{2}$. The obtained profiles are substituted into Eq. (3.32) to evaluate the grand potential of the system. As shown in Appendix E, some of the integrations indicated in these equations are analytically tractable, reducing the dimensionality of the integrals in Eq. (3.32) to at most four and those in Eqs. (3.35) and (3.36) to at most three.

3.2.4 Bulk properties

In the absence of the external field, the thermodynamic properties of a homogeneous system can be easily derived from Eq. (3.32). Let $q^{ion} = 0$, then Eq. (3.36) has a trivial solution of

$q^{eff}(r) = 0$. In fact, if $q^{eff}(r) = 0$, $U(1)$ given by Eq. (3.19) becomes zero and hence $m(1)$ is constant. Then the angular averages of the total multipole moments on the molecules 1 and 2 are all zero, for these angular averaged tensors are spherically symmetric as well as traceless. Since $\phi^{mp}(1,2)$ is a sum of the terms proportional to the total multipole moments of the molecules 1 and 2, the terms involving $\phi^{mp}(1,2)$ in Eq. (3.36) are zero and Eq. (3.36) is identically satisfied. This also means that under the mean field approximation employed in the present work, bulk properties of the system are, in the absence of the external field, the same as those of the system of molecules without polarizabilities or permanent multipole moments.

Setting $n(r)$ to a constant n in Eq. (3.32), we obtain the Helmholtz free energy density:

$$\begin{aligned} f(T,n) &= -p + \mu n \\ &= -k_B T n \log f_R + f^d(n) - \frac{1}{2}\alpha^{att} n^2. \end{aligned} \tag{3.37}$$

Note that $\Omega = -pV$ for a homogeneous system. f_R is the contribution from the free rotation of a molecule, the value of which is $8\pi^2$ in general and equals 4π for a linear molecule. α^{att} is defined here by

$$\begin{aligned} \alpha^{att} &\equiv -\frac{1}{V}\iint d\mathbf{r}_1\, d\mathbf{r}_2\, H(r_{12}-d)\,\phi^{att}(r_{12}) \\ &= -\int d\mathbf{r}_{12}\, H(r_{12}-d)\phi^{att}(r_{12}). \end{aligned} \tag{3.38}$$

For the particular choice of $\phi^{att}(r_{12})$ given by Eq. (3.3), one has

$$\alpha^{att} = \frac{4\pi}{3}\epsilon^{att} d^3. \tag{3.39}$$

Equation (3.37) is a fundamental equation of the isotropic system. Note that Eq. (3.37) is essentially the same as for the isotropic system of molecules without polarizability or permanent multipole moments. f_R merely affects the value of $f(T,n)$ at the standard state. From Eq. (3.37) by well known thermodynamic relations, one obtains

$$\mu(T,n) = -k_B T \log f_R + \mu^d(n) - \alpha^{att} n; \tag{3.40}$$

$$p(T,n) = n\mu^d(n) - f^d(T,n) - \frac{1}{2}\alpha^{att} n^2. \tag{3.41}$$

At a given temperature, the coexisting bulk densities are determined by

$$\begin{aligned} \mu_l(T, n_l^{eq}) &= \mu_v(T, n_v^{eq}); \\ p_l(T, n_l^{eq}) &= p_v(T, n_v^{eq}), \end{aligned} \tag{3.42}$$

where the subscripts l and v refer to liquid and vapor, respectively. The spinodal curve which divides the metastable and unstable regions in $T - n$ phase diagram is obtained by

$$\frac{\partial p}{\partial n} = 0. \tag{3.43}$$

The critical point is located in the phase diagram by Eq. (3.43) and

$$\frac{\partial^2 p}{\partial n^2} = 0, \tag{3.44}$$

with a numerical solution

$$\begin{aligned} y_c &= \frac{\pi}{6} d^3 n_c \\ &\approx 0.13044; \\ \frac{1}{k_B T_c} &\approx 2.6503 \left(\frac{1}{\epsilon^{att}} \right). \end{aligned} \tag{3.45}$$

3.3 Solution Methods for the Equilibrium Profiles

Given T/T_c and supersaturation S, defined as the ratio of the metastable vapor pressure to the equilibrium vapor pressure, we can calculate, via Eqs. (3.40)-(3.42), the chemical potential μ of the system and the densities of the bulk liquid n_l and vapor n_v at that chemical potential. For thus obtained μ and n_v, Eqs. (3.35) and (3.36) have to be solved simultaneously with the boundary conditions given by Eq. (3.33) and

$$n(r) \longrightarrow n_v \qquad \text{as} \qquad r \longrightarrow \infty. \tag{3.46}$$

Let $\delta n(r)$ and $\delta q^{eff}(r)$ be the deviations of $n(r)$ and $q^{eff}(r)$, respectively, from the exact solutions of Eqs. (3.35) and (3.36). Expanding $\Omega[n, q^{eff}]$ around the approximate profiles and ignoring the higher order, one finds that the error in Ω, which we denote by $\Delta\Omega$, due

to the deviations of $n(r)$ and $q^{eff}(r)$ from the exact solutions, satisfies

$$\begin{aligned} |\Delta\Omega| &\leq \int d\mathbf{r}_1 \left| \frac{\delta\Omega}{\delta n(r_1)} \delta n(r_1) \right| + \int d\mathbf{r}_1 \left| \frac{\delta\Omega}{\delta q^{eff}(r_1)} \delta q^{eff}(r_1) \right| \\ &\leq n_{max} \int d\mathbf{r}_1 \left| \frac{\delta\Omega}{\delta n(r_1)} \right| + \left| q^{ion} \right| \int d\mathbf{r}_1 \left| \frac{\delta\Omega}{\delta q^{eff}(r_1)} \right|, \end{aligned} \tag{3.47}$$

where $n_{max} = \sqrt{2}/d^3$ is the density at the closest packing. Note that the re-scaled charge $q^{eff}(r_1)$ never exceeds q^{ion}. We define

$$\begin{aligned} \Delta_n &\equiv n_{max} \int d\mathbf{r}_1 \left| \frac{\delta\Omega}{\delta n(r_1)} \right| \\ \Delta_q &\equiv \left| q^{ion} \right| \int d\mathbf{r}_1 \left| \frac{\delta\Omega}{\delta q^{eff}(r_1)} \right| \end{aligned} \tag{3.48}$$

and demand that both Δ_n and Δ_q be sufficiently small.

Under a condition that nucleation takes place, Eqs. (3.35) and (3.36) have two sets of solutions for $n(r)$ and $q^{eff}(r)$. One is for a metastable state exhibiting the vapor solvation of an ion and the other is for a critical nucleus, which corresponds to a saddle point in the functional space. The metastable profiles for $n(r)$ and $q^{eff}(r)$ are obtained by iteration. In particular, we start from the initial guess

$$q^{eff}(r) = q^{ion} \qquad \text{and} \qquad n(r) = n_v. \tag{3.49}$$

For this $n(r)$, we can solve Eq. (3.36) by iteration until Δ_q becomes sufficiently small. The resulting $q^{eff}(r)$ is used in Eq. (3.35), which is now iterated just once. Using $n(r)$ and $q^{eff}(r)$ thus obtained as the next guess, we repeat the same procedure until both Δ_n and Δ_q become sufficiently small. To obtain the critical nucleus by iteration, we take

$$q^{eff}(r) = q^{ion} \qquad \text{and} \qquad n(r) = \begin{cases} n_l & r \leq R \\ n_v & \text{otherwise} \end{cases} \tag{3.50}$$

as the initial guess and proceed in the same manner as for the metastable nucleus. If R is too small, the nucleus shrinks as the iteration proceeds, while it grows if R is too large. Starting from several values of R, it is possible to find R^* such that the nucleus neither shrinks nor grows as the iteration is repeated. In the actual computation, R^* was identified with that which yields, after some steps of iteration, $n(r)$ that minimizes Δ_n. Then, this

$n(r)$ was used with the corresponding $q^{eff}(r_1)$ as the initial guess in solving Eq. (3.35) more accurately by the Newton-Raphson method, after which the iterative solution of Eq. (3.36) follows. Using $n(r)$ and $q^{eff}(r)$ thus obtained as the next guess, we repeatedly applied the process until both Δ_n and Δ_q become sufficiently small. The grand potential Ω of a system was calculated from Eq. (3.32) for the obtained equilibrium profiles. The reversible work of nucleation $\Delta\Omega$, not to be confused with that in Eq. (3.47), was calculated as the difference of Ω for the critical nucleus and for the metastable nucleus.

Finally, the boundary of the system is taken to be a sphere, the radius r_0 of which is sufficiently large so that $n(r_0)$ and $q^{eff}(r_0)$ attain their limiting values n_v and q^{ion}/ε_v. Here ε_v is the dielectric constant of the bulk vapor of density n_v. There are two contributions to the free energy density at $r_1 < r_0$ resulting from the interaction across the system boundary at r_0. One is through $\phi^{att}(r_{12})$ and can be evaluated analytically. The other is through $\phi^{mp}(1,2)$, which was calculated numerically by noting that the contribution to the free energy density at r_1 comes from only those molecules in the spherical shell of $r_L < r < r_1 + d$, where r_L is the larger of $r^{ion} + \frac{d}{2}$ and $r_1 - d$. (See Appendix E.) The free energy density in $r_1 > r_0$ is determined by T, n_v, ε_v, and $|q^{ion}|$, being a constant which is same for the critical nucleus and for the metastable nucleus. This allows one to calculate the free energy difference between two systems which have the same T, n_v, ε_v, and $|q^{ion}|$ without introducing any truncation error.

3.4 Results and their Implications

In applying the above density functional theory to a particular substance, one needs to know its critical temperature T_c, the molecular diameter d, the polarizabilities, and the permanent multipole moments. The value of T_c is generally available[80] and d can be estimated from the molecular geometry. The values of the polarizabilities and the permanent multipole moments can be obtained from quantum mechanical calculations. The results are available for some materials, e.g., $(CH_3)_2O$, CH_3OH, CH_4, CS_2, and H_2O.[81–86] Among these, perhaps the most interesting case would be H_2O. However, any sensible treatment of water requires a proper account of hydrogen bonding and is not attempted in the current work. We have limited our application to ion-induced nucleation of CS_2, CH_4, and CCl_4. Except for CCl_4, these materials are rarely used in experiments, yet they are highly symmetric, thereby

Table 3.1: Material constants for CS_2 and CH_4 (Refs. 83,86) a_0 and e are Bohr radius and the electron charge, respectively. As indicated by the superscript (B), tensor components are expressed in body fixed coordinate system. Values of the other tensor components are readily deduced from those given here from the molecular symmetry. The C-Cl bond length is taken from Ref. 87, while the values of the critical temperature are taken from Ref. 80. b is defined in Eq. (3.54). The values of the polarizabilities and the permanent multipole moments for CCl_4 are estimated from the corresponding values for CH_4 as explained in Sec. IV-B.

	CS_2	CH_4	CCl_4
T_c	552 K	190.5 K	556.6 K
d	$\sim 5.868\,a_0$ (S-S distance)	$\sim 4.104\,a_0$ (2× C-H distance)	$\sim 6.654\,a_0$ (2× C-Cl distance)
b	97.62	404.4	85.40
μ	0	0	0
Θ	$\Theta_{33}^{(B)} = 2.425\,\lvert e\rvert {a_0}^2$	0	0
Ω	0	$\Omega_{123}^{(B)} = 2.410\,\lvert e\rvert {a_0}^3$	$\Omega_{123}^{(B)} = -10.98\,\lvert e\rvert {a_0}^3$
Φ	$\Phi_{3333}^{(B)} = 140.1\,\lvert e\rvert {a_0}^4$	$\Phi_{3333}^{(B)} = -7.690\,\lvert e\rvert {a_0}^4$	$\Phi_{3333}^{(B)} = 58.07\,\lvert e\rvert {a_0}^4$
α	$\alpha_{11}^{(B)} = \alpha_{22}^{(B)} = 36.58\,{a_0}^3$ $\alpha_{33}^{(B)} = 93.14\,{a_0}^3$	$\alpha_{33}^{(B)} = 15.98\,{a_0}^3$	$\alpha_{33}^{(B)} = 72.80\,{a_0}^3$
A	0	$A_{1,23}^{(B)} = 9.46\,{a_0}^4$	$A_{1,23}^{(B)} = 71.44\,{a_0}^4$

reducing the computational work, while still serving to illustrate some of the essential features of ion-induced nucleation. The values of the molecular parameters used in this work are given in Table 3.1.

We non-dimensionalized relevant quantities by model parameters: d as the length scale, $k_B T_c$ as the energy scale, and $|e|$ for electric charge, where e is the electron charge. Non-dimensionalized quantities are denoted by $\tilde{}$ (tilde).

3.4.1 CS_2

Figure 3.2 shows the density profile $n(r)$ of CS_2 obtained at $\widetilde{T}$=0.55 and supersaturation $S = 2$. As mentioned in Sec. 3.3, a metastable profile shows solvation of the ion. Volume exclusion due to the ion surface, which is regarded as a hard wall, is apparent outside the first coordination shell. The general feature of particular interest is that near the ion surface, the number density $n(r)$ is higher when $q^{ion} < 0$ both for the metastable and for the critical nucleus than when $q^{ion} > 0$. This indicates that the ion-molecule interaction

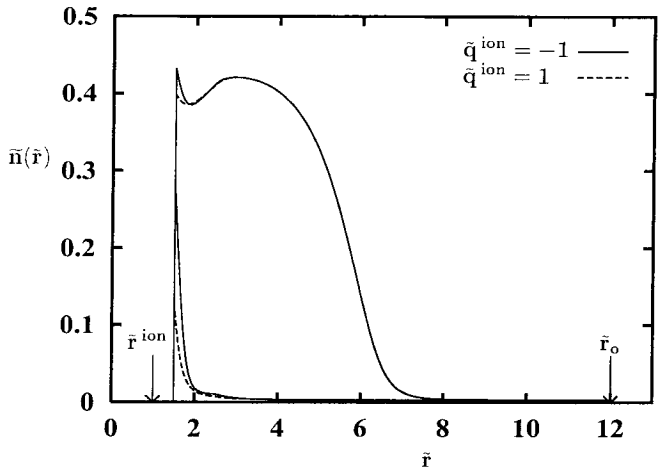

Figure 3.2: Equilibrium density profiles of CS_2 at $\widetilde{T}$= 0.55 and $S = 2$. For each value of $\tilde{q}^{ion}$, the lower profile corresponds to the metastable nuclei, while the upper profile represents the critical nuclei.

is stronger if $q^{ion} < 0$, implying some sort of asymmetry in the interaction. To see this more explicitly, consider the bare ion-molecule interaction energy $U^b(1)$, which is obtained by setting $q^{eff}(r_1) = q^{ion}$ in Eqs. (3.19)-(3.21):

$$U^b(1) = -\frac{1}{2} q^{ion^2} u^{pol}(1) + q^{ion} u^P(1). \tag{3.51}$$

Since CS_2 is a linear centro-symmetric molecule, $U^b(1)$ depends only on the ion-molecule separation r_1 and the angle θ_1 between the radial direction $\mathbf{r}_1$ and C-S bond. We plotted $U^b(1)$ in Fig. 3.3 as a function of $|\cos\theta_1|$ at $r_1 = 1.5d$, namely at the minimum ion-molecule separation when $r^{ion} = d$. The sign dependence of $U^b(1)$ shown in Fig. 3.3 can be readily understood as follows. As shown in Fig. 3.4, the first term in Eq. (3.51) is minimum when the C-S bond lines up with the electric field due to q^{ion}, irrespective of its sign, while the second term yields the minimum value at the angle which changes from $|\cos\theta_1| = 1$ to $\cos\theta_1 \approx 0.45$ as q^{ion} changes its sign from negative to positive. Stated differently, when $q^{ion} < 0$, the polarizabilities and the permanent multipole moments work constructively to orient the molecule along the direction of the electric field while they work rather destructively if $q^{ion} > 0$.

The sign dependence of $U^b(1)$ is present for a molecule even with only a single permanent

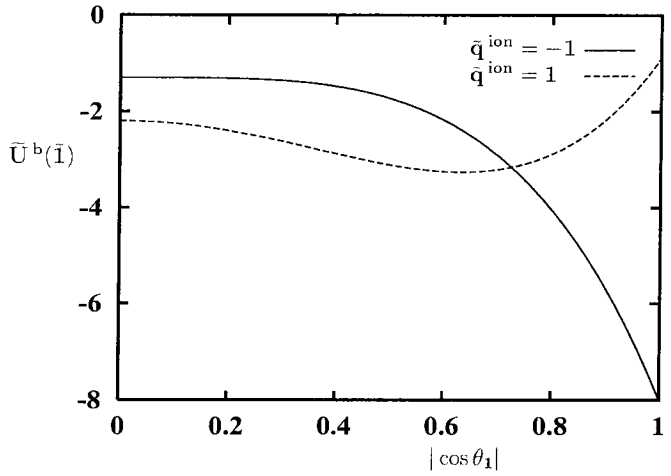

Figure 3.3: The bare ion-molecule interaction potential $\widetilde{U}^b(\widetilde{1})$ for CS_2 at $\widetilde{r}_1 = 1.5$ and $|\widetilde{q}^{ion}|$=1.

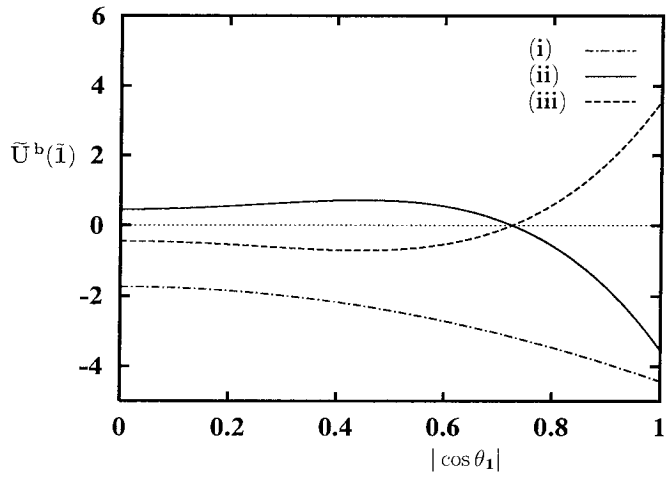

Figure 3.4: Contributions for $\widetilde{U}^b(\widetilde{1})$ from (i) the polarizabilities $(-\frac{1}{2}\, q^{ion^2} u^{pol}(1)/k_B T_c)$ and the permanent multipole moments $(q^{ion} u^P(1)/k_B T_c)$ with (ii) $\widetilde{q}^{ion} = -1$ and (iii) $\widetilde{q}^{ion} = 1$.

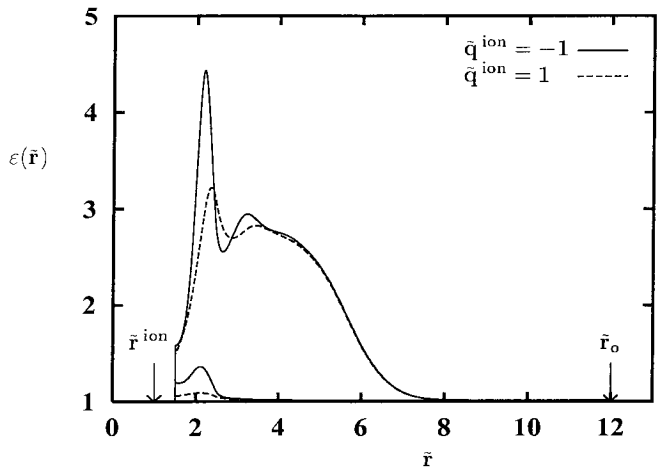

Figure 3.5: Variation of the local dielectric constant $\varepsilon(\widetilde{r})$ corresponding to the density profile $\widetilde{n}(\widetilde{r})$ given in Fig. 3.2. For each value of $\widetilde{q}^{ion}$, the lower profile corresponds to the metastable nuclei, while the upper profile represents the critical nuclei.

multipole moment, higher than the dipole, without polarizabilities. Thus in the case of a linear centro-symmetric molecule, the interaction energy between the ion (point charge) and the quadrupole moment of the molecule depends quadratically on $\cos\theta_1$, attaining the minimum value at $\cos\theta_1 = 0$ for one sign of the ion charge which is, in general, different from what is obtained at $\cos\theta_1 = \pm 1$ as the minimum for the other sign of the ion charge. Such possibility of producing the sign effect from a single permanent multipole moment is not pursued here, for the contribution to $U^b(1)$ from each one of the permanent multipole moments or the polarizabilities is comparable to each other at least for those molecules close to the ion.

The sign dependence of $U^b(1)$ is counteracted to some extent by the dielectric response of the condensing molecules. Figure 3.5 shows the variation of the local dielectric constant $\varepsilon(r)$ corresponding to the density profile $n(r)$ shown in Fig. 3.2. For a given value of r, a profile with a smaller value of $\varepsilon(r)$ applies for the metastable nucleus while the larger corresponds to the critical nucleus. Clearly, the effective electric field around the ion is weaker when $q^{ion} < 0$ compared to the case of $q^{ion} > 0$. Recall the definition of $\varepsilon(r)$ given in Eq. (3.18).

Density profiles of CS_2 in the case of $\widetilde{q}^{ion} = -1$ are shown in Fig. 3.6 at $\widetilde{T} = 0.55$ for

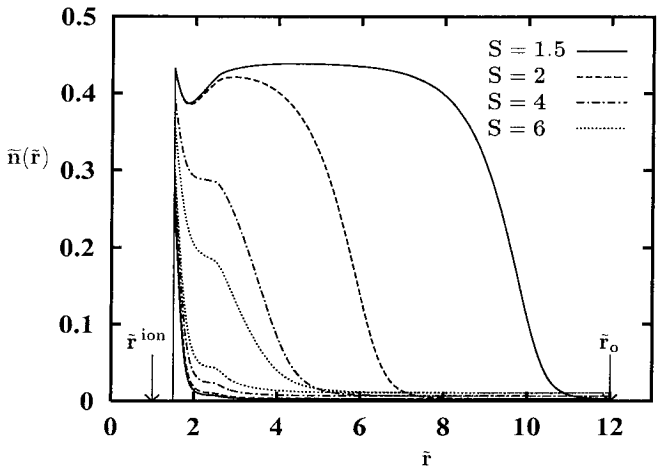

Figure 3.6: Variation in the density profiles $\widetilde{n}(\widetilde{r})$ of CS_2 with the Supersaturation S. $\widetilde{T}$= 0.55 and $\widetilde{q}^{ion} = -1$.

several values of the supersaturation. Figure 3.6 shows a similar feature to that observed in our previous work on ion-induced nucleation of a dipolar fluid.[41] Namely, a metastable nucleus grows as S increases, while the critical nucleus shrinks. These two profiles eventually coincide at a certain supersaturation $S < S_{max}$, where S_{max} is the supersaturation at the spinodal, indicating the onset of instability of the vapor phase in the presence of the ion. These trends can be explained by a completely parallel argument to that given previously[41] and will not be repeated here.

Figure 3.7 shows the local dielectric constant profile $\varepsilon(r)$ under the same condition as for the Fig. 3.6. Comparing Fig. 3.2 with Fig. 3.5 and Fig. 3.6 with Fig. 3.7, one finds that $\varepsilon(r)$ at r is roughly proportional to the local density $n(r)$ at that point. A remarkable exception is the sharp peak in $\varepsilon(r)$ near the ion surface and the oscillation following the peak; the latter is particularly clear for a large nucleus. To understand this behavior, we obtained $\varepsilon(r)$ at $\widetilde{T}$= 0.55 corresponding to a simpler density profile $n(r) = n_{max}$. Figure 3.8 shows that the sharp peak followed by the oscillation persists even if $n(r)$ is constant throughout. As shown in Appendix E, only those molecules in the spherical shell $r_L < r < r_1 + d$ contribute to the dielectric constant $\varepsilon(r_1)$ at r_1. In the present case of uniform density, the number of molecules $N_\varepsilon(r_1)$ in this spherical shell is proportional to the volume of the shell and a monotonically increasing function of r_1. On the other hand, as shown in Appendix E, contributions to the integral in Eq. (3.36) tend to cancel and the average total multipole

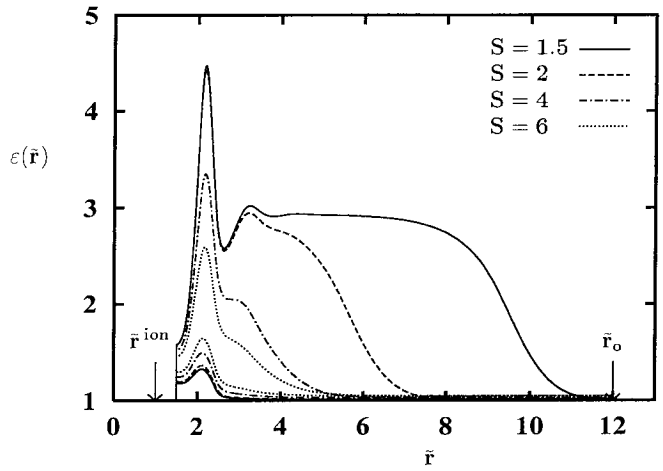

Figure 3.7: Local dielectric constants $\varepsilon(\tilde{r})$ corresponding to the density profiles shown in Fig. 3.6.

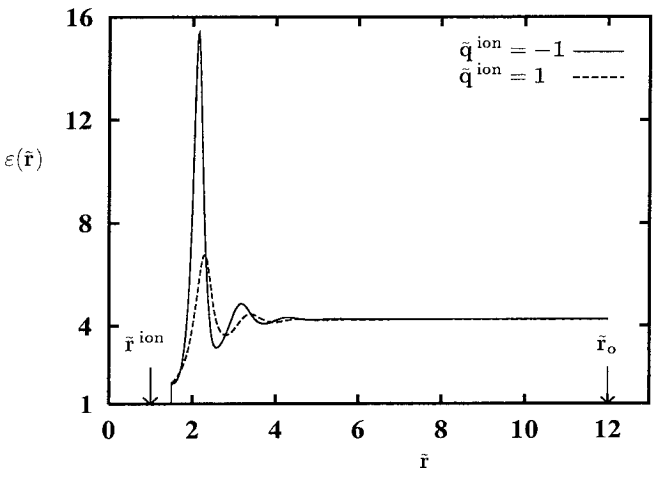

Figure 3.8: Local dielectric constants $\varepsilon(\tilde{r})$ at $\widetilde{T}$= 0.55 corresponding to the density profile $n(r) = n_{max}$.

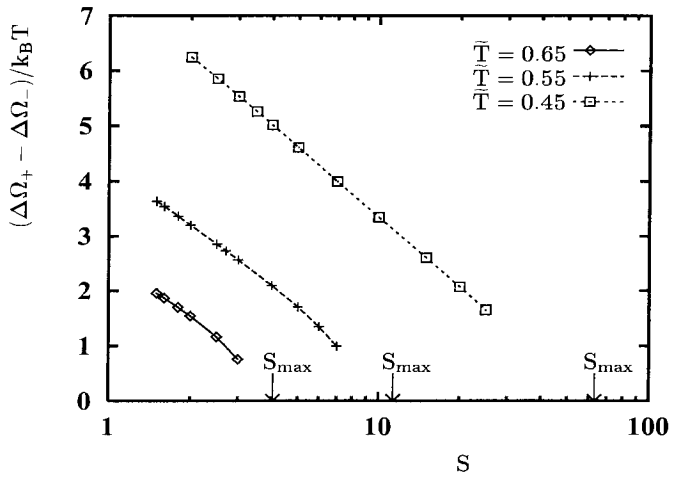

Figure 3.9: The difference in the reversible work of nucleation of CS_2 between the cases of $\widetilde{q}^{ion} = 1$ and $\widetilde{q}^{ion} = -1$. $\widetilde{r}^{ion} = 1$. Three values of S_{max} represent the supersaturation at the spinodal. From the left, they correspond to $\widetilde{T}$= 0.65, $\widetilde{T}$= 0.55, and $\widetilde{T}$= 0.45, respectively.

moments on a molecule decrease as r_1 is increased, both of which reduce the magnitude of the integral in Eq. (3.36). At the $r_1 \longrightarrow \infty$ limit, the increase in $N_\varepsilon(r_1)$ balances exactly the decrease in the magnitude of the integral to yield the constant value of $\varepsilon(\infty)$. However, when $r_1 < r^{ion} + \frac{3}{2}d$, the increase in $N_\varepsilon(r_1)$ is due partially to the increase in the spherical shell thickness, which leads to the steep increase in $\varepsilon(r_1)$ in this range of r_1. Now, the existence of a peak implies that there must be a competing factor with this steep increase in $\varepsilon(r_1)$. To see how this happens, first recall that $\varepsilon(r_1)$ is essentially the reciprocal of the effective electric field due to q^{ion} and other molecules in $r_L < r_2 < r_1 + d$, the field by the latter being in the opposite direction to the former. When $\varepsilon(r_2)$ is larger, the electric field at r_1 created by those molecules in this region is smaller, causing the decrease in $\varepsilon(r_1)$. A peak in $\varepsilon(r)$ near the ion arises as a result of these two competing factors. The same mechanism is responsible for the oscillation of $\varepsilon(r)$ mentioned above.

Figure 3.9 shows the difference between the reversible work $\Delta\Omega_+/k_BT$ of nucleation of CS_2 on a positive ion and that $(\Delta\Omega_-/k_BT)$ on a negative ion. Calculations were performed close to but below the supersaturation at which the metastable nucleus reaches its stability limit. For both cases, this happens at $S < S_{max}$, but first for the case of $q^{ion} < 0$ as the result of the preference to the negative ion shown by $U^b(1)$. Strictly speaking, one has to

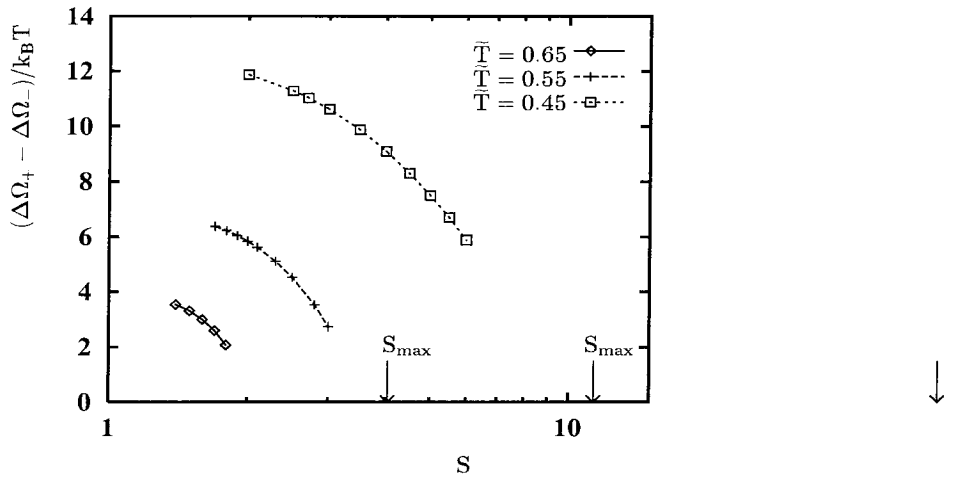

Figure 3.10: Same as Fig. 3.9, but for CH_4. S_{max} for $\widetilde{T}$= 0.45 is not shown in the figure.

take into account the effect of the dielectric response of the condensing molecules. In all of our calculations for CS_2, however, we found that the quantities defined as

$$\begin{aligned} \Delta\Omega^{critical} &\equiv \Omega_+^{critical} - \Omega_-^{critical} \\ \Delta\Omega^{metastable} &\equiv \Omega_+^{metastable} - \Omega_-^{metastable} \end{aligned} \tag{3.52}$$

were both positive, being consistent with the sign preference of $U^b(1)$. Here $\Omega^{critical}$ and $\Omega^{metastable}$, respectively, denote the grand potential of a system with a critical nucleus and a metastable nucleus. We see that the observed sign preference of the reversible work is also consistent with that shown by $U^b(1)$. As we shall see below, however, the latter is not always the case. A similar monotonic decrease in $\Delta\Omega_+ - \Delta\Omega_-$ with increasing S is observed to that found previously for dipolar molecules.[41]

3.4.2 CH_4 and CCl_4

Figure 3.10 shows the sign preference in the case of CH_4. A similar trend is found to the case of CS_2. In Fig. 3.11, we show the sign preference of the reversible work for CH_4 and CCl_4. In both calculations, $\widetilde{T}$= 0.55 and r^{ion} is set equal to the diameter of a CH_4 molecule.

The calculation for CCl_4 is only qualitative. Since not all of the required molecular parameters are available for this molecule, we estimated them from the corresponding values

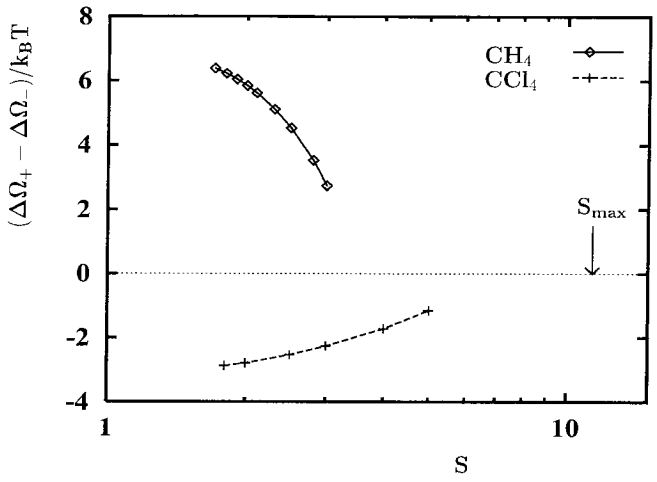

Figure 3.11: The sign preference in the reversible work of nucleation of CH_4, and CCl_4 at $\widetilde{T}$= 0.55. r^{ion} is chosen to be the same as the diameter of a CH_4 molecule.

for CH_4. We simply assumed that the polarizabilities and the permanent multipole moments scale with proper powers of the molecular size and that the permanent multipole moments have a sign opposite to those of CH_4. The latter assumption follows from the relative electronegativites:[87] Cl > C > H.

Here again, calculations are made close to but below the supersaturation at which a metastable nucleus becomes unstable. From Fig. 3.11, it is observed that the ion is more effective for CH_4 both in reducing the nucleation barrier and in producing the sign preference. When non-dimensionalized, $U^b(1)$ scales with a dimensionless quantity b:

$$\widetilde{U}(\widetilde{1}) \equiv \frac{U^b(1)}{k_B T_c} \sim b, \tag{3.53}$$

where

$$b \equiv \frac{e^2}{dk_B T_c}. \tag{3.54}$$

A larger value of b implies a stronger ion-molecule interaction and hence a larger reduction in the nucleation barrier. In general, the asymmetry in the ion-molecule interaction is still buried in the dimensionless $\widetilde{U}^b(\widetilde{1})/b$, the magnitude of b dictating the sensitivity of the system to this asymmetry. In the present case where the polarizabilities and the permanent multipole moments are estimated as above, $\widetilde{U}^b(\widetilde{1})$ for CCl_4 differs from that for CH_4 only

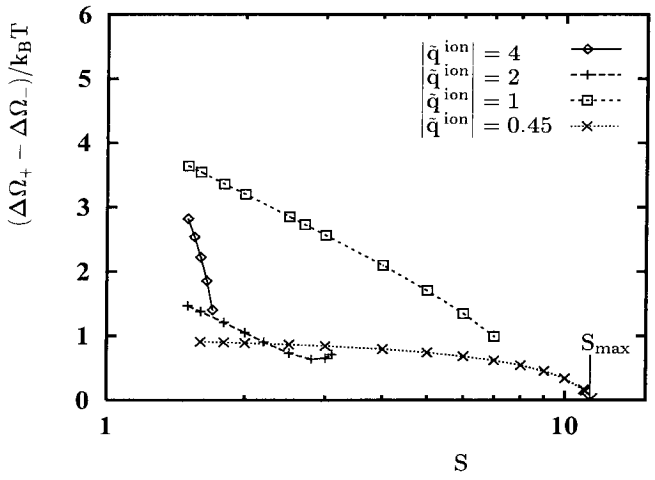

Figure 3.12: Effect of $|q^{ion}|$ on the sign preference in the reversible work of nucleation of CS_2 at $\widetilde{T}$= 0.55. $\widetilde{r}^{ion}$=1.

by the value of b. Results shown in Fig. 3.11 are consistent with the values of b given in Table. 3.1. Also, Fig. 3.11 shows that the reversal of the sign of the permanent multipole moments results in reversing the sign preference, as one can see from Eq. (3.51). It should be noted here that the difference in electronegativity between Cl and C ($\sim$ 0.5) is larger than that between C and H ($\sim$ 0.4).[87] Thus, our prediction on the sign preference for CCl_4 is considered to be a lower bound to a true value.

3.4.3 Effect of r^{ion} and q^{ion}

In the foregoing, we have shown that the sign preference in the reversible work of nucleation arises from the asymmetric nature in the ion-molecule interaction. One can change the strength of this interaction by changing either q^{ion} or r^{ion}. Figure 3.12 shows the effect of $|q^{ion}|$ on the sign preference in ion-induced nucleation of CS_2, while Fig. 3.13 shows the effect of r^{ion}. From Figs. 3.12 and 3.13, we see that the metastable nucleus reaches its stability limit faster as the electric displacement due to the ion becomes stronger. This follows from the fact that for a given value of the supersaturation S, the metastable nucleus becomes larger with increasing ion-molecular interaction, while the critical nucleus shrinks. However, Figs. 3.12 and 3.13 show that increasing the ion-molecule interaction does not necessarily increase the sign preference, for when this interaction is increased, so

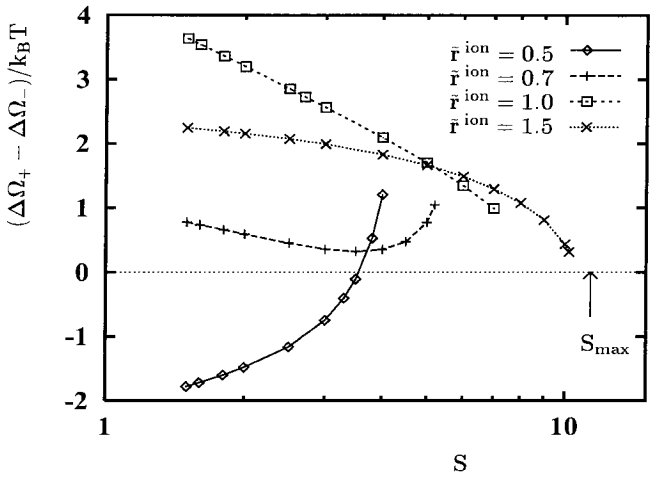

Figure 3.13: Effect of r^{ion} on the sign preference in the reversible work of nucleation of CS_2 at $\widetilde{T}$= 0.55. $|\tilde{q}^{ion}|$=1

is the dielectric response of the condensing fluid. In this strong ion-molecule interaction regime, however, contributions from hyperpolarizabilities neglected in Eq. (3.4) may become significant,[76] since the interaction energy between the ion and these hyperpolarizabilities scales with some power of q^{ion} higher than unity.[78,79] A change in q^{ion} affects the ion-molecule interaction $U^b(1)$ rather uniformly for all the molecules within the whole system, while changing r^{ion} alters the relative importance of the terms in $U^b(1)$ mainly for those molecules close to the ion. This explains the qualitative difference between Fig. 3.12 and Fig. 3.13.

A rather striking feature to be observed in Fig. 3.13 is the reversal in the sign preference that occurs at lower supersaturation with $r^{ion} = 0.5d$. To see its implication, first rewrite the sign preference $\Delta\Omega_+ - \Delta\Omega_-$ as follows:

$$\begin{aligned}
\Delta\Omega_+ - \Delta\Omega_- &= (\Omega_+^{critical} - \Omega_+^{metastable}) - (\Omega_-^{critical} - \Omega_-^{metastable}) \\
&= (\Omega_+^{critical} - \Omega_-^{critical}) - (\Omega_+^{metastable} - \Omega_-^{metastable}) \\
&= \Delta\Omega^{critical} - \Delta\Omega^{metastable}. \qquad (3.55)
\end{aligned}$$

We show each term in Eq. (3.55) separately in Fig. 3.14, which indicates that both $\Delta\Omega^{critical}$ and $\Delta\Omega^{metastable}$, in fact, preserve the sign preference that is indicated by $U^b(1)$. However,

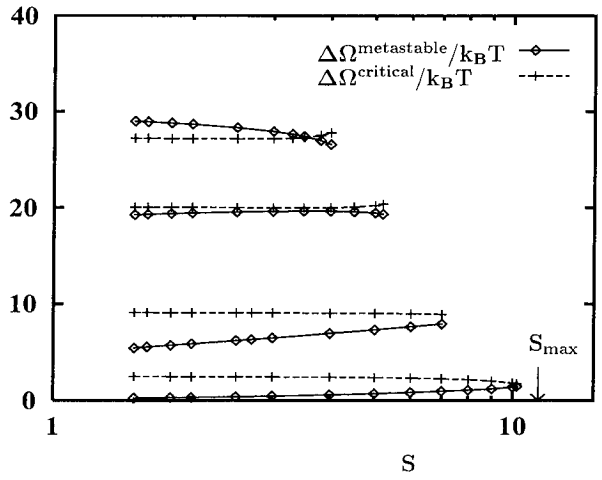

Figure 3.14: Variations of $\Delta\Omega^{critical}/k_BT$ and $\Delta\Omega^{metastable}/k_BT$ with supersaturation S for various values of r^{ion}. From the top, they correspond to the case of $\widetilde{r}^{\,ion} = 0.5$, $\widetilde{r}^{\,ion} = 0.7$, $\widetilde{r}^{\,ion} = 1.0$, and $\widetilde{r}^{\,ion} = 1.5$, respectively. $\widetilde{T}$= 0.55 and $|\widetilde{q}^{\,ion}|$=1

when the ion-molecule interaction is increased near the ion as a result of decreasing r^{ion}, it is counteracted by the dielectric response of the condensing fluid in this region. The effect is more significant for clusters with higher density, namely for critical nuclei at lower supersaturation, thereby causing $\Delta\Omega^{critical}$ to become smaller than $\Delta\Omega^{metastable}$.

In all calculations the sign preference toward a negative ion was recovered as the stability limit is approached. This is only obvious, for

$$\Delta\Omega_+ - \Delta\Omega_- \sim \Delta\Omega_+ > 0 \tag{3.56}$$

in this limit as long as the sign preference in the sense mentioned above Eq. (3.52) is preserved. One can also alter the sign preference in the reversible work by choosing a different value of q^{ion} or r^{ion} for a positive ion from that of a negative ion. In this respect, it is important to actually identify the ion involved in experiments on ion-induced nucleation. We note recent progress in this direction reported by Kane *et al.*[44]

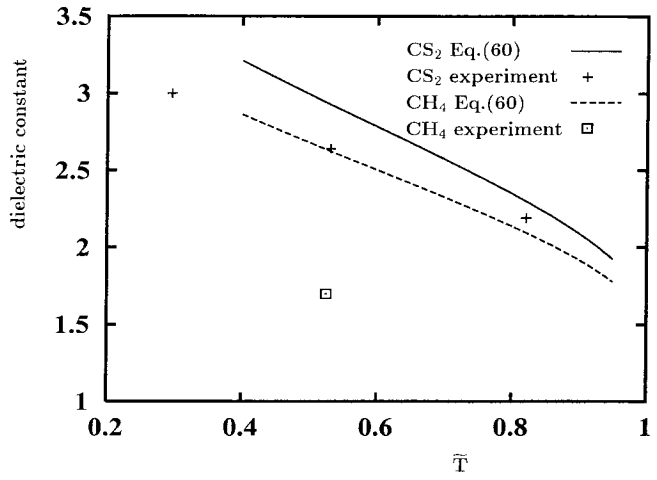

Figure 3.15: Comparison of the values of dielectric constant of bulk liquid obtained from the present theory (Eq. (3.60)) and experiments.

3.4.4 The validity of the model representation

To evaluate the validity of the current model representation of a molecule, we calculated the dielectric constant ε_l of the bulk liquid phase. The intensive state of the liquid is chosen to be the one at vapor-liquid coexistence. When the density profile

$$n(r) \longrightarrow n_l \qquad \text{as} \qquad r \longrightarrow \infty \tag{3.57}$$

is substituted, Eqs. (3.18) and (3.36) yields a solution with a limiting behavior

$$\varepsilon(r) \longrightarrow \varepsilon_l \qquad \text{as} \qquad r \longrightarrow \infty. \tag{3.58}$$

We can obtain this ε_l by solving Eq. (3.36) numerically and setting

$$\varepsilon_l \approx \varepsilon(r_0). \tag{3.59}$$

Alternatively, we may ignore the higher permanent multipole moments and hyperpolarizability to find that

$$\varepsilon_l = 1 + \frac{16\pi\mu_\alpha^{(P)}\mu_\alpha^{(P)}}{9k_BT} n_l \qquad \text{(polar-nonpolarizable molecule)}$$

$$\varepsilon_l = 1 + \frac{8\pi\alpha_{\alpha\alpha}}{9} n_l \qquad \text{(nonpolar-polarizable molecule)} \qquad (3.60)$$

Calculated values of ε_l are compared in Fig. 3.15 against the experimental values obtained at 1 atm.[80] In the case of CS_2, the predicted values of ε_l agree well with the data, though the disagreement is quite large ($\sim$ 130 %) for CH_4. In light of the approximations involved in our model representation, the agreement is noteworthy and the model captures many of the most important characteristics of intermolecular or ion-molecule interactions.

3.5 Summary and Conclusions

In this paper, we have shown that the sign preference in ion-induced nucleation can be explained in terms of the asymmetric nature of the ion-molecule interaction. Consistent treatment of such molecular characteristics is achieved by means of a statistical mechanical density functional theory. Within the framework of a mean field theory, the grand potential is obtained in terms of two order parameters, the particle number density $n(r)$ and the re-scaled ion charge $q^{eff}(r)$, the latter taking account of the dielectric response of the condensing molecules. When the intensive state of the supersaturated vapor is specified, the stationarity condition of the grand potential uniquely determines a critical nucleus and a metastable nucleus for given values of model parameters.

All the molecular parameters used in the present work, if not already available, can be obtained from quantum mechanical calculations. Although the current theory is applicable for both polar and non-polar materials, we have confined our application of the theory to ion-induced nucleation of CS_2 and CH_4, for which the required molecular parameters are readily accessible.[83,86] When the electric displacement due to an ion is sufficiently weak, the calculated reversible work shows a preference consistent with that of the bare ion-molecule interaction potential. In particular, a preference is exhibited toward a negative ion, influencing the nucleation rate by factors of 10 to 10^2 for CS_2 and 10 to 10^5 for CH_4. The predicted sign preference decreases with increasing supersaturation. Qualitative prediction of the ion-induced nucleation of CCl_4 reveals that this substance should exhibit a preference toward positive ions, in agreement with existing data.[60] Qualitatively different behavior was observed for the predicted sign preference when the electric displacement due to an ion is increased.

Our theory at this stage is at best semi-quantitative both in the model representation and in the theoretical treatment. First, we placed polarizabilities and permanent multipole moments at the center of a spherical molecule. Such representation, however, is valid only when the ion-molecule or intermolecular separation is large in comparison to the molecular dimension. To some extent, one could relax this limitation by distributing the polarizabilities and the multipole moments among various sites in a molecule.[88–90] Part of the molecular symmetry is captured in our model through the tensors representing polarizabilities and permanent multipole moments. However, actual molecular shape is yet another important factor in determining the packing structure of molecules around the ion. Proper account of this effect requires an intermolecular potential with an anisotropic repulsive part.

Secondly, we have characterized an ion by its charge and radius, and the ion-molecule interaction is assumed to be purely electrostatic along with the hard core repulsion at the ion surface. It was shown by Spears[76] that as long as chemical bonding is negligible, the ion-molecule interaction can indeed be quantitatively treated by an electrostatic model, while the details of the repulsive interaction and the polarizability of the ion were also shown to be important. On the other hand, one would not expect the present theory to be applicable to a system where the chemical nature of the interaction between the ion and molecules plays an important role.[77] Further complication arises since ions present in the experiments are often complex molecules such as $H^+(H_2O)_n$ rather than simply ionized atoms. Then, the ion itself must be treated by means of statistical mechanics. Also, we avoided the explicit consideration of the fluctuation of an ion within the nucleus by taking the position of the point charge as the origin. It is expected that at least part of this contribution to the free energy cancels out when taking the difference between two states in obtaining the reversible work. In a more accurate model representation, one would have to treat the system as a binary in which the ion is the second component at extremely low concentration.

Finally, a better treatment of the pair-correlation function than that in a mean field theory, along with the above mentioned model representation of a molecule, will undoubtedly give a better description of the fluid structure within the cluster. Thus the density profile near the ion will exhibit oscillations resembling that near a hard wall, which can either enhance or reduce the oscillatory behavior in the local dielectric constant near the ion. Spontaneous polarization may be observed at the interface as a result of the inhomogeneity in density. Nevertheless, it is clear that some of the most important characteristics

of ion-induced nucleation have been captured in the present theory, which forms a basis for explaining this well known phenomenon that has hitherto remained inexplicable within the classical framework.

Acknowledgments[42]

This work was supported by National Science Foundation grant ATM-9307603.

Chapter 4 Direct Evaluation of the Equilibrium Distribution of Physical Clusters by a Grand Canonical Monte Carlo Simulation

A new approach to cluster simulation is developed in the context of nucleation theory. This approach is free of any arbitrariness involved in the definition of a cluster. Instead, it preferentially and automatically generates the physical clusters, defined as the density fluctuations that lead to nucleation, and determines their equilibrium distribution in a single simulation, thereby completely bypassing the computationally expensive free energy evaluation that is necessary in a conventional approach. The validity of the method is demonstrated for a single component system using a model potential for water under several values of supersaturation.

4.1 Introduction

When a vapor is brought to supersaturation, relaxation occurs toward the more stable liquid phase. The initial stage of this phase transition is the formation of a critical nucleus as a result of spontaneous density fluctuations in the metastable vapor phase. Since not all of the density fluctuations lead to nucleation, Reiss *et al.*[48–53] posed a question regarding how to identify a physical cluster, which is defined as a density fluctuation that participates in the nucleation event. Moreover, if nucleation theory is to be formulated in terms of a cluster, as in the classical theory,[1] its precise characterization is the prerequisite of the theory. One of the quantities of central importance to nucleation theory is the equilibrium cluster size distribution, the average number of clusters of different sizes per unit volume. Once the distribution is determined, a rate theory can then describe the event of nucleation,[1] such as its transient or steady state behavior. Since the number density of a given cluster is related to the reversible work to form this cluster in the vapor phase, a cluster simulation in the context of nucleation usually focuses on evaluating the free energy of the clusters.

A cluster simulation is commonly realized by confining a fixed number of molecules, say i, in a spherical container of volume v concentric with the center of mass of i molecules. To the

extent that these i molecules actually form a cluster and that its thermodynamic properties are nearly independent of v over a wide range of v, Lee *et al.*[91] characterized the cluster by its size i alone. We refer to this cluster as the LBA cluster. In an attempt to identify a physical cluster, Reiss *et al.*[48–53] characterized the cluster by both i and v. The latter is related to the distance from the cluster's center of mass to the nearest ideal gas molecule, which serves as an index to organize the counting procedure in enumerating the configurational space of the entire vapor phase that is regarded as an ideal gas mixture of monomers and clusters of various sizes. As they have pointed out,[48–52] however, the identification of a physical cluster has to reflect the dynamics of the nucleation process. Thus, in their approach, it is the rate theory[52] that determines whether a particular i/v cluster participates in the nucleation event. Insofar as the cluster size distribution is obtained indirectly from the free energy, which in turn is evaluated through thermodynamic integration,[47] the simulation has to be carried out at many values of temperature for each cluster size i or each pair of values of i and v in the case of the i/v cluster. For this reason, the i/v-cluster was also studied by computationally less demanding density functional theory.[92]

In this work, we present a new approach to the problem which directly implements the stochastic evolution of a physical cluster in the form of a grand canonical Monte Carlo simulation.[47] Our approach is conceptually simpler than the i/v cluster and offers several attractive features. The simulation preferentially generates the physical clusters during the course of the simulation without any prior knowledge regarding the details of their identity. Their equilibrium distribution is, at least in principle, directly determined from a single simulation, which permits one to completely bypass the expensive free energy evaluation. The grand canonical Monte Carlo simulation presents an additional advantage of efficiently sampling the various relevant configurations even for a cluster of highly associative molecules. Finally, the approach maintains its simplicity regardless of the complexity of the intermolecular interaction arising, for example, from the presence of a molecular polarizability or three-body potentials.

The remainder of the paper is organized as follows. In Sec. 4.2.1, we review a conceptual aspect in formulating nucleation theory, which clarifies the context in which a physical cluster should be introduced into the theory. Details of the method to identify and characterize the physical cluster are given in Sec. 4.2.2 followed by Sec. 4.2.3 that describes how to evaluate, from a single simulation, the equilibrium distribution of the physical clusters.

The method is applied in Sec. 4.3 to water using the SPC/E model[93] to illustrate its utility. The paper then concludes in Sec. 4.4 with a brief discussion on the implications of our work.

4.2 Theory

4.2.1 General concept

We first review a conceptual aspect in describing a nucleation process. In principle, a fundamental microscopic theory can describe the time evolution of the density fluctuations that occur spontaneously in a metastable state and eventually lead to the formation of a new phase. In the framework of classical mechanics, for example, one determines the phase space trajectory that brings the system from the metastable phase to the more stable phase. When the average is taken over all possible initial microstates consistent with the metastable phase, one obtains a statistical description of the phase transition. In search for a macroscopic description of the process, one introduces a coarse graining into the microscopic theory, namely a number of microstates are grouped together as one entity, which we temporarily call a macrostate, and the deterministic elements in the fundamental microscopic theory are replaced by a probabilistic description providing the transition rates between these macrostates, each of which is now characterized by average properties of the microstates contributing to it. Reiss *et al.*[48–52] addressed this aspect as an "inversion of the order of averaging." It is by no means a peculiarity in nucleation theory, rather it is a central theme of statistical physics. The method is valid if, for example, the system can be divided into many statistically independent small parts and an experiment is not sufficiently sensitive to probe beyond the average behavior of these small parts.

Needless to say, it is a difficult task to explicitly carry out the approach just mentioned. However, nucleation theory is concerned with the initial stage of the phase transition, i.e., formation of a critical nucleus as a result of the spontaneous density fluctuations occurring in the parent phase in metastable equilibrium. Thus, equilibrium statistical mechanics should suffice in identifying the microstates relevant in nucleation. Consequently, one can introduce the macrostates through the coarse graining of the configurational space of the system constrained in the metastable state. It remains to specify the statistical ensemble most suitable in identifying a physical cluster. In the present context, a physical cluster is defined as a density fluctuation in the metastable phase that leads to nucleation.[48–53] If

the entire vapor phase is taken as a system, the coarse graining itself does not allow one to identify the physical cluster, for a macrostate introduced in this procedure represents a group of points in the configurational space of the entire vapor. Even though it is still possible to *define* a cluster, it merely serves as a counting procedure in enumerating the configurational space. Apparently, the definition is not unique since one can organize the counting in an arbitrary fashion. Any arbitrariness in defining the cluster must be removed by the rate theory appropriate for that definition. This implies that neither the cluster thus defined nor the rate theory is completely free of a non-physical aspect. In developing a molecular level theory, however, we demand that the cluster introduced into the theory or the rate theory taken separately be subject to a direct physical interpretation. Thus, we take a system so that the identification of a physical cluster and its characterization in terms of a macrostate are accomplished as a result of the coarse graining. In this work, we restrict ourselves to the case of vapor to liquid homogeneous nucleation in a single component system. The formalism developed here can be extended to a binary system or heterogeneous nucleation, for example.

4.2.2 Identification of a physical cluster

Suppose that the entire vapor phase of volume V_{tot} is divided into small cells of equal volume V and assume that V satisfies the following two conditions.[26] On one hand, V is sufficiently macroscopic in the sense that these cells can be regarded as statistically independent, which permits one to describe the nucleation process in the entire vapor by focusing on a single cell of volume V. In other words, performing an experimental measurement on the whole vapor phase is equivalent to taking an ensemble average on one of the cells. The appropriate statistical ensemble is a grand canonical ensemble.[94] On the other hand, V is small enough that the probability of finding more than one uncorrelated density fluctuation that participates in the nucleation process at any instant is negligible, which implies that there is at most one cluster in the cell. Thus, a proper coarse graining of the configurational space of the grand canonical ensemble should lead to an identification of a physical cluster. The appropriate partition function for one such cell is

$$\Xi(\beta, V, z) = \sum_{N=0}^{N_{cut}} \frac{z^N}{N!} \int d\{N\} e^{-\beta U_N}, \tag{4.1}$$

where $\beta = (k_B T)^{-1}$ with k_B and T being the Boltzmann factor and the absolute temperature, respectively. z is the fugacity of the molecule and N is the total number of molecules in the system, whose translational and orientation coordinates are collectively denoted by $\{N\}$. The total potential energy of the system is denoted by U_N. The summation with respect to N is bounded by N_{cut} to constrain the system to the metastable equilibrium. Equation (4.1) suggests that one can classify the microstates by N alone or N and U_N. Complication arises, however, since V is macroscopic and most of the fluctuations in N and U_N have very little to do with the nucleation process. Thus, among the various microstates consistent with a given value of N and a given interval of U_N, only a small fraction of them actually participate in the nucleation event and hence contain a physical cluster. In the language of Sec. 4.2.1, this means that a finer coarse graining than achieved by N or N and U_N is required to identify the microstates containing a physical cluster.

A conventional approach to identify the relevant microstates is to *a priori* define a set of clusters from which the physical clusters are isolated. For example, Band[13,14] and Stillinger[95] defined a cluster such that a molecule is considered to be a part of it if the distance between the molecule and at least one of the molecules of the cluster is less than a certain cutoff distance. In the LBA cluster,[91] every molecule in the system of volume $v \ll V$ is regarded as a part of the cluster. When either the cutoff distance or v is chosen so that the thermodynamic properties of the cluster are insensitive to it, the resulting cluster is identified as the physical cluster. In the i/v cluster,[48–53] every molecule in the system of volume v is also regarded as a part of the cluster. The i/v cluster differs from the LBA cluster in that the physical clusters are isolated from the various i/v clusters through an appropriate rate theory.[52] The assumption implicit in these approaches is that the arbitrarily defined clusters form a superset of the physical clusters. It is not even obvious, however, that all the relevant microstates are distributed primarily among the clusters that are to be isolated as physical or that all the irrelevant microstates are distributed primarily among the clusters that are to be discarded as non-physical. For example, consider two microstates: one with an i/v cluster and the other with an i/v' cluster and suppose that the configurations of molecules inside v and v' are identical and that these two clusters differ only by their values of v, namely by the locations of the nearest ideal gas molecules. If the i/v cluster is a physical one and $v \ll v'$, the i/v' cluster is most likely a non-physical one, for the assumed configuration in the i/v' cluster is unfavorable because of the translational entropy

of the molecules and may not be sampled at all during a simulation of a finite length of time. Artifacts of this kind would be removed, if possible at all, only by an intractably complicated rate theory.

One must realize that whether or not a given microstate contains a physical cluster, and hence is relevant in a nucleation event, is completely determined by the system itself. Thus, it is most straightforward to directly isolate the physical clusters from the entire microstates accessible to the system rather than indirectly by means of an arbitrarily defined cluster. The remaining task is simply to devise an effective simulation method for this purpose in such a way that no prior knowledge is required as to the detailed identity of the physical clusters. Let us first define the excess number of molecules N_c and the excess potential energy U_c by

$$\begin{aligned} N_c &\equiv N - n_v V \\ U_c &\equiv U_N - u_v V, \end{aligned} \tag{4.2}$$

where n_v and u_v are the number density of molecules and the average potential energy per unit volume in the vapor phase, respectively. Note that N_c is, in general, not an integer or necessarily positive. During a simulation, N and U_N, hence N_c and U_c, fluctuate. For a macroscopic V, these fluctuations are caused primarily by those due to each of the vapor molecules. Fluctuations of this kind are undesirable in identifying the physical clusters since they have very little to do with the nucleation process. In a grand canonical ensemble, however, their effect on N_c or U_c can be made negligible by decreasing the volume until it satisfies

$$n_v V \ll 1. \tag{4.3}$$

In this limit, the system contains, on average, no vapor molecule and thus the simulation preferentially generates the microstates containing a physical cluster. In fact, the probability of finding at least one vapor molecule in the system is, assuming the ideal gas behavior of the vapor phase, given by $1 - e^{-n_v V} \approx n_v V$, which is negligible as a result of Eq. (4.3). To achieve the coarse grained description, one can characterize the physical cluster by the excess quantities N_c and U_c since the dominant contribution to them now arises from the presence of the cluster. A more detailed characterization of the cluster is clearly possible.

In what follows, however, we focus solely on N_c since the inclusion of U_c or some other quantities does not affect the theoretical development given below. We refer to the physical cluster characterized in this manner as an N_c-cluster.

In view of Eq. (4.3), we may redefine N_c by

$$N_c \equiv N, \tag{4.4}$$

so that N_c is a non-negative integer. In short, our approach is to perform a grand canonical Monte Carlo simulation[47] on the system of microscopic volume V satisfying Eq. (4.3) allowing the number of molecules N_c to fluctuate from 0 to N_{cut}. All of the molecules found inside the system at a given instant are regarded as forming a physical cluster. To constrain the system to the metastable equilibrium, while still sampling a critical nucleus, N_{cut} introduced in Eq. (4.1) must be chosen to slightly exceed the size of the critical nucleus. Among the microstates contributing to the N_c-cluster, there are undoubtedly configurations in which some of the molecules are more properly regarded as a part of the vapor. The extent to which such configurations contribute to thermodynamic properties of the N_c-cluster, and hence the transition rates between the various N_c-clusters, clearly depends on V. This V dependence is neither an artifact nor an arbitrariness of the theory, rather the magnitude of the vapor contributions reflects the focus of our coarse grained description of the nucleation phenomenon. Because of Eq. (4.3), however, the vapor contribution is on average negligible. Consequently, the volume dependence is expected to be negligible as well and we shall not dwell upon this issue any further.

Some words on V are in order. Clearly, V has to be larger than the spatial extent of a physical cluster in it. That the system is microscopic does not affect the applicability of the statistical mechanical description. It is sufficient to assume a weak coupling between the system and its surroundings.[94] Both conditions are trivially satisfied in the case of vapor to liquid nucleation, in which the molar volume in the vapor phase is considerably larger than the physical dimension of the cluster and the interaction between the vapor molecules and a cluster can be ignored. If, on the other hand, V cannot be chosen to satisfy Eq. (4.3), the very concept of cluster is no longer relevant in describing nucleation, for the correlation between the system inside V and the surrounding is appreciable in this case. In other words, our method is applicable whenever the concept of cluster is relevant in nucleation and *vice*

versa, implying that clusters identified in our method are in fact physical clusters.

4.2.3 The equilibrium cluster size distribution

Besides providing a natural way to identify and characterize the physical clusters, the grand canonical ensemble allows one to obtain the equilibrium cluster size distribution directly from a single simulation without an expensive free energy evaluation. Since the distribution is of central importance in nucleation theory, we examine this possibility in detail.

To derive the expression for the equilibrium cluster size distribution $c(N_c)$, suppose that the whole vapor phase of volume V_{tot} is divided into cells of equal volume V, where V satisfies Eq. (4.3). Because of Eq. (4.3), most of the cells contain no molecules at all and those containing an N_c-cluster, including $N_c = 1$, are on average spatially distant. Thus, as we discussed at the end of Sec. 4.2.2, each cell is only weakly coupled with its surrounding cells and one can assume that the cells are all statistically independent. Consequently, the average number of the N_c-cluster inside the entire vapor of volume V_{tot} is given by

$$\frac{V_{tot}\,\Xi_c(\beta, V, z; N_c)}{V\,\Xi(\beta, V, z)}, \tag{4.5}$$

where Ξ_c is the term for which $N = N_c$ in the grand canonical partition function Ξ:

$$\Xi_c(\beta, V, z; N_c) \equiv \frac{z^{N_c}}{N_c!} \int d\{N_c\} e^{-\beta U_{N_c}}. \tag{4.6}$$

Equation (4.5) can be rationalized as follows: V_{tot}/V is the total number of the cells, while

$$p(N_c) \equiv \frac{\Xi_c(\beta, V, z; N_c)}{\Xi(\beta, V, z)} \tag{4.7}$$

is the normalized probability of finding an N_c-cluster in a given cell. Dividing the expression Eq. (4.5) by V_{tot}, we obtain the desired number density:

$$c(N_c) = \frac{1}{V}\, p(N_c). \tag{4.8}$$

Since the cluster can be formed anywhere in the volume V, we have

$$p(N_c) \sim V, \tag{4.9}$$

provided that care is taken to avoid the surface effect. As we shall see shortly, the implementation of this condition in a simulation is trivial. Thus, $c(N_c)$ given by Eq. (4.8) is independent of V as it should be.

In principle, one can determine the normalized probability $p(N_c)$ from a single simulation simply by counting the number of events in which N_c molecules are found in the system. Because of the condition Eq. (4.3), however, the system contains no molecules at all for most of the time and the states with $N_c \geq 1$ will be hardly sampled. To avoid this, we perform a simulation by fixing one molecule at the center. Provided that the boundary of the system is far from the molecules forming a cluster, the problem associated with the surface effect mentioned above is also resolved. Namely, the volume dependency Eq. (4.9) is rigorously obtained if integration with respect to the coordinates of the molecule thus fixed is performed analytically by ignoring the surface effect.

Since the precise size of the critical nucleus is not known prior to a simulation, the appropriate value of N_{cut} is also unknown. It is then convenient to perform a simulation by allowing N_c to fluctuate from unity to N_{max} chosen to be sufficiently large compared to the expected value of N_{cut}. Clearly, the normalized probability $p_s(N_c)$ obtained from the simulation differs from $p(N_c)$, since the former is normalized in the interval $[1, N_{max}]$, while the latter must be normalized in $[0, N_{cut}]$. To express $p(N_c)$ in terms of $p_s(N_c)$, we first note that the ratio $p_s(N_c)/p(N_c)$ is a common constant for $N_c = 1, \cdots, N_{cut}$. In fact,

$$\frac{p_s(N_c)}{p(N_c)} = \frac{\Xi_c(N_c)/\Xi'}{\Xi_c(N_c)/\Xi}, \tag{4.10}$$

where Ξ' is a grand canonical partition function of the system when N_c is constrained to $N_c = 1, \cdots, N_{max}$. Next, note that the ratio $p(0)/p(1)$ can be obtained analytically if the interaction between the system and the surroundings is ignored:

$$\frac{p(0)}{p(1)} = \frac{1}{z\Omega V}, \tag{4.11}$$

where Ω arises from the integration with respect to the orientational coordinates. Equations (4.10) and (4.11) can be used with the normalization requirement of $p(N_c)$ to obtain

$$p(0) = \frac{p_s(1)}{p_s(1) + z\Omega V\sigma}$$

$$p(N_c) = \frac{z\Omega V p_s(N_c)}{p_s(1) + z\Omega V \sigma} \qquad (N_c = 1, \cdots, N_{cut}), \tag{4.12}$$

where we define

$$\sigma \equiv \sum_{N_c=1}^{N_{cut}} p_s(N_c). \tag{4.13}$$

The equilibrium distribution $c(N_c)$ immediately follows from Eq. (4.8). The second of Eq. (4.12) satisfies Eq. (4.9). To see this, note that $p_s(N_c)$ is independent of V since both Ξ_c and Ξ' are proportional to V. Upon ignoring the terms of the second order in $z\Omega V$ or higher, Eq. (4.12) yields Eq. (4.9).

The simulation becomes impractical as the free energy barrier of nucleation exceeds several k_BT since clusters around the critical size are hardly reached. To overcome this difficulty, one can simply perform a series of simulations allowing N_c to fluctuate in the intervals $[1, N_1], [N_1, N_2], \cdots, [N_n, N_{max}]$. The probability $p_s(N_c)$ readily follows by demanding its continuity. This is an example of the umbrella sampling.[96] The validity of this approach depends on the assumption that N_i molecules form a cluster in the simulation constrained in $[N_i, N_{i+1}]$, which is reasonable since the system, when viewed as a closed one with N_i molecules inside, is at least N_i-fold more supersaturated than the vapor phase as is seen from Eq. (4.3):

$$\frac{N_i}{V} \gg N_i n_v. \tag{4.14}$$

The fact that N_c is constrained in the interval $[N_i, N_{i+1}]$ does not imply that the same set of N_i molecules remains in the system as if they were forming a core on which other molecules condense. Instead, any molecule in the system are subject to a trial annihilation in the grand canonical Monte Carlo simulation as far as N_c exceeds N_i. This is especially important to sample efficiently all the relevant configurations of clusters of highly associative molecules.

The time scale for a cluster to reach the internal mechanical equilibrium is many orders of magnitude shorter than that for the cluster to exchange a molecule with the vapor phase. Therefore, it is a common practice to assume that the configurational integral of an N_c-cluster is independent of the fugacity. Under this assumption, the results obtained at fugacity z' can be used to estimate $c(N_c)$ at a different fugacity z''. To see this, it is

sufficient to note that

$$p_s(z'', N_c) = \frac{\Xi'(z')}{\Xi'(z'')} \left(\frac{z''}{z'}\right)^{N_c} p_s(z', N_c), \tag{4.15}$$

substitution of which in Eq. (4.12) with z replaced by z'' in the latter reveals that the unknown constant $\Xi'(z')/\Xi'(z'')$ cancels out. It should be noted here that the assumption leading to Eq. (4.15) is not valid if the N_c-cluster has more than one conformational isomer that cannot establish a chemical equilibrium among themselves within the time period required for the cluster to change its size. In fact, a change in the fugacity affects the condensation rate of a vapor molecule, while having a minimal effect, if at all, on the evaporation rate, which differs from one isomer to another. Consequently, the probability distribution of isomers accounted for under the N_c-cluster, and hence the thermodynamic properties of the N_c-cluster, depends on the fugacity. In this case, one has to perform a separate simulation for each value of the fugacity.

Finally, we address a consistency issue. For simplicity, we assume that the vapor phase can be regarded as an ideal gas, for which $z\Omega = n_v$. Strictly speaking, the 1-cluster cannot be identified with a vapor monomer, since the former excludes other molecules from V because of the approximate definition Eq. (4.4) of N_c, while the latter does not under the ideal gas approximation. In fact, one can easily show that $c(1) \neq n_v$: Ξ_c in Eq. (4.6) can be evaluated to be $n_v V$ for the 1-cluster, while for an ideal gas

$$\Xi = e^{n_v V}, \tag{4.16}$$

yielding

$$c(1) = n_v e^{-n_v V}. \tag{4.17}$$

The factor of $e^{-n_v V}$ is a work term arising from the volume exclusion just mentioned. However, this distinction is completely insignificant since $e^{-n_v V} \approx 1$. Alternatively, one can consistently recover the monomer concentration by setting $V = 0$ in Eq. (4.17).

4.2.4 Alternative interpretation

We have assumed in Sec. 4.2.2 that the physical clusters, namely the density fluctuations that participate in the nucleation event, can be identified with the density fluctuations

other than those due to each of the vapor molecules. The validity of this assumption can be addressed only through an explicit formulation of the approach discussed in Sec. 4.2.1. Given the intractability of the formulation, however, it is of interest to present a heuristic argument to motivate our grand canonical Monte Carlo simulation from an alternative point of view.

Let us focus on an arbitrarily chosen monomer in the vapor phase and define an open system of volume V centered at the monomer. The volume V is taken to be sufficiently small compared to the molar volume of the vapor molecules:

$$V \ll \frac{1}{n_v}, \tag{4.18}$$

which is nothing more than Eq.(4.3). If the stochastic evolution of the system is followed throughout the entire nucleation process, one would find, for most of the cases, that the system contains the same monomer alone even after nucleation took place. However, if the monomer we chose was a successful one, we find that it acquires other vapor molecules, which then form a cluster. If nucleation process is a formation of a cluster of this kind as is pictured in the classical nucleation theory, but with a sufficient number of molecules to reach a critical size, the physical clusters are identified simply by following the stochastic evolution of a system that contains a successful monomer. Provided that this stochastic evolution can be described as a Markov process, a monomer can be made to be a successful one by employing a sufficiently high frequency of the trial creation and annihilation of molecules in the system. This is legitimate since a fundamental property of the Markov process guarantees that the limiting distribution of the Markov process, such as the statistical weight of each microstates and $p_s(N_c)$, is independent of the frequency, as long as the microscopic reversibility is satisfied by the transition rates between microstates.[47] Our grand canonical Monte Carlo simulation can be viewed as a straightforward implementation of this idea. Conceptually, however, the point of view taken in Sec. 4.2.2 was preferred since it highlights the subtle difference between our method of identifying the physical clusters and the conventional ones that require an *a priori* definition of clusters and the necessity of the term $N_c = 0$ in normalizing $p(N_c)$ is readily understandable.

Finally, we note that the physical clusters generated in the simulation are consistent with an intuitive definition of clusters. To see this, note that, in our simulation, N_c is

always larger than $n_v V \ll 1$, the average number of molecules in V when filled with the uniform vapor. Thus, on average, any attempted Monte Carlo move to create a molecule in the system will be accepted with higher probability if the newly created molecule interacts more favorably with the rest of the molecules, while as soon as a molecule evaporates from the cluster, it is more likely to be removed from the system upon its trial annihilation.

4.3 Application to SPC/E Water

As an illustration, we applied the present method to water using the SPC/E model,[93] which is a three interaction sites model without any polarizability known to reproduce some of the bulk liquid properties of water. It should be noted that the interaction potential in a small object such as a cluster and that in the bulk phase can be quite different.[97] Thus, the model may not be accurate for simulating the properties of clusters. We shall not pursue the issue here. Instead, we stress that more realistic model potentials can be employed without any modification to the theory.

We carried out the simulation at $T = 298.15$K for several values of the fugacity. The system is taken as a spherical container of radius 15 Å. Other details of the simulation conditions are summarized in Table 4.1. We sampled the value of N_c once every 10^2 Monte Carlo steps and performed each simulation until each N_c-cluster was sampled about 10^4 times. This translates to about 10^6 Monte Carlo steps for each N_c-cluster. During one Monte Carlo step, translation and rotation is made on average once on every molecule in the system, except for that at the center which undergoes rotation only. Care must be taken to ensure the microscopic reversibility upon a trial creation or annihilation of a molecule. Thus, during each Monte Carlo step, either trial creation or annihilation of a molecule is performed with equal probability. When N_c is at its lower bound, the trial annihilation is rejected with certainty. Likewise for a trial creation when N_c is at the upper bound.

Figures 4.1-4.5 show snapshots[98] taken rather arbitrarily from the simulation. The compact configuration shown in each of the figures clearly qualifies as a cluster. Extensive hydrogen bond network is also observed. Comparison of Figs. 4.1-4.3 reveals that very different configurations are sampled even in this highly associative substance, showing a clear advantage of the grand canonical simulation.

The equilibrium cluster size distribution is shown in Fig. 4.6. For simplicity, we have set

Table 4.1: Conditions of the simulation.

No.	$z\Omega$ [Å^{-3}]	$n_v V$ [a]	N_i [b]
S1	0.23×10^{-5}	0.325×10^{-1}	1,16
S2	0.16×10^{-5}	0.226×10^{-1}	1, 4, 8, 20, 26
S3	0.12×10^{-5}	0.170×10^{-1}	1, 3, 7, 11, 16, 22, 30, 38
S4	0.1×10^{-5}	0.141×10^{-1}	1, 3, 6, 10, 16, 24, 32, 40, 44
S5	0.8×10^{-6}	0.113×10^{-1}	1, 3, 6, 9, 12, 16, 20, 28, 36, 44, 50, 55

[a]Under the ideal gas approximation, $n_v = z\Omega$.
[b]End values of N_c in the umbrella sampling.

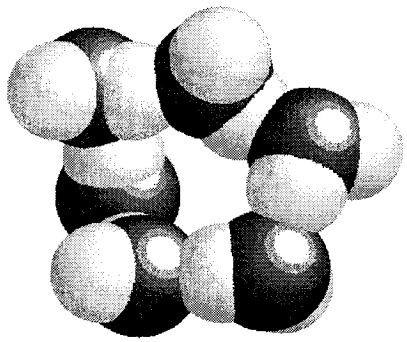

Figure 4.1: A snapshot of a 6-cluster forming a cyclic hexamer. At $T = 298.15$ K and $z\Omega = 0.1 \times 10^{-5}$ Å^{-3}. N_c is confined in the interval $[6, 10]$.

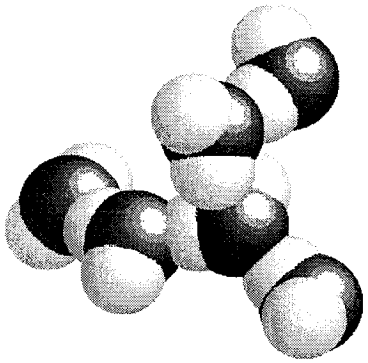

Figure 4.2: A snapshot of a 6-cluster. At $T = 298.15$ K and $z\Omega = 0.1 \times 10^{-5}$ Å^{-3}. N_c is confined in the interval $[6, 10]$.

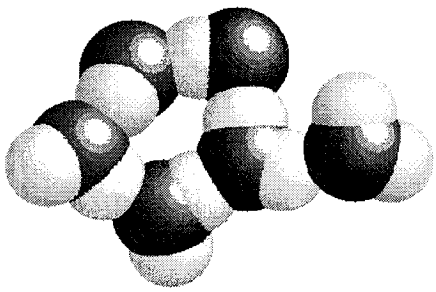

Figure 4.3: A snapshot of a 6-cluster as a cyclic pentamer with an additional molecule. At $T = 298.15$ K and $z\Omega = 0.1 \times 10^{-5}$ Å^{-3}. N_c is confined in the interval $[6, 10]$.

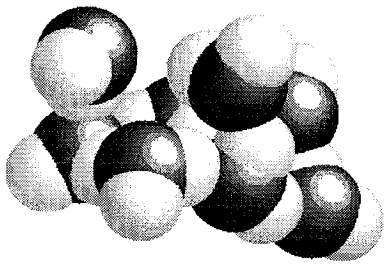

Figure 4.4: A snapshot of an 8-cluster. At $T = 298.15$ K and $z\Omega = 0.1 \times 10^{-5}$ Å^{-3}. N_c is confined in the interval $[6, 10]$.

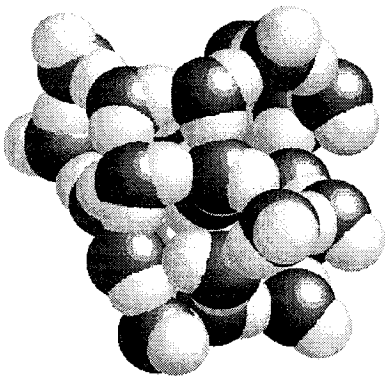

Figure 4.5: A snapshot of a 25-cluster. At $T = 298.15$ K and $z\Omega = 0.1 \times 10^{-5}$ Å^{-3}. N_c is confined in the interval $[24, 32]$.

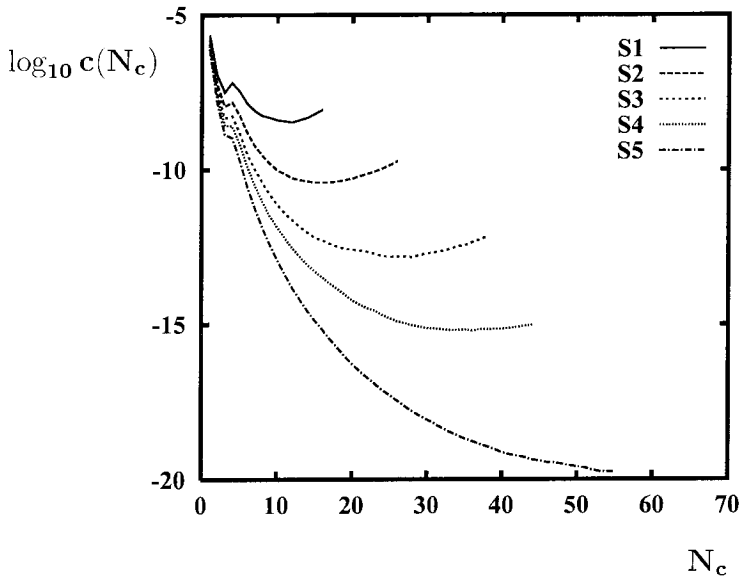

Figure 4.6: Cluster size distribution at $T = 298.15$K. $c(N_c)$ is in Å^{-3}. The conditions of simulation for S1, ..., S5 are given in Table 4.1.

$N_{cut} = N_{max}$ in Eq. (4.13). Since we are to describe the event of nucleation as a stochastic evolution of an N_c-cluster, the relevant reversible work $W^{rev}(N_c)$ to form this N_c-cluster is related to its probability $p(N_c)$ or the concentration $c(N_c)$. In this work, we have taken a point of view that a cluster is the density fluctuation in the vapor confined in the metastable state. The reversible work $W^{rev}(N_c)$ appropriate for this fluctuation picture is

$$\beta W^{rev}(N_c) \equiv -\log p(N_c). \tag{4.19}$$

In classical theory, the N_c-cluster is regarded as a product of the reaction

$$N_c \ \mathrm{X} \rightleftharpoons \mathrm{X}_{N_c}, \tag{4.20}$$

where X denotes a monomer. In this reaction picture, $W^{rev}(N_c)$ is more properly defined by

$$\beta W^{rev}(N_c) \equiv -\log \frac{c(N_c)}{n_v}. \tag{4.21}$$

The appearance of n_v is reasonable since the formation of the N_c-cluster starts from a

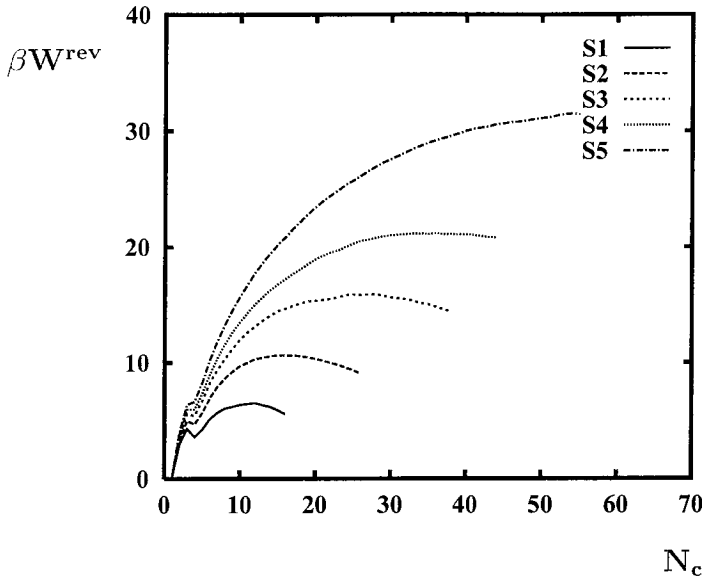

Figure 4.7: The reversible work of cluster formation at $T = 298.15$K. The conditions of simulation for S1, ..., S5 are given in Table 4.1.

monomer. In the case of vapor to liquid nucleation, both the fluctuation picture and the reaction picture appear quite reasonable. Hence, we expect that the rate theory appropriate for the fluctuation picture and that for the reaction picture will yield a consistent description of the nucleation phenomenon. In fact, $c(N_c)$ is independent of which picture is employed. In the following, we focus on $\beta W^{rev}(N_c)$ defined by Eq. (4.21), which is shown in Fig. 4.7. For high enough values of the fugacity, $\beta W^{rev}(3)$ is found to be a local maximum, which presumably is due to the inability to form a stable hydrogen bond network in the 3-cluster caused by the lack of the polarizability in the model potential. Though this result is most likely an artifact of the model potential, we note that such a nontrivial detail is easily captured in the present approach.

To assess the validity of the assumption implicit in Eq. (4.15), we compare $\beta W^{rev}(z, N_c)$ at $z\Omega = 0.1 \times 10^{-5}\text{Å}^{-3}$ that is obtained directly from simulation at this value of the fugacity with $\beta W^{rev}(z, N_c)$ obtained through Eq. (4.15) using $p_s(z', N_c)$ for other values of the fugacity z', where in Eq. (4.15) we set $z'' = z$. The result is shown in Fig. 4.8 and indicates that the configurational integral, and hence the Helmholtz free energy, of an N_c-cluster is nearly independent of the value of the fugacity. The result has several important

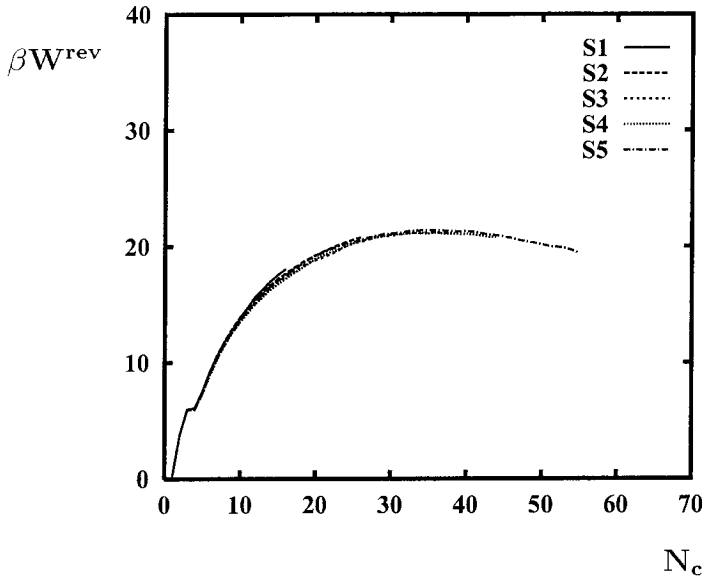

Figure 4.8: Comparison of the reversible work of cluster formation at $T = 298.15$K and $z\Omega = 0.1 \times 10^{-5}$ Å^{-3} obtained directly at this value of $z\Omega$ (S4) with the same quantity obtained through Eq. (4.15) by using other values of $z\Omega$ (S1, S2, S3, S5). The conditions of simulation for S1, ..., S5 are given in Table 4.1.

implications. First of all, this is the first example in which the fugacity independence of the thermodynamic properties of a cluster is actually *demonstrated* rather than simply *assumed.* Secondly, if one assumes this fugacity independence from the outset, then the agreement among various simulations provides an independent check that the configurational integral is properly evaluated in each simulation. This is rather remarkable since 10^6 Monte Carlo steps are hardly enough to achieve this kind of convergence for water if a canonical ensemble is employed. Next, one can significantly reduce the computational effort. Namely, when a simulation is performed at a certain value of the fugacity, the result can be used to calculate the reversible work at any value of the fugacity, provided that N_{max} used in the simulation is larger than N_{cut} appropriate for the fugacity of interest. Finally, $\beta W^{rev}(z, N_c)$ evaluated using $p_s(z', N_c)$ should increase with z', reflecting a contribution from the configurations accounted for under the N_c-cluster with some of the molecules being more properly regarded as a part of vapor, since such configurations are energetically unfavorable and tend to increase the free energy of the N_c-cluster. The fact that $\beta W^{rev}(z, N_c)$ depends only negligibly on z' implies that the V dependence of the thermodynamic properties of the N_c-cluster is

also negligible as we claimed near the end of Sec. 4.2.2.

4.4 Concluding Remarks

We have presented a new approach in identifying a physical cluster. Our approach differs from the conventional one in that no intermediate cluster such as the LBA cluster or the i/v cluster is introduced, from which the physical clusters have to be isolated either by adjusting the parameter v or by resorting to a rate theory. Thus, the assumption implicit in the conventional approach that the physical clusters form a subset of these intermediate clusters is avoided. Our basic idea is to follow the stochastic evolution of a system while suppressing the fluctuations irrelevant to the nucleation event. In doing so, we demonstrate the utility of a grand canonical Monte Carlo simulation. Thus, the simulation preferentially samples the physical clusters *without any prior knowledge regarding their detailed identity*, and then *directly* determines their equilibrium distribution. The latter feature permits one to completely bypass the expensive free energy calculation; this in turn opens up a possibility of employing more realistic intermolecular potentials that have been hitherto computationally prohibitively expensive. With an efficient method in both identifying the physical clusters and determining their equilibrium distribution, one is now in a position to initiate a rate theory to capture the full molecular level details of the nucleation process.

Acknowledgments[99]

The authors wish to express gratitude to Professor Howard Reiss and his co-workers for the series of insightful papers[48–53] and fruitful discussions, which led them to appreciate the importance of the physical clusters in the context of nucleation theory. This work was supported by National Science Foundation grant ATM-9614105. Z.-G. W. acknowledges support from the Camille and Henry Dreyfus Foundation and the Alfred P. Sloan Foundation.

Chapter 5 Binary Nucleation of Sulfuric Acid-Water: Monte Carlo Simulation

We have developed a classical mechanical model for the H_2SO_4/H_2O binary system. Monte Carlo simulation was performed in a mixed ensemble, in which the number of sulfuric acid molecules is fixed while that of water molecules is allowed to fluctuate. Simulation in this ensemble is computationally efficient compared to conventional canonical simulation, both in sampling very different configurations of clusters relevant in nucleation and in evaluating the free energy of cluster formation. The simulation yields molecular level information, such as the shape of the clusters and the dissociation behavior of the acid molecule in the cluster. Our results indicate that the clusters are highly nonspherical as a result of the anisotropic intermolecular interactions and that a cluster with a given number of acid molecules has several very different conformations, which are close in free energy and hence equally relevant in nucleation. The dissociation behavior of H_2SO_4 in a cluster differs markedly from that in bulk solution and depends sensitively on the assumed value of the free energy f_{hb} of the dissociation reaction $H_2SO_4+H_2O \rightarrow HSO_4^- \cdot H_3O^+$. In a small cluster, no dissociation is observed. As the cluster size becomes larger, the probability of having an $HSO_4^- \cdot H_3O^+$ ion pair increases. However, in clusters relevant in nucleation, the resulting ion pairs remain in contact; about 240 water molecules are required to observe behavior that resembles that in bulk solution. If a larger value of f_{hb} is assumed to reflect its uncertainty, the probability of dissociation becomes negligible. A reversible work surface obtained for a condition typical of vapor to liquid nucleation suggests that the rate-limiting step of new particle formation is a binary collision of two hydrated sulfuric acid molecules. The ion pairs formed by dissociation play a key role in stabilizing the resulting cluster. The reversible work surface is sensitive to the assumed value of f_{hb}, thus pointing to the need of an accurate estimate of the quantity either by *ab initio* calculations or experiments.

5.1 Introduction

The theory of binary nucleation dates back to a paper by Reiss.[4] Despite successive modification accounting for transient behaviors and paths in the vicinity of the saddle point,[100–105] the theory is an extension of classical nucleation theory for single component systems. While the classical theory[1–3] is presently the only practical approach for predicting nucleation rates, limitations of the theory, arising from its macroscopic nature, are well known. Thus, there has been a great interest in establishing molecular level approaches to nucleation.

One of the most important binary nucleating systems is H_2SO_4/H_2O, to which numerous papers are devoted on both theoretical[106–121] and experimental[122–127] fronts. Comparisons of classical predictions with experimental data for H_2SO_4/H_2O nucleation, while not extensive, yield conflicting results as to the validity of the classical theory.[114,123,124,126,127] Thus, it is of great interest on both fundamental and practical grounds, to seek a molecular level description of binary H_2SO_4/H_2O nucleation.

There are two major trends in developing a molecular level theory of nucleation. One is a molecular level simulation,[47–53,91,128] which can be applied regardless of the complexity of the intermolecular interaction. However, the free energy of a cluster, the quantity of central importance in nucleation theory, is usually evaluated by integrating its internal energy obtained at different temperatures from separate simulations. This aspect renders the approach computationally demanding and, as a result, virtually all of the simulations are limited to a single component system. The alternative approach is to use statistical mechanical density functional theory,[32] first applied to homogeneous nucleation by Oxtoby and Evans.[33] In this approach, the grand potential of the system is written as a functional of order parameters. Then, the stationarity condition of the grand potential determines the order parameters for the critical nucleus and the corresponding grand potential follows from the functional. When a cluster possesses a high degree of symmetry and the intermolecular potential is relatively simple, this approach is computationally far less demanding, allowing one to investigate a much wider range of the parameter space. Thus, one usually employs model potentials that capture the essential features of the molecules under consideration. When the results are compared against predictions from classical theory, which uses bulk thermodynamic quantities obtained from the same theoretical framework, one can isolate the deviations from the classical predictions arising from the molecular level details. Al-

though the approach is more approximate compared to molecular simulation, the theory is extremely powerful in addressing the deviations in a semi-quantitative manner and has been employed to investigate several interesting systems[34–42] for which no simulation has been performed. The theory was recently applied to a ternary system.[43]

In the present case of H_2SO_4/H_2O binary system, however, the density functional theory does not offer any advantage over simulation, for the intermolecular potentials that can faithfully represent the system is very complicated and as a result of the strongly anisotropic intermolecular interactions, a small cluster is expected to be highly non-spherical. Consequently, we resort to a method of computer simulation, in particular Monte Carlo simulation, since we are primarily concerned with equilibrium properties of the clusters. To our knowledge, the present work is the first example in which an extensive evaluation is made of the free energy of cluster formation in a binary system. The lack of a simulation work in a binary system is a result of the extensive computation involved in the free energy calculation. Thus, one of our goals in the present work is to establish a simulation technique that considerably reduces the computational effort.

The intermolecular interaction potential is the fundamental information prerequisite in applying a molecular theory. To reproduce this potential in a simple way, one usually represents a molecule as a set of interaction sites rigidly held together in its representative geometry. The interaction parameters are then optimized to reproduce *ab initio* results for geometries and energies of small clusters or certain bulk thermodynamic properties. The main concern in this approach is the quality of the potential thus obtained. For example, the necessity of incorporating molecular polarizabilities or three-body potentials in accurately reproducing the energy and the geometry of a cluster is often stressed.[97,129] In the case of a cluster of highly associative molecules, however, simulation must be performed for a very long period of time to sample faithfully the relevant parts of the phase space. For a water cluster, for example, this is necessary because the strong intermolecular interaction arising from an extensive hydrogen bond network hinders the evolution of the cluster from one structure to another, even though very different structures have to be taken into account in evaluating the thermodynamic properties of the cluster. In the present case of the H_2SO_4/H_2O system, even stronger hydrogen bonds are expected to be involved,[130] as is suggested by the relatively high boiling point of the pure acid (330°C). Thus, in order to perform a feasible calculation to obtain the free energy of the clusters, we must be content

with simple model potentials.

Nonetheless, simulation provides significant molecular level insight that is otherwise unattainable. Since the size of a typical cluster, containing a few acid molecules and several tens of water molecules, is smaller than the Bjerrum length, the distance at which the Coulombic interaction of a pair of ions becomes comparable with the thermal energy, the dissociation behavior of a sulfuric acid molecule in the cluster can be quite different from that in bulk solution. In classical nucleation theory, however, the reversible work of cluster formation is expressed in terms of bulk thermodynamic quantities. It follows that the reversible work estimated by classical theory may not reflect the true dissociation behavior in the cluster, whose effect can be addressed only by a molecular approach. Another conceptually, if not quantitatively, important problem relates to the very foundation of the thermodynamics of interfaces. Unless a cluster is spherical on average, the formalism loses its validity as the thickness of the interfacial region becomes non-negligible compared to the size of the cluster itself.[5] As mentioned above, however, a small cluster is expected to be highly non-spherical even after a thermal average is taken.

Given the limitations on the quality of the intermolecular potentials, a sensible way to address the effect of the molecular level details is to compare the results from simulation with the classical predictions obtained by using bulk thermodynamic properties for the system with the same model potentials used in simulation. Computation involved in determining these properties from simulation with the required accuracy is demanding and beyond the scope of this work. Instead, we shall directly compare the reversible work surface from simulation with the classical predictions for a real H_2SO_4/H_2O system.

This paper is organized as follows. The model potential is developed in Sec. 5.2. In Sec. 5.3, we derive the expression for the reversible work of cluster formation. In this section we employ a mixed ensemble, in which the number of water molecules is allowed to fluctuate while that of acid molecules is fixed. As a result, a cluster is characterized solely by the number of acid molecules inside it. In Sec. 5.4, we characterize a cluster by the numbers of molecules of both water and acid and derive the expressions for the reversible work and the equilibrium distribution for this cluster. The resulting expressions can be readily evaluated from the results of the mixed ensemble simulation. Section 5.5 describes certain details of the simulation. Results of simulation are presented in Sec. 5.6, where a comparison is made between the reversible work from molecular simulation and that from

classical theory. The paper concludes in Sec. 5.7 with a brief discussion on the implications of our work.

5.2 Model

Given the possibility of dissociation and protonation of the molecules involved, conceptually the simplest approach is to represent the H_2SO_4/H_2O system as a mixture of reactive species of water, sulfate ion, and proton. In the initial stage of this work, we investigated this possibility[131] and encountered serious difficulties. Briefly, to take advantage of the existing models for water[93] and sulfate ion,[132] a proton was described as a unit charge $|e|$, where e is the charge of an electron, with Lennard-Jones parameters that reproduce O-H bond energies of hydronium ion and sulfuric acid. Since both bond energies are of the order of 10^2 kcal/mol, however, protons rarely change their positions during a simulation. Consequently, the system becomes locked into a local minimum dictated mainly by the initial configuration of protons. This behavior is in serious contradiction with the experimental value of the activation energy for proton transfer in water, which is estimated to be about a few kcal/mol.[133,134]

An alternative model was proposed by Hale and Kathmann,[135] in which a partial charge less than $|e|$ is assigned to a proton. Although the model cannot describe either dissociation of acid or protonation of water, and hence is inapplicable for the present purpose of addressing the dissociation behavior in a cluster, it can explicitly incorporate internal rotations and vibrations of O-H bonds in a sulfuric acid molecule. Such internal degrees of freedom can be important. In a $H_2SO_4 \cdot H_2O$ dimer in vacuum, for example, the potential energy barrier for internal rotation of the O-H bonds of the acid molecule is estimated to be 5.2 kcal/mol by *ab initio* calculation at the MP2/3-21g** level of theory,[136] suggesting a possibility of more than one conformation of the dimer. Some of these conformations become unavailable to the dimer as it is transferred from the vapor phase to the bulk liquid solution simply because of the dissociation of the acid molecule. This indicates that the contribution to the dimer free energy from certain conformations is not included in the classical description which relies on bulk thermodynamic properties. Thus, the loss of an available conformation can contribute to an error in the classical free energy prediction.

Attempts to develop a dissociative model pose serious problems. Note that a proton in

a dissociative model must carry a unit charge of $|e|$. In reality, however, its effective charge certainly is less than $|e|$, since a proton exists by forming a chemical bond to an oxygen from water or sulfate ion. Moreover, when one of the O-H bonds is broken and another is formed, the entire electronic structure of the molecules involved changes. This is inherently a quantum mechanical effect, which, when reproduced in the realm of classical mechanics, requires fairly detailed interaction potentials including explicit polarizabilities and three-body potentials, as illustrated by a dissociative model for pure water.[137,138] To develop a dissociative model for the present system, substantial amount of data on energies and structures of sulfuric acid-water complexes are required. In this context, we note that the three-body potential can be quite sensitive to the exact environment. Thus, the dissociative model for pure water[137,138] is unlikely to remain valid in the present system. However, available literature dealing with such complexes is very limited. Apparently, only one such paper exists,[139] which provides interaction energies with partially optimized geometries of the neutral complex $H_2SO_4 \cdot H_2O$ and the ionic complex $HSO_4^- \cdot H_3O^+$. The lack of necessary information precludes an effort to develop a detailed interaction potential.

An *ab initio* molecular dynamics[140–143] approach, in which atomic nuclei are treated classical mechanically while the electronic degrees of freedom are treated explicitly by quantum mechanical density functional theory,[144] appears to be an interesting alternative. In this approach, no model potential needs to be specified, rather it is calculated on-the-fly during the course of simulation. However, its application is currently limited to investigating dynamics that occur on the time scale of the order of picosecond and is not yet practical in evaluating free energy.

The approach adopted here is to treat the dissociated and undissociated states as distinct. Since a proton exists primarily as a part of either sulfuric acid or hydronium ion rather than as a free ion, and the second dissociation of sulfuric acid is negligible compared to the first, one can introduce water, hydronium ion, sulfuric acid, and bisulfate ion as the constituent molecules. A molecule is modeled as a set of interaction sites rigidly held together at a representative geometry. It is well known that nonadditive interactions, arising from molecular polarizabilities and three-body interactions, play an important role in both the energetics and the structures of clusters.[97,129] Nonetheless, the enormous computational effort involved in free energy calculation and the lack of either experimental or quantum mechanical data indicate one should adopt the simplest possible potential, namely a pair-

Table 5.1: Interaction parameters for water and hydronium ion.

	water	hydronium ion
A_O^2 [kcal Å^{12}/mol]	0.62935 $\times 10^6$	0.38931 $\times 10^6$
C_O^2 [kcal Å^6/mol]	0.62545 $\times 10^3$	0.65328 $\times 10^3$
z_O	-0.8476 $\|e\|$	-0.2480 $\|e\|$
z_H	0.4238 $\|e\|$	0.4160 $\|e\|$
r(O-H) [Å]	1.000	0.973
$\angle$ H-O-H	109.47°	111.6°

Table 5.2: Lennard-Jones parameters of sulfuric acid molecule and bisulfate ion.

	sulfur site	oxygen sites
A_i^2 [kcal Å^{12}/mol]	0.40063×10^7	0.76351×10^6
C_i^2 [kcal Å^6/mol]	0.20016×10^4	0.78154×10^3

wise additive potential. Even then, in this four component system, there are as many as ten distinct interaction pairs, while the available data cover only four of them. For example, in addition to the data on the two complexes mentioned above, various water-water interaction potentials are available. Protonated water clusters have been a focus of extensive studies on both experimental[145–148] and theoretical[149–153] fronts. To estimate the remainder of the interactions, however, one needs to invoke some kind of mixing rule, which in turn requires that all of the pair interactions be described by the same type of function. In this work, the interaction potential $u_{\alpha\beta}$ between molecules α and β is assumed to be the sum of Coulombic and Lennard-Jones interactions,

$$u_{\alpha\beta} = \sum_{i \text{ on } \alpha} \sum_{j \text{ on } \beta} \left(\frac{z_i z_j}{r_{ij}} + \frac{A_i A_j}{r_{ij}^{12}} + \frac{C_i C_j}{r_{ij}^{6}} \right), \tag{5.1}$$

where r_{ij} is the distance between sites i and j and the summation is taken over all intermolecular interaction sites.

The model parameters are given in Tables 5.1—5.3. The notations for the interaction sites for sulfuric acid and bisulfate ion are defined in Fig. 5.1. The geometries for these species are given in Table 5.4

and discussed below. Parameters for water correspond to the SPC/E potential,[93] which is known to reproduce certain bulk properties of pure water including the coexistence den-

Table 5.3: Partial charges on H_2SO_4 and HSO_4^-.

interaction site	H_2SO_4	HSO_4^-
S	2.8528 $\|e\|$	2.8272 $\|e\|$
O_1	-1.0325 $\|e\|$	-1.2942 $\|e\|$
$O_1\prime$	-1.0325 $\|e\|$	-1.1482 $\|e\|$
O_2	-0.9582 $\|e\|$	-0.9615 $\|e\|$
$O_2\prime$	-0.9582 $\|e\|$	-0.9615 $\|e\|$
H_1	0.5643 $\|e\|$	—
$H_1\prime$	0.5643 $\|e\|$	0.5382 $\|e\|$

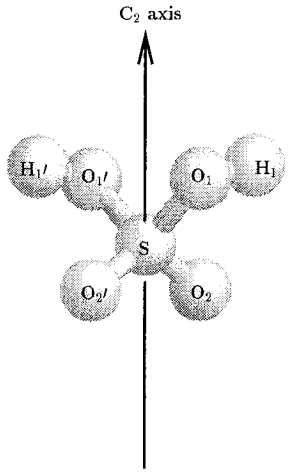

Figure 5.1: Model of a sulfuric acid molecule showing notations and C_2 axis.

Table 5.4: Sulfuric acid molecule geometry adopted in this work.

r(O_1-H_1)	0.97 Å
r(S-O_1)	1.574 Å
r(S=O_2)	1.422 Å
$\angle$(H_1-O_1-S)	108.5°
$\angle$(O_1-S-$O_1\prime$)	101.3°
$\angle$(O_2=S=$O_2\prime$)	123.3°
τ($H_1O_1SO_2$)[a]	20.8°
τ(P_1P_2) [b]	88.4°

[a] Looking down the O_1-S bond. The H_1O_1 projection must be rotated clockwise by 20.8° to be *cis* to the O_2-S bond.

[b] Angle between $O_1SO_1\prime$ and $O_2SO_2\prime$ planes. The small deviation from exactly perpendicular planes brings O_2 and $O_2\prime$ closer to $O_1\prime$ and O_1, respectively.

Table 5.5: Enthalpy of hydration from simulation and experimental values.

$n-1,n$	$-\Delta U_{n-1,n}$ [kcal/mol][a,b]	$-\Delta H_{n-1,n}$ [kcal/mol][a,c]
0,1	25.35	31.6
1,2	23.74	19.5
2,3	21.98	17.9
3,4	11.42	12.7
4,5	10.92	11.6
5,6	10.43	10.7

[a] $\Delta U_{n-1,n} \equiv U_n - U_{n-1}$, likewise for $\Delta H_{n-1,n}$.
[b] This work. Simulation performed at 298.15 K.
[c] Experimental data of Lau et al.[145]

sities[154] and the surface tension.[155,156] Parameters for the other molecules require explanation.

As mentioned above, protonated water clusters have been studied extensively and various interaction potentials have been proposed.[157–160] However, none assumes a form as simple as Eq. (5.1). Thus, it is necessary to develop a potential as follows. First, the geometry of the hydronium ion is taken from the accurate theoretical determination by Rodwell and Radom.[161] Each atomic site bares a partial charge while the Lennard-Jones parameters are assigned only for the oxygen sites. Then, these parameters are tuned to reproduce the experimentally determined enthalpy of hydration of the ion hydrated up to six water molecules.[145] The difference between enthalpy and internal energy is ignored for simplicity. In parameterizing the partial charge on oxygen, either negative or positive charge can be assigned, yielding a similar overall agreement to the experimental enthalpy of hydration. However, the assignment of a negative charge resulted in interaction parameters that are closer to the values for SPC/E water and is preferred on the basis that the protonation of a molecule should not significantly change its interaction parameters. The resulting hydration energies are compared with experimental values in Table. 5.5. Except for the first few hydrates, the agreement is fair.

The experimentally determined geometry is adopted for sulfuric acid[130] as shown in Fig. 5.1 and Table 5.4. A partially optimized geometry for bisulfate ion was obtained by Kurdi and Kochanski[139] using *ab initio* calculation. In their calculation, $\angle$ S-$O_1\prime$-$H_1\prime = 114°$ was obtained. However, the value is probably an overestimate insofar as the corresponding

Table 5.6: Energy and geometry of $H_2SO_4 \cdot H_2O$ neutral complex. Comparison between simulation and "exact" values.

	This work[a]	Experiment[b]	Kurdi[c]	Morokuma[d]	Lay[e]
energy [kcal/mol]	-15.76	—	-15.769	≈ -10.00	-25.37
O-O_1 distance [Å][f]	2.662	—	2.656	≈ 2.696	2.553
dipole moment of H_2SO_4 [Debye]	2.718	2.72515	—	—	2.2989

[a]Simulation was carried out at 0.1 K.
[b]Kuczkowski *et al.*[130]
[c]*Ab initio* SCF-MO-LCGO calculation by Kurdi and Kochanski.[139]
[d]*Ab initio* calculation by Morokuma and Muguruma[162] at the fourth-order MP4SDQ level with zero-point correction. The values cited here are estimated from their figures.
[e]*Ab initio* calculation by Lay[136] at the MP2/3-21g** level.
[f]O is on water while O_1 is on sulfuric acid.

value for sulfuric acid was overestimated by 11.5°. In the present work, we simply use the same value as for sulfuric acid. We also ignore the slight ($\approx 0.5°$) deviation between the C_2 axes of the angle O_1-S-$O_1\prime$ and O_2=S=$O_2\prime$. In other words, bisulfate ion was obtained from sulfuric acid by removing the proton H_1 and shortening the bond length r(S-O_1) to 1.48Å. In determining interaction parameters for these molecules, *ab initio* results[139] on the potential energies and geometries of $H_2SO_4 \cdot H_2O$ and $HSO_4^- \cdot H_3O^+$ were used. The experimentally obtained dipole moment of sulfuric acid[130] provided additional information. The information, however, is simply not sufficiently extensive to determine all of the parameters. To further facilitate the parameterization, the Lennard-Jones parameters for these molecules were assumed to be the same as those of sulfate ion[132] and only the partial charges were adjusted. In addition, partial charges on O_2 and $O_2\prime$ sites of bisulfate ion are assumed to be equal, though these two sites are not equivalent. The resulting interaction energies and geometries are compared with the *ab initio* results in Table 5.6 and 5.7 for sulfuric acid and

bisulfate, respectively. In Table 5.6, other sets of *ab initio* results are shown. Judged from the level of the theory, the results by Morokuma and Muguruma[162] are perhaps the most accurate. Nonetheless, we employ the results by Kurdi and Kochanski[139] since the corresponding data for $HSO_4^- \cdot H_3O^+$ are available only in their paper. Because of some model parameters left unadjusted, the model is expected to be sufficiently flexible to incorporate additional data as they become available.

Table 5.7: Energy and geometry of $HSO_4^- \cdot H_3O^+$ ionic complex. Comparison between simulation and *ab initio* results.

	This work[a]	"Exact" value[b]
energy [kcal/mol]	−136.39	−136.39
O-O_1 distance [Å][c]	2.380	2.326
∠ O_1-H_1-O[c]	174.6°	180°
∠ O_1-H-O[c]	168.9°	180°

[a]Simulation was carried out at 0.1 K.
[b]*Ab initio* SCF-MO-LCGO calculation by Kurdi and Kochanski.[139]
[c]H and O are the atomic sites on hydronium ion, O_1 is on sulfuric acid, and H_1 refers to the position of the proton if the S-O_1 bond is shortened to 1.48 Å without removing H_1 from H_2SO_4.

An iterative method similar to that suggested by Halley *et al.*[138] is used to find the optimum sets of parameters. First, simulation was carried out with some reasonable values of the parameters, for which the difference between the calculated and "exact" energies and structures of the complexes were evaluated. New sets of parameters were obtained by randomly perturbing the old parameters, which in turn were used to generate the next trial parameters only if they resulted in a decrease of the deviation. The process was repeated until no further decrease of the deviation is achieved.

5.3 Reversible Work of Cluster Formation

In this section, we derive a statistical mechanical expression for the reversible work of cluster formation from a H_2SO_4/H_2O binary vapor. Since the vapor phase serves as a reference state in calculating the reversible work, its precise nature has to be specified first. Most of the acid molecules in the vapor exist as hydrates so that the number of the sulfuric acid monomers is significantly smaller than the total number of acid molecules.[109,110,113,114,117,118,163] In deriving the statistical mechanical expression for the reversible work of cluster formation, it is most convenient to take a reference state in which molecules exist as monomers forming an ideal gas mixture. Once the reversible work is obtained as a function of monomer concentration of acid molecules, it is an easy task, if so desired, to re-express it as a function of the number density of all sulfuric acid molecules calculated regardless of hydration state.[109,113,117] The same applies to the total number of water molecules if hydrate forma-

tion leads to a serious depletion of water.[15,117]

Inside the vapor phase, we take a system of volume V which satisfies the following two conditions.[26] On one hand, V is sufficiently macroscopic in the sense that its coupling with the surrounding vapor is sufficiently weak. Then the statistical properties of the system are determined by the grand canonical ensemble.[94] On the other hand, V is small enough that the probability of finding more than one uncorrelated density fluctuation that participates in the nucleation process at any instant is negligible, which implies that there is at most one cluster in the system. Then, the reversible work W^{rev} to form a cluster inside V from the reference state is given by

$$\beta W^{rev} = -\log \frac{\Xi^c}{\Xi^r}, \tag{5.2}$$

where $\beta \equiv (k_B T)^{-1}$ with k_B and T being the Boltzmann constant and the absolute temperature, respectively. Ξ^r is the partition function of the system constrained to be in the reference state, while Ξ^c is evaluated under the constraint that the system contains a cluster. Assuming the ideal gas behavior in the reference state,

$$\begin{aligned} \Xi^r(T, V, \mu_w, \mu_s) &= \sum_{N_w=0}^{\infty} \sum_{N_a=0}^{\infty} \frac{1}{N_w!} \left(\frac{q_w e^{\beta\mu_w}}{\Lambda_w^3} V\Omega \right)^{N_w} \frac{1}{N_a!} \left(\frac{q_s e^{\beta\mu_s}}{\Lambda_s^3} V\Omega \right)^{N_a} \\ &= e^{(n_w+n_s)V}, \end{aligned} \tag{5.3}$$

where the subscripts w and s refer to water and sulfuric acid, respectively. The molecular partition functions of the α-molecule are given by q_α and Λ_α^3, the former arising from the internal degrees of freedom of the molecule and the latter from the kinetic energy of translation and rotation. μ_α is the chemical potential of the α-component in the reference state and Ω arises from the integration over the orientational coordinates of a molecule. Here, the symmetry number of a molecule is absorbed in q_α. Finally, n_α is the number density of the α-component in the reference state, where we have made use of the fact that

$$n_\alpha = \frac{q_\alpha e^{\beta\mu_\alpha}\Omega}{\Lambda_\alpha^3}. \tag{5.4}$$

In a single component system, a cluster simulation is commonly realized by confining a fixed number of molecules, say i, in a spherical container of volume v concentric with the center of mass of i molecules. To the extent that these molecules actually form a cluster and

the thermodynamic properties of the cluster are nearly independent of v over a wide range of v, Lee *et al.*[91] characterized the cluster by its size i alone. The exclusive use of a canonical ensemble in cluster simulation stems from the fact that clusters are unstable with respect to change in their size. In the H_2SO_4/H_2O binary system, there are as many as 300 clusters assuming that the maximum numbers of H_2SO_4 and H_2O molecules in a cluster are 3 and 100, respectively. If a canonical ensemble is employed, expensive thermodynamic integration has to be carried out to evaluate the free energy of each cluster. One can significantly reduce the computational effort by devising simulation that preferentially samples clusters relevant in nucleation, i.e., those found along the valley passing through the saddle point of the reversible work surface. Under conditions typical of sulfuric acid-water binary nucleation, $n_s \ll n_w$. Moreover, when the relative humidity is less than 100%, the sulfuric acid hydrate cannot grow indefinitely without acquiring more acid molecules. Thus, during the time period required for a cluster to either acquire or lose an acid molecule, the cluster reaches *stable* partial equilibrium with respect to its internal degrees of freedom and the exchange of water molecules.[107,109,110] These clusters in *stable* partial equilibrium are, in fact, those found along the valley of the free energy surface. Thus if we employ the mixed ensemble in which the number of water molecules is allowed to fluctuate while that of sulfuric acid molecules is fixed, simulation will preferentially generate the clusters relevant in nucleation. In this approach, a cluster is characterized only by the number N_a^c of sulfuric acid molecules in it. For brevity, we refer to this cluster as the N_a^c-cluster. Our goal here is to express Ξ^c in terms of the partition function of the N_a^c-cluster in the mixed ensemble. As we shall discuss in Sec. 5.4, the free energy of the cluster characterized by both N_a^c and N_w^c, the latter being the number of water molecules in it, can be easily obtained from simulation on the N_a^c-cluster.

Recently, we developed a new approach to cluster simulation in a single component system using a grand canonical ensemble.[99] The method is free of any arbitrariness involved in the definition of a cluster. Instead, it preferentially generates the physical clusters, defined as the density fluctuations that participate in nucleation,[48–53] and directly determines their equilibrium distribution without the computationally demanding free energy evaluation. In the present case of H_2SO_4/H_2O binary system, however, Monte Carlo moves to create or annihilate an acid molecule will rarely be accepted since a hydrogen bond network will be seriously disturbed in the process. The present approach of using the mixed ensemble can

be regarded as an application of the grand canonical ensemble approach to heterogeneous nucleation, in which a fixed number of acid molecules in the cluster, as a whole, are regarded as a heterogeneous nucleation site.

We first obtain the partition function Φ^c for the mixed ensemble under the constraint that the system contains an N_a^c-cluster. Once Φ^c is obtained, Ξ^c follows immediately. Since n_s is many orders of magnitude smaller than the corresponding value in the cluster, we can divide the acid molecules in the system to N_a^c belonging to the cluster and N_a^v regarded as part of the vapor. Although no dissociation is allowed in the vapor in accord with the choice of the reference state, possible dissociation in the cluster is an essential feature of the system. We denote the number of resulting bisulfate ions and hydronium ions by N_i. In our model representation of H_2SO_4/H_2O binary system using the four distinct molecular species, we then have

$$\begin{aligned}\Phi^c(\beta, V, \mu_w, N_a^v, N_a^c) &= \frac{1}{N_a^v!}\left(\frac{q_s V\Omega}{\Lambda_s^3}\right)^{N_a^v} \sum_{N_i=0}^{N_a^c} \frac{1}{(N_a^c - N_i)!}\left(\frac{q_s}{\Lambda_s^3}\right)^{N_a^c - N_i} \frac{1}{N_i!}\left(\frac{q_b}{\Lambda_b^3}\right)^{N_i} \frac{z_h^{N_i}}{N_i!} \\ &\quad \times \sum_{N_w=0}^{\infty} \frac{z_w^{N_w}}{N_w!} \int d\{N\} e^{-\beta U_N}, \end{aligned} \tag{5.5}$$

where the subscripts b and h refer to bisulfate ion and hydronium ion, respectively. We have defined the fugacities z_w of water and z_h of hydronium ion by

$$z_w \equiv \frac{q_w e^{\beta\mu_w}}{\Lambda_w^3} \qquad \text{and} \qquad z_h \equiv \frac{q_h e^{\beta\mu_w}}{\Lambda_h^3}, \tag{5.6}$$

respectively, and assumed that the N_a^v sulfuric acid vapor molecules can be treated as an ideal gas to integrate out their contribution in the configurational integral. As a result, N stands for $N_a^c + N_i + N_w$, whose translational and orientational degrees freedom are collectively denoted by $\{N\}$ in the configurational integral. Note that in the definition of z_h, Eq. (5.6), the chemical potential of water is used since hydronium ions are formed from water, to which the system is open. To clarify this point, Eq. (5.5) is derived in Appendix F starting from a dissociative model. Note that the configurational integral is taken over all configurations consistent with the N_a^c-cluster. This constraint is well-defined and presents no difficulty in evaluating the integral. In fact, as we will see below, the partition function to be evaluated by simulation involves only N_a^c acid molecules. Moreover, the boiling point

of pure sulfuric acid is much higher (330°C) than the temperature of interest, where acid molecules are bound together regardless of the value of V. This means that no explicit consideration is necessary to impose the constraint that the N_a^c acid molecules form a cluster. Finally, multiplying Φ^c by $e^{\beta\mu_s(N_a^v+N_a^c)}$ and summing over N_a^v, we can convert Φ^c to Ξ^c:

$$\begin{aligned}\Xi^c(\beta,V,\mu_w,\mu_s;N_a^c) &= \sum_{N_a^v=0}^{\infty} e^{\beta\mu_s(N_a^v+N_a^c)}\Phi^c(\beta,V,\mu_w,N_a^v,N_a^c) \\ &= e^{n_s V}\left(\frac{q_s e^{\beta\mu_s}}{\Lambda_s^3}\right)^{N_a^c}\sum_{N_i=0}^{N_a^c}\frac{\chi^{N_i}}{(N_a^c-N_i)!N_i!}\frac{z_w^{N_i}}{N_i!} \\ &\quad\times\sum_{N_w=0}^{\infty}\frac{z_w^{N_w}}{N_w!}\int d\{N\}e^{-\beta U_N}, \end{aligned} \tag{5.7}$$

where χ is defined by

$$\chi = \frac{q_b q_h}{q_s q_w}\frac{\Lambda_s^3\Lambda_w^3}{\Lambda_b^3\Lambda_h^3}. \tag{5.8}$$

Clearly, $-k_BT\log\chi$ is the free energy of the reaction

$$H_2SO_4 + H_2O \rightarrow HSO_4^- + H_3O^+, \tag{5.9}$$

where each molecule is considered to be isolated in vacuum.

If the summation with respect to N_i in Eq. (5.7) is to be evaluated directly in a single simulation, it must be possible to replace a sulfuric acid-water neutral pair with a bisulfate-hydronium ion pair via a trial move in Monte Carlo simulation. This trial move, however, will almost certainly be rejected since it will seriously disturb the hydrogen bond network in the cluster, costing a very high energy. Instead, each term in the summation over N_i must be calculated separately. In particular, the simulation focuses on evaluating the expression

$$\Xi_w^c(\beta,V,\mu_w,N_a^c,N_i) \equiv \sum_{N_w=0}^{\infty}\frac{z_w^{N_w}}{N_w!}\int d\{N\}e^{-\beta U_N} \tag{5.10}$$

for each value of N_i, the number of the ion pairs in the system. Except for the analytically tractable factors, Ξ_w^c is the partition function in the mixed ensemble of an N_a^c-cluster whose dissociation state is specified by N_i. Eq. (5.10) cannot be evaluated in a single simulation. Instead, it must be evaluated by means of a thermodynamic integration.[47] An expression for

$\Xi_w^c(\beta, V, \mu_w, N_a^c, N_i)$ convenient for this purpose is derived in Appendix G. Using Eq. (G48) in Eq. (5.7), we obtain

$$\begin{aligned}
&\Xi^c(\beta, V, \mu_w, \mu_s; N_a^c) \\
&= e^{(n_s+n_w)V}(n_s V)^{N_a^c} \sum_{N_i=0}^{N_a^c} \frac{n_w^{N_i}}{N_i!(N_a^c - N_i)!} \left[\frac{\chi}{\Omega}\int d1\, e^{-\beta u_{hb}(1)}\right]^{N_i} \\
&\times \exp\left\{-\int_{\beta_0}^{\beta} [< U_N >_{n_{w0}} - N_i < u_{hb} >]\, d\beta \right. \\
&\qquad \left. + \int_{\log n_{w0}}^{\log n_w} [< N_w >_\beta - n_w V]\, d\log n_w \right\},
\end{aligned} \tag{5.11}$$

which, when substituted into Eq. (5.2) along with Eq. (5.3), yields

$$e^{-\beta W^{rev}(\beta,V,\mu_w,\mu_s;N_a^c)} = (n_s V)^{N_a^c} \sum_{N_i=0}^{N_a^c} e^{-\beta\phi(\beta,V,\mu_w,N_a^c,N_i)}, \tag{5.12}$$

where we define

$$\begin{aligned}
&\beta\phi(\beta, V, \mu_w, N_a^c, N_i) \\
\equiv\ & -\log \frac{n_w^{N_i}}{N_i!(N_a^c - N_i)!} + \beta N_i f_{hb}(\beta) \\
&+ \int_{\beta_0}^{\beta} [< U_N >_{n_{w0}} - N_i < u_{hb} >]\, d\beta - \int_{\log n_{w0}}^{\log n_w} [< N_w >_\beta - n_w V]\, d\log n_w,
\end{aligned} \tag{5.13}$$

where β_0 is chosen to be sufficiently small that the system can be regarded as an ideal gas composed of water, sulfuric acid, and bisulfate-hydronium ion pairs. n_{w0} is the smallest of the number density of water molecules in vapor that we are interested in and u_{hb} is the intermolecular potential between HSO_4^- and H_3O^+. The thermal average $< \cdots >_x$ is evaluated at a fixed value of x, which remains constant along the integration path. The thermal average $< u_{hb} >$ is calculated in the canonical ensemble of a single $HSO_4^- \cdot H_3O^+$ ion pair. $f_{hb}(\beta)$ is the free energy required to make the ion pair in the system from sulfuric acid and water forming an ideal gas confined in the unit volume at β and is defined through the relation

$$e^{-\beta f_{hb}(\beta)} \equiv \frac{\chi}{\Omega}\int d1 e^{-\beta u_{hb}(1)}. \tag{5.14}$$

When n_w is expressed in $Å^{-3}$, the distance in the integral of Eq. (5.14) has to be measured in Å so that Eq. (5.13) is dimensionally consistent.

5.4 Reversible Work Surface and the Cluster Size Distribution

In the previous section, a cluster is characterized by N_a^c alone. In classical nucleation theory, however, it is customary to characterize a cluster by both N_a^c and N_w^c. To obtain the expression for the reversible work to form this (N_a^c, N_w^c)-cluster, we must first specify how to define N_w^c for a particular configuration of molecules in the system. Let us consider an excess quantity defined by

$$N_w^{ex} \equiv N_w - n_w V, \tag{5.15}$$

which is zero for a uniform vapor. However, during a simulation in the mixed ensemble, N_w, and hence N_w^{ex}, fluctuates. For a macroscopic V, this fluctuation arises primarily from that due to the vapor molecules. Fluctuations of this kind have very little to do with the nucleation process and should not be counted as part of a cluster. In the mixed ensemble, however, their effect on N_w^{ex} can be made negligible by decreasing the volume until it satisfies

$$n_w V \ll 1. \tag{5.16}$$

In this limit, the system contains, on average, no vapor molecule. In fact, the probability of finding at least one vapor molecule of water in the system is, assuming the ideal gas behavior of the vapor phase, given by $1 - e^{-n_w V} \approx n_w V$, which is negligible as a result of Eq. (5.16). Thus, one can attribute the non-zero value of N_w^{ex} to the presence of a cluster, which suggests that one may define

$$\begin{aligned} N_w^c &\equiv N_w^{ex} + N_i \\ &= N_w + N_i - n_w V, \end{aligned} \tag{5.17}$$

where we include hydronium ions in the definition since the ions are formed from water. In view of Eq. (5.16), we may redefine N_w^c by

$$N_w^c \equiv N_w + N_i, \tag{5.18}$$

namely, all the water molecules, whether or not protonated, in the system can be regarded as a part of the cluster. The (N_a^c, N_w^c)-cluster thus defined is a physical cluster in the sense that it represents density fluctuations relevant in nucleation.[99]

We note that the clusters generated in simulation are consistent with an intuitive definition of clusters. To see this, note that, except when $N_w^c = 0$, N_w^c is always larger than $n_w V (\ll 1)$, the average number of water molecules in V when filled with the uniform vapor. Thus, on average, any attempted Monte Carlo move to create a molecule in the system will be accepted with higher probability if the newly created molecule interacts more favorably with the rest of the molecules, while as soon as a molecule evaporates from the cluster, it is more likely to be removed from the system upon its trial annihilation.

Some words on V are in order. Clearly, V has to be larger than the spatial extent of a cluster in it. That the system is microscopic does not affect the applicability of the statistical mechanical description. It is sufficient to assume a weak coupling between the system and its surroundings.[94] Both conditions are trivially satisfied in the present case of vapor to liquid nucleation, where the molar volume in the vapor phase is considerably larger than a physical dimension of the cluster and the interaction between the vapor molecules and a cluster can be ignored.

The expression for the reversible work to form an (N_a^c, N_w^c)-cluster can be easily obtained. In fact, the grand canonical partition function Ξ^c of the (N_a^c, N_w^c)-cluster is obtained from Eq. (5.7) by keeping only the term $N_w = N_w^c - N_i$ in the sum over N_w. Thus,

$$\begin{aligned}
& \Xi^c(\beta, V, \mu_w, \mu_s; N_a^c, N_w^c) \\
= \; & e^{n_s V} \left(\frac{q_s e^{\beta \mu_s}}{\Lambda_s^3} \right)^{N_a^c} \sum_{N_i=0}^{N_a^c} \frac{\chi^{N_i}}{(N_a^c - N_i)! N_i!} \frac{z_w^{N_i}}{N_i!} \frac{z_w^{N_w}}{N_w!} \int d\{N\} e^{-\beta U_N} \\
= \; & e^{n_s V} \left(\frac{q_s e^{\beta \mu_s}}{\Lambda_s^3} \right)^{N_a^c} \sum_{N_i=0}^{N_a^c} \frac{\chi^{N_i}}{(N_a^c - N_i)! N_i!} \frac{z_w^{N_i}}{N_i!} \\
& \times \Xi_w^c(\beta, V, \mu_w, N_a^c, N_i) p(\beta, V, \mu_w, N_a^c, N_i, N_w^c - N_i),
\end{aligned} \tag{5.19}$$

where p is defined by

$$p(\beta, V, \mu_w, N_a^c, N_i, N_w) \equiv \frac{\frac{{z_w}^{N_w}}{N_w!} \int d\{N\} e^{-\beta U_N}}{\sum_{N_w=0}^{\infty} \frac{{z_w}^{N_w}}{N_w!} \int d\{N\} e^{-\beta U_N}}, \tag{5.20}$$

which is the normalized probability of finding N_w water molecules in the system containing N_a^c acid molecules, N_i of which are ions, and is directly obtained from a single simulation. Since Eq. (5.19) differs from Eq. (5.7) only by a factor of p, one can obtain the desired

expression from Eq.(5.12):

$$\begin{aligned} & e^{-\beta W^{rev}(\beta,V,\mu_w,\mu_s;N_a^c,N_w^c)} \\ = \; & (n_s V)^{N_a^c} \sum_{N_i=0}^{N_a^c} e^{-\beta\phi(\beta,V,\mu_w,N_a^c,N_i)} p(\beta,V,\mu_w,N_a^c,N_i,N_w^c-N_i). \end{aligned} \tag{5.21}$$

The equilibrium cluster size distribution $c(\beta,\mu_w,\mu_s,N_a^c,N_w^c)$ can be obtained as follows. Suppose that the entire vapor phase of volume V_{tot} is divided into small cells of volume V. Because of Eq. (5.16) and $n_s \ll n_w$, most of the cells contain no molecules at all and those containing a cluster or a monomer are on average spatially distant. Thus, one can assume that all of the cells are statistically independent. Then, the average total number of the (N_a^c,N_w^c)-clusters in V_{tot} is given by

$$\frac{V_{tot}\,\Xi^c(\beta,V,\mu_w,\mu_s;N_a^c,N_w^c)}{V\,\Xi(\beta,V,\mu_w,\mu_s)}, \tag{5.22}$$

where Ξ is the grand canonical partition function of the system of volume V taken in the vapor. In calculating Ξ, all the possible microstates consistent with the metastable state have to be accounted for. However, since the system contains no molecules at all for most of the time, it can be approximated as ideal gas:

$$\Xi(\beta,V,\mu_w,\mu_s) \approx \Xi^r(\beta,V,\mu_w,\mu_s). \tag{5.23}$$

When divided by V_{tot}, the expression Eq. (5.22) becomes

$$c(\beta,\mu_w,\mu_s,N_a^c,N_w^c) = \frac{e^{-\beta W^{rev}(\beta,V,\mu_w,\mu_s;N_a^c,N_w^c)}}{V}, \tag{5.24}$$

where we used Eq. (5.2). As Eq. (5.2) indicates, $e^{-\beta W^{rev}}$ is the probability of finding the (N_a^c,N_w^c)-cluster in the system relative to the reference state. Since the cluster can be found anywhere in the system and the event of finding it at one place or another is mutually exclusive, $e^{-\beta W^{rev}}$ is proportional to V, indicating that c is independent of volume as required.

Finally, we address a consistency issue. Strictly speaking, neither (0,1)-cluster nor (1,0)-cluster is a vapor monomer of water or acid molecule, respectively, since these clusters exclude water vapor from the system of volume V because of the definition Eq. (5.18),

while the monomers do not. In fact, one can readily show that

$$c(1,0) = n_s e^{-n_w V}, \tag{5.25}$$

where the term for $N_i = 1$ is ignored in Eq. (5.19), and that

$$c(0,1) = n_w e^{-n_w V}. \tag{5.26}$$

However, this distinction is completely insignificant since $e^{-n_w V} \approx 1$. Alternatively, one can consistently recover the monomer densities by setting $V = 0$ in Eqs. (5.25) and (5.26).

5.5 Details of the Simulation

First, we briefly describe some of the details of the simulation. The system is defined as a spherical cavity of radius 50 Å. We studied the clusters of $N_a^c = 1, 2, 3$. As pointed out in Sec. 5.3, for a given value of N_a^c, there are $N_a^c + 1$ clusters to be simulated separately corresponding to the different dissociation states defined by N_i. Thus, there are nine clusters in total. For each of the clusters, the initial configuration of the molecules is created as follows. The sulfur site of a sulfuric acid molecule or a bisulfate ion is placed at the center of the cavity and the rest of the molecules, including a certain number of water molecules, are placed randomly inside the system. After sufficient equilibration at $T = 303.15$ K and $n_w = 0.1048 \times 10^{-6}$Å^{-3}, corresponding to a relative humidity of about 10% if the actual vapor pressure of water is used,[164] the configuration is used as the initial configuration for the simulations at the nearby values of T and n_w. The process is repeated to obtain the initial configuration of the whole range of T and n_w studied. After equilibration, which typically takes $10^5 - 10^6$ Monte Carlo steps, N_w and U_N are sampled for about $10^7 - 10^9$ Monte Carlo steps. Sampling is made every 10^3 steps for short runs and every 10^4 steps for long runs. Here, one Monte Carlo move consists of (i) trial random translation and rotation of molecules in the system and (ii) one trial grand canonical move, namely a trial creation or annihilation of a water molecule. Molecules to be moved are chosen randomly so that each molecule is picked up once per Monte Carlo step on average. The maximum displacement for a trial translation and the maximum angle for a trial rotation are tuned during the simulation so that the acceptance ratio, defined as the ratio between the number

Table 5.8: Conditions of the simulation. T=298.15 K

No.	n_w [Å^{-3}]	n_wV	Relative humidity [%][a]
S1	0.1048×10^{-6}	0.5487×10^{-1}	13.65
S2	0.2×10^{-6}	0.1047	26.06
S3	0.3×10^{-6}	0.1571	39.08
S4	0.3839×10^{-6}	0.2010	50.01
S5	0.5×10^{-6}	0.2618	65.13
S6	0.6×10^{-6}	0.3142	78.17

[a]Saturation pressure of water is assumed to be 23.71 mmHg.[164]

of accepted trial moves and the total number of the trial moves, stays around 50%. As discussed in Appendix H, a molecule at the center of the system undergoes rotation only.

To evaluate the temperature integration in Eq. (5.13), simulation is performed at 298.15 K and higher temperatures, the highest of which is chosen so that the integrand $[< U_N >_{n_{w0}} - N_i < u_{hb} >]$ is negligible at this temperature and depends on the values of both N_a^c and N_i. For example, it is 500 K for $(N_a^c, N_i) = (1, 0)$, while 2400 K for $(N_a^c, N_i) = (3, 3)$. Also, $n_{w0} = 0.1048 \times 10^{-6}$Å^{-3}. In evaluating the second integral of Eq. (5.13), simulation is carried out at $n_w = 0.1048 \times 10^{-6}$, 0.2×10^{-6}, 0.3×10^{-6}, 0.3839×10^{-6}, 0.5×10^{-6}, and 0.6×10^{-6} Å^{-3} as summarized in Table 5.8.

Further technical details of the simulation is discussed in Appendices G—I. In Appendix G, a criterion is discussed on the adequacy of the number of intermediate points used to evaluate the thermodynamic integrations. In Appendix H, a criterion in choosing the system volume V is discussed from a point of view somewhat different from that of Lee *et al.*[91] Finally, under a reasonable approximation, one can dispense with the integration with respect to n_w indicated in Eq. (5.13), which results in the improvement of the computational efficiency by a factor of several. The method is discussed in Appendix I.

5.6 Results and Discussion

5.6.1 Shape of the clusters

Snapshots[98] of the clusters are shown in Figs. 5.2—5.7, where sulfur sites, oxygen sites, and hydrogen sites are colored red, dark blue, and white, respectively. Fig. 5.2 shows a hydrate of a sulfuric acid molecule, in which a loop of hydrogen bonds is formed from the H_1 site to

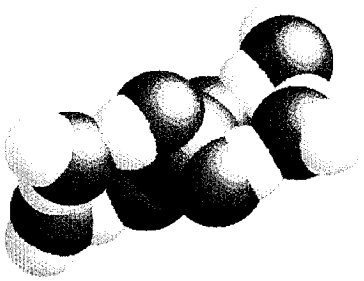

Figure 5.2: A cluster with $N_a^c = 1, N_i = 0$ at $T = 298.15$ K and $n_w = 0.6 \times 10^{-6}$ Å^{-3}.

the O_2 site of the acid with two water molecules, similarly for $H_1\prime$ to $O_2\prime$. In hydrates with fewer water molecules, the hydrogen bonds are formed preferentially from the H_1 and $H_1\prime$ protons to oxygens of water molecules. One end of the hydrogen from a water attached to the H_1 site, for example, forms a distant hydrogen bond to the O_2 site.

Figures 5.3, 5.4, and 5.5 show clusters with two sulfuric acid molecules. Note that the acid molecules directly form two hydrogen bonds in Fig. 5.3, while one of them is mediated by a water molecule in Fig. 5.4. Around room temperature and at all values of n_w investigated in this work, these two configurations are representative of the connectivity of the acid molecules. Since interconversion of these two conformations requires one or two hydrogen bonds to be broken first, the Monte Carlo lifetimes of the conformations are fairly long, being of the order of 10^7 steps. As the value of n_w is increased, configurations similar to Fig. 5.4 become more probable than those similar to Fig. 5.3. The configuration in Fig. 5.5 can be regarded as an intermediate between those two. Note that $N_w^c = 5$ in both Figs. 5.3 and 5.4. However, it is unlikely that interconversion between these two conformations occurs in a canonical simulation since it would involve diffusion of a water molecule over several Angstroms on the cluster surface where no favorable interaction site exists. This shows a clear advantage of the mixed ensemble simulation over a conventional one in a canonical

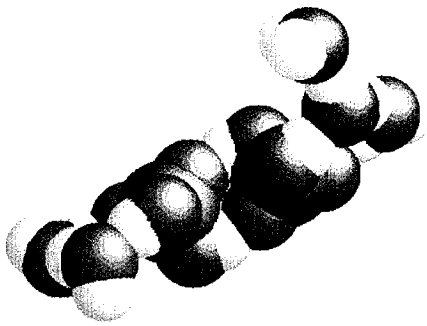

Figure 5.3: A cluster with $N_a^c = 2, N_i = 0$ at $T = 298.15$ K and $n_w = 0.5 \times 10^{-6}$ Å^{-3}.

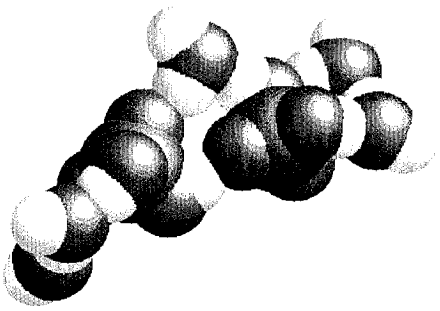

Figure 5.4: A cluster with $N_a^c = 2, N_i = 0$ at $T = 298.15$ K and $n_w = 0.6 \times 10^{-6}$ Å^{-3}.

Figure 5.5: A cluster with $N_a^c = 2, N_i = 0$ at $T = 298.15$ K and $n_w = 0.6 \times 10^{-6}$ Å^{-3}.

ensemble. This effectiveness in sampling very different relevant configurations has been stressed in a simulation work that determines the solvation shell structure of protein and nucleic acid,[165] for example.

Similar connectivity is observed in Fig. 5.6 for clusters with three sulfuric acid molecules. An additional complication arises in this case, however, since the acid molecules can now form a ring (Fig. 5.7). As is seen from Figs. 5.6 and 5.7, acid molecules in the ring conformation tend to form hydrogen bonds preferentially with water molecules than among themselves in comparison to those in the linear conformation, leading to larger clusters. Since both conformations are observed in the simulation, the corresponding free energies are expected to be close, the difference being the order of $k_B T$. To understand its implication, we monitored the quantity

$$\beta W \equiv \beta U_N - \log \frac{(n_w V)^{N_w}}{N_w!}, \tag{5.27}$$

which plays the same role as βU_N in a canonical ensemble in that the statistical weight of a given microstate is proportional to $e^{-\beta W}$. The data from simulation of 7×10^8 Monte Carlo steps were divided into small blocks, each of which corresponding to 10^7 Monte Carlo

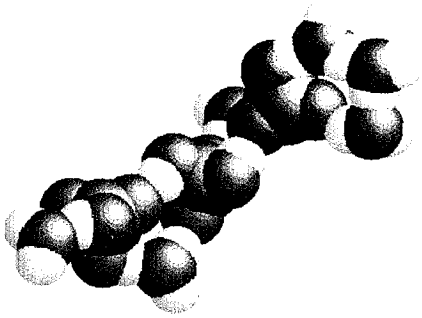

Figure 5.6: A cluster with $N_a^c = 3, N_i = 0$ at $T = 298.15$ K and $n_w = 0.6 \times 10^{-6}$ Å^{-3} showing a linear conformation.

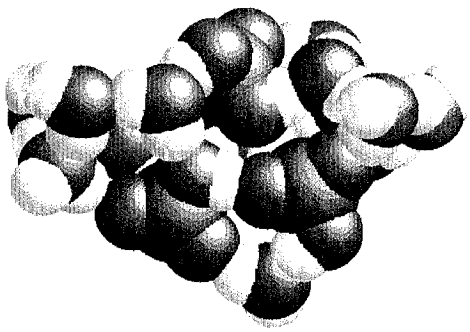

Figure 5.7: A cluster with $N_a^c = 3, N_i = 0$ at $T = 298.15$ K and $n_w = 0.6 \times 10^{-6}$ Å^{-3} showing a ring conformation.

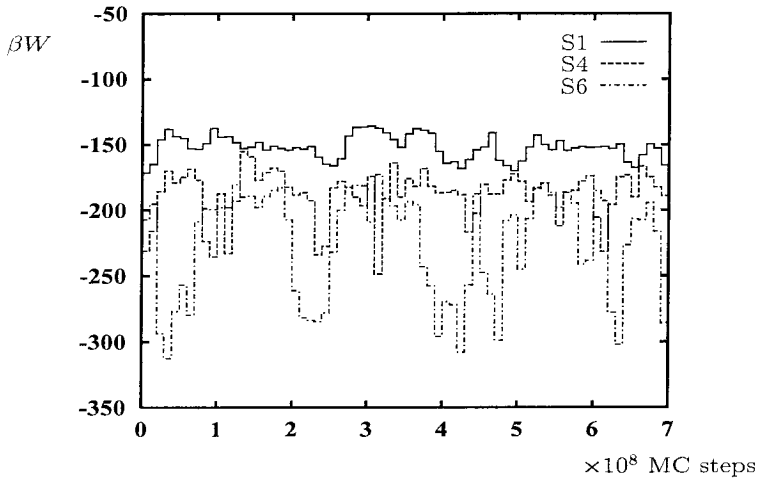

Figure 5.8: The change in the block average of βW. The size of each block is 10^7 MC steps. The conditions of simulation for S1, S4, and S6 are given in Table 5.8.

steps, and the average of βW was calculated for each block. Fig. 5.8 shows the variation of this block average of βW for three values of n_w. Larger, i.e., less negative, values of βW correspond to the linear conformation while the smaller values of βW correspond to the ring conformation. Despite the large difference in βW, both linear and ring conformations are observed. This means that the ring conformation is entropically unfavorable since it attracts more water molecules, confining them to a far smaller volume than V. As these water molecules evaporate, the cluster returns to the linear conformation. From Fig. 5.8, it is clear that additional Monte Carlo steps are required to achieve good statistics. Nonetheless, qualitative trends are already present. For example, the ring conformation appears more frequently as n_w is increased.

None of the clusters shown here possesses a spherical or an axial symmetry. Given the fairly long lifetime of each conformation of the clusters, the same is expected to be true even after the thermal average is taken. Thus, the thermodynamic description of the clusters is no longer amenable to Gibbs' prescription.[5] In particular, the thermodynamic quantities cannot be classified into extensive and intensive ones, which is a prerequisite in deriving the familiar Gibbs-Duhem relation, for example. It seems hardly profitable to try to extend Gibbs' interfacial thermodynamics to include such cases, since the quantities introduced into such a theory are unlikely to be subject to experimental measurement. This in turn highlights the importance of the molecular level approach.

Table 5.9: Heat of formation.

molecule	ΔH_f [kcal/mol]
H_2O [a]	− 57.80
H_2SO_4 [b]	-175.67 ± 1.912
H_3O^+ [b]	142 ± 1
HSO_4^- [b]	-227.77 ± 4.063

[a]Prigogine and Defay[166]
[b]Lias *et al.*[167]

5.6.2 Estimate of the value of f_{hb}

To evaluate the reversible work to form an N_a^c-cluster or an (N_a^c, N_w^c)-cluster, from Eqs. (5.12) or (5.21), the value of f_{hb} defined by Eq. (5.14) is required. Using the heat of formation of the molecules given in Table 5.9 and ignoring the entropic effect, we obtain

$$-k_B T \log \chi \approx 147.70 \pm 6.98 \qquad \text{kcal/mol.} \tag{5.28}$$

To evaluate the remaining factor in Eq. (5.14), we introduce the approximation

$$\frac{1}{\Omega} \int d1 e^{-\beta u_{hb}(1)} \approx \frac{v_f \omega_f}{\Omega} e^{-\beta < u_{hb} >}, \tag{5.29}$$

where v_f and ω_f respectively denote the volume and the solid angle over which H_3O^+ can fluctuate with respect to HSO_4^-. We approximate their values as the cubic of the maximum displacement and angle used for the trial Monte Carlo move. Then

$$\begin{aligned} v_f &\approx 0.25^3 \text{Å}^3 \\ \omega_f &\approx 0.3^3. \end{aligned} \tag{5.30}$$

From simulation, $< u_{hb} >= 135.04 \pm 0.01$ kcal/mol at $T = 298.15$ K. Since Å^3 in v_f cancels out Å^{-3} of n_w in Eq. (5.13), we can omit the unit of volume here to obtain

$$-k_B T \log \frac{1}{\Omega} \int d1 e^{-\beta u_{hb}(1)} \approx -127.85 \pm 0.01 \qquad \text{kcal/mol.} \tag{5.31}$$

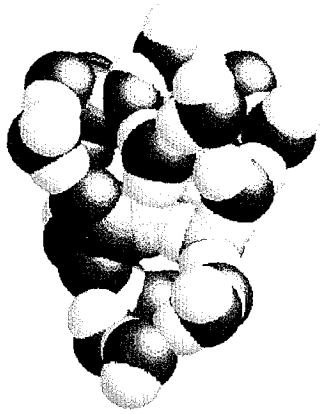

Figure 5.9: A cluster with $N_a^c = 2, N_i = 1$ at $T = 298.15$ K and $n_w = 0.6 \times 10^{-6}$ Å^{-3}.

Combining Eqs. (5.28) and (5.31), we obtain

$$f_{hb} \approx 19.85 \pm 6.99 \qquad \text{kcal/mol.} \tag{5.32}$$

In what follows, we adopt 20 kcal/mol as the value of f_{hb}. At $T = 298.15$ K, the indicated uncertainty in this quantity is as large as $12k_BT$. Effects of this uncertainty will be addressed subsequently.

5.6.3 Dissociation of H_2SO_4 in a cluster

Snapshots of clusters containing a $HSO_4^- \cdot H_3O^+$ ion pair are shown in Figs. 5.9 and 5.10, in which atomic sites are colored as before with the exceptions for the O_1 site of bisulfate ion and the oxygen site of hydronium ion, which are, respectively, colored green and light blue. In Fig. 5.9, a hydrogen from H_3O^+ forms a hydrogen bond directly to the O_1 site of HSO_4^-, while in Fig. 5.10, H_3O^+ forms hydrogen bonds to oxygen sites of H_2O and H_2SO_4. In both clusters, however, there is no intervening molecule between the ion pair. The same holds true for ion pairs buried in 97 water molecules as shown in Fig. 5.11. The water molecules start to intervene in the ion pairs as the number of water molecules exceeds about 240 as

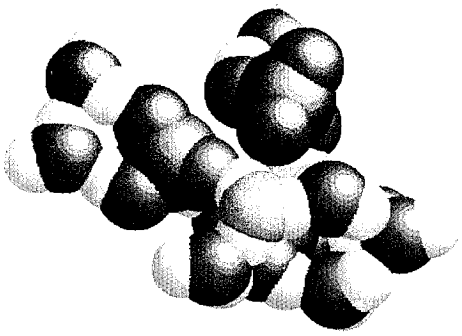

Figure 5.10: A cluster with $N_a^c = 3, N_i = 1$ at $T = 298.15$ K and $n_w = 0.3839 \times 10^{-6}$ Å^{-3}.

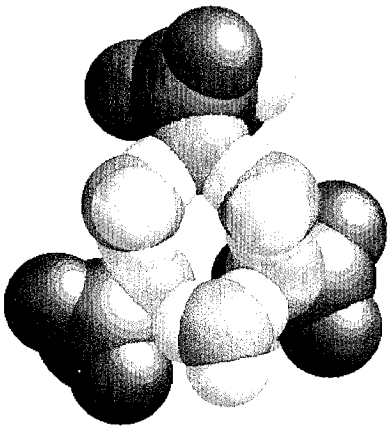

Figure 5.11: Ion pairs forming a core inside the cluster with $N_w^c = 97$. $N_a^c = 3$, $N_i = 3$ at $T = 298.15$ K and $n_w = 0.6 \times 10^{-6}$ Å^{-3}. Water molecules are not shown.

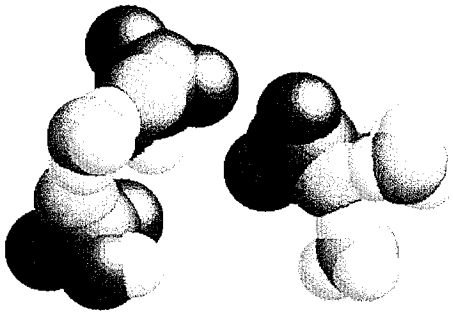

Figure 5.12: Ion pairs forming a core inside the cluster with $N_w^c = 243$. $N_a^c = 3$, $N_i = 3$ at $T = 298.15$ K and $n_w = 0.6 \times 10^{-6}$ Å^{-3}. Water molecules are not shown.

shown in Fig. 5.12. Thus our simulation suggests that, as far as the dissociation behavior of H_2SO_4 is concerned, at least about 240 water molecules are required to attain a behavior that resembles the bulk solution.

The fact that there is no separation of ion pairs in a small cluster does not imply that dissociation is not important in the cluster. As an $H_2SO_4 \cdot H_2O$ neutral dimer dissociates to an $HSO_4^- \cdot H_3O^+$ ion pair, its net dipole moment increases to attract more water molecules. (If these dimers are placed in vacuum, the dipole moment changes from 3.28 Debye to 12.0 Debye at 298.15 K upon dissociation.) Consequently, the potential energy of the cluster decreases. Whether or not dissociation occurs in a given N_a^c-cluster is determined by the free energy $\phi(N_a^c, N_i)$, defined by Eq. (5.13), of the cluster as a function of N_i. The quantity is shown in Fig. 5.13 for the case of $N_a^c = 3$ at $T = 298.15$ K for three values of n_w. Clearly, dissociation occurs for all cases. The increase in $\beta\phi$ is observed as N_i changes from 0 to 1 when $n_w = 0.1048 \times 10^{-6}$ Å^{-3}, reflecting the fact that the ion pair cannot attract sufficient water molecules when placed in vapor with such a low water concentration. If 27 kcal/mol is assumed for the value of f_{hb}, however, we find that dissociation no longer occurs for this N_a^c-cluster (Fig. 5.14). This change at the qualitative level points to the necessity of a more

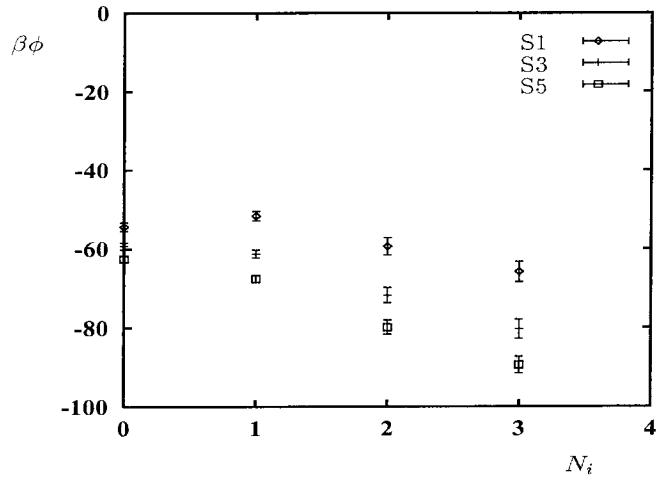

Figure 5.13: Free energy of the N_a^c-cluster as a function of the dissociation state defined by N_i. $N_a^c = 3$ and $T = 298.15$ K. f_{hb}=20 kcal/mol. The conditions of simulation for S1, S3, and S5 are given in Table 5.8.

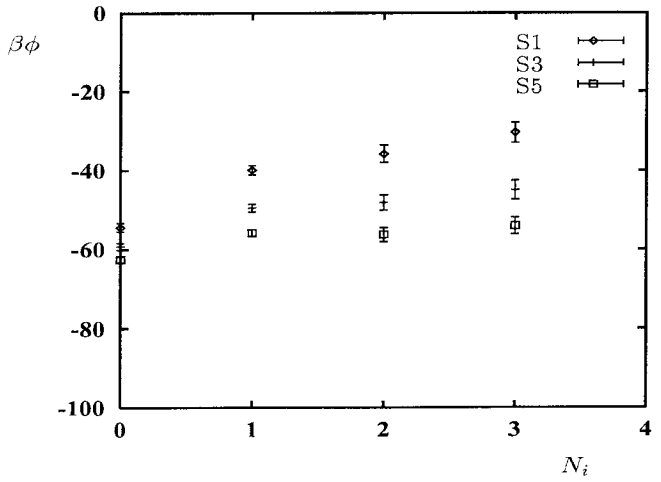

Figure 5.14: Free energy of the N_a^c-cluster as a function of the dissociation state defined by N_i. $N_a^c = 3$ and $T = 298.15$ K. f_{hb}=27 kcal/mol. The conditions of simulation for S1, S3, and S5 are given in Table 5.8.

accurate estimate of the value f_{hb}.

5.6.4 Effect of hydration

In Eqs. (5.12) and (5.21), n_s represents the number density of unhydrated sulfuric acid molecules in accordance with the choice of our reference state in calculating the reversible work. In reality, however, most acid molecules exist as hydrates and one can specify only the total number density n_s^{tot}. Thus, we must express n_s in terms of n_s^{tot}. The derivation given here is analogous to the corresponding one in classical theory.[109, 113, 117]

Since a given acid molecule is either hydrated or unhydrated regardless of its dissociation state, we have

$$n_s^{tot} = \sum_{N_a^c=1} \sum_{N_w^c} N_a^c \, c(N_a^c, N_w^c). \tag{5.33}$$

From Eqs. (5.21) and (5.24), we obtain

$$n_s^{tot} = \frac{1}{V} \sum_{N_a^c=1} N_a^c \, (n_s V)^{N_a^c} \sum_{N_i=0}^{N_a^c} e^{-\beta\phi(N_a^c, N_i)}, \tag{5.34}$$

where we have made use of the normalization condition

$$\sum_{N_w=0} p(\beta, V, \mu_w, N_a^c, N_i, N_w) = 1. \tag{5.35}$$

Assuming that the hydrates are dominated by those containing only one acid molecule ($N_a^c = 1$), we find that

$$\begin{aligned} p_0 &\equiv \frac{n_s}{n_s^{tot}} \\ &\approx \left[\sum_{N_i=0}^{1} e^{-\beta\phi(1, N_i)} \right]^{-1}. \end{aligned} \tag{5.36}$$

In the following, we assume that $n_s^{tot} = 0.1 \times 10^{-13} \text{Å}^{-3}$, which is typical of experiment in H_2SO_4/H_2O binary nucleation.[127]

5.6.5 Reversible work of cluster formation and comparison with classical predictions

Recall that the cluster size distribution is given in the classical nucleation theory by

$$c(N_a^c, N_w^c) = n_w \exp[-\beta W^{classical}(N_a^c, N_w^c)], \tag{5.37}$$

where $W^{classical}$ is the reversible work of cluster formation evaluated by the classical theory. Thus, rewriting Eq. (5.24) as

$$c(N_a^c, N_w^c) = n_w \exp[-\beta W^{rev}(N_a^c, N_w^c) - \log(n_w V)], \tag{5.38}$$

we find that a sensible comparison is made between our molecular theory and the classical by comparing the quantity defined by

$$\beta w^{REV(N_a^c, N_w^c)} \equiv \beta W^{rev}(N_a^c, N_w^c) + \log(n_w V) \tag{5.39}$$

against $\beta W^{classical}(N_a^c, N_w^c)$. Similar quantities can be defined for an N_a^c-cluster by summation with respect to N_w^c of Eqs. (5.37) and (5.38). Thus, we compare $W^{classical}(N_a^c)$ defined by

$$\exp[-\beta W^{classical}(N_a^c)] \equiv \sum_{N_w^c=0}^{\infty} \exp[-\beta W^{classical}(N_a^c, N_w^c)] \tag{5.40}$$

with $w^{REV}(N_a^c)$ defined by

$$\exp[-\beta w^{REV}(N_a^c)] \equiv \sum_{N_w^c=0}^{\infty} \exp[-\beta w^{REV}(N_a^c, N_w^c)]. \tag{5.41}$$

The upper limit (∞) of the summation is only formal since the summand decays quickly as N_w^c is increased when the relative humidity is less than 100%.

Figure 5.15 compares the reversible work βw^{REV} of the N_a^c-cluster formation obtained by assuming the value of 20 kcal/mol for f_{hb} with $\beta W^{classical}$ obtained by the classical theory.[168] While classical theory predicts that a 3-cluster is still subcritical, our simulation predicts that a 2-cluster is the critical nucleus for conditions S1 to S4 and that βw^{REV} decreases monotonically with N_a^c for conditions S5 and S6. (See Table 5.8.) This means that the rate-limiting step of new particle formation is the binary collision of sulfuric acid

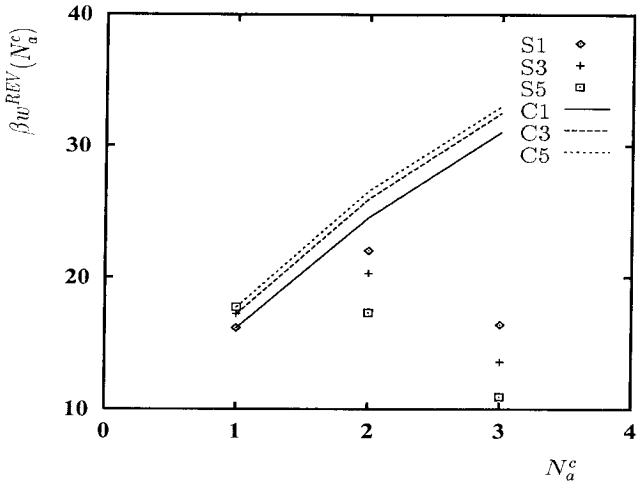

Figure 5.15: Reversible work of N_a^c-cluster formation at $T = 298.15$ K. Calculated with $f_{hb} = 20$ kcal/mol. The conditions of simulation for S1, S3, and S5 are given in Table 5.8. C1 shows the classical prediction under the condition S1. Similarly for C3 and C5.

molecules. Note that classical theory predicts that $\beta W^{classical}$ increases as n_w is increased. This trend reflects the fact that a higher value of n_w results in more significant depletion of the acid molecules and reverses as N_a^c becomes large enough so that the cluster is a critical nucleus. When 27 kcal/mol is employed for the value of f_{hb}, the results of our simulation become more or less comparable with the classical prediction as shown in Fig. 5.16. This indicates that the large discrepancy between the molecular theory and the classical as observed in Fig. 5.15 arises from the difference in the behavior of a cluster involving the $HSO_4^- \cdot H_3O^+$ ion pairs.

To obtain more detailed information regarding the clusters with ion pairs, we calculated βw^{REV} of the (N_a^c, N_w^c)-cluster formation for the condition S3. The results are shown in Figs. 5.17 and 5.18 for the case of $f_{hb} = 20$ kcal/mol and 27 kcal/mol, respectively. Figures 5.17 and 5.18 also compare the simulation against the classical prediction. For small values of N_w^c the agreement is surprisingly good. Figure 5.17 shows a double minimum in the reversible work. The minimum for the larger values of N_w^c corresponds to the clusters with ion pairs, while the contribution to the minimum for the smaller values of N_w^c arises from the undissociated states, since the $HSO_4^- \cdot H_3O^+$ ion pair has a larger dipole moment than the $H_2SO_4 \cdot H_2O$ neutral dimer and hence can attract more water molecules (as discussed in Sec. 5.6.3). From Fig. 5.17, the dominant cluster for the case of $N_a^c = 1$ is the (1,4)-cluster. If two (1,4)-cluster collide without losing a water molecule, the resulting (2,8)-cluster is

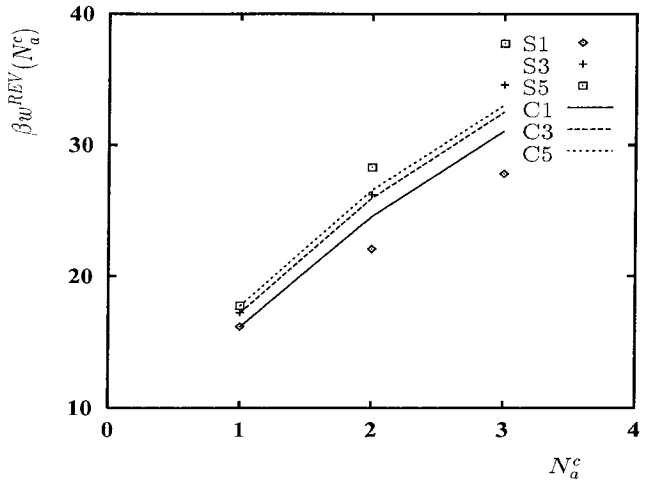

Figure 5.16: Reversible work of N_a^c-cluster formation at $T = 298.15$ K. Calculated with $f_{hb} = 27$ kcal/mol. The conditions of simulation for S1, S3, and S5 are given in Table 5.8. C1 shows the classical prediction under the condition S1. Similarly for C3 and C5.

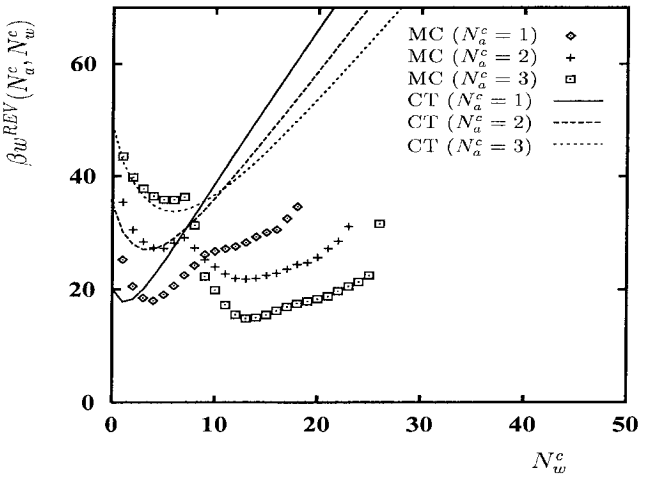

Figure 5.17: Reversible work of (N_a^c, N_w^c)-cluster formation at $T = 298.15$ K and $n_w = 0.3 \times 10^{-6}$ Å^{-3}. Calculated with $f_{hb} = 20$ kcal/mol. CT and MC denote the classical prediction and the results of simulation, respectively.

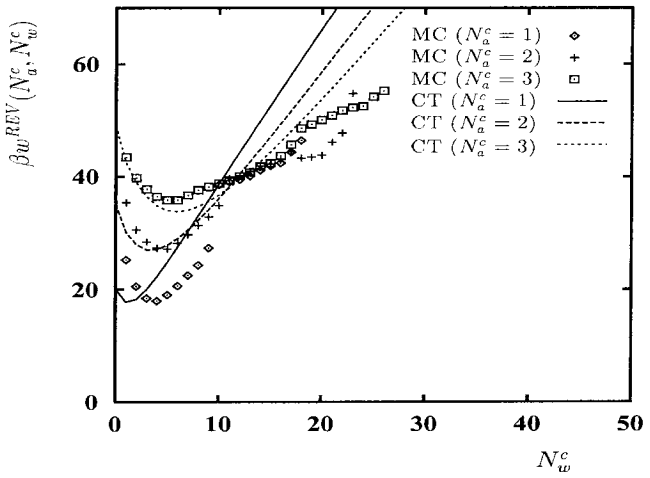

Figure 5.18: Reversible work of (N_a^c, N_w^c)-cluster formation at $T = 298.15$ K and $n_w = 0.3 \times 10^{-6}$ Å^{-3}. Calculated with $f_{hb} = 27$ kcal/mol. CT and MC denote the classical prediction and the results of simulation, respectively.

already in the state with one or two dissociated acid molecules, and hence can attract more water molecule to form a stable cluster. Figure 5.17 further indicates that, upon acquiring one more sulfuric acid molecule, even more stable cluster results. We note that the most probable number of water molecule in 3-cluster is comparable with that in 2-cluster. This means that some of the water molecules have to evaporate after 2-cluster captures an acid hydrate. When f_{hb} is increased from 20 kcal/mol to 27 kcal/mol to reflect its uncertainty, the resulting reversible work surface changes markedly and our simulation becomes more or less comparable with the classical prediction. This sensitivity to f_{hb} again stresses the importance of the accurate estimation of this quantity.

Next, we draw attention to the distribution of acid hydrates, for which $N_a^c = 1$. Both Figs. 5.17 and 5.18 show that the dominant hydrates contain four water molecules, which is larger than the classical prediction of two hydrating water molecules at relative humidity less than 100%.[109, 113, 114] To identify the origin of this discrepancy, we calculated the average interaction energy of the $H_2SO_4 \cdot H_2O$ dimer at $T = 298.15$ K and obtained -13.7 kcal/mol, which is 0.9 kcal/mol lower than the classical prediction of the first hydration enthalpy (-12.8 kcal/mol) estimated by Mirabel and Ponche.[108] This difference of 0.9 kcal/mol is far from insignificant. For example, Fig. 5.19 compares the result of the simulation and the classical predication on the fraction of unhydrated acid molecules p_0 given by Eq. (5.36). Clearly, our simulation predicts far more significant depletion of the unhydrated acid concen-

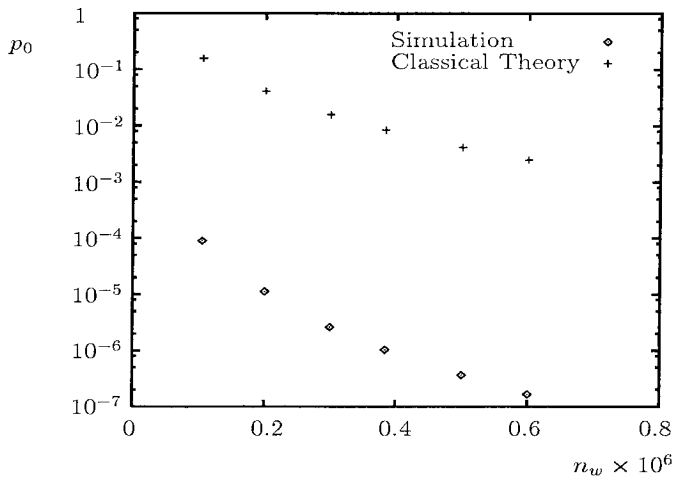

Figure 5.19: Comparison of the probability that a sulfuric acid molecule is unhydrated. At $T = 298.15$ K. Calculated with $f_{hb} = 20$ kcal/mol.

tration as a result of hydration. Thus, the agreement between simulation and the classical prediction at small values of N_w^c is most likely a result of the cancellation of errors. Such sensitivity of the hydrates distribution points to the critical importance of an accurate *ab initio* calculation to enable the accurate determination of the model potentials. We note that p_0 is quite insensitive to the value of f_{hb}, which indicates that no appreciable dissociation occurs in hydrates with one acid molecule as seen also from Figs. 5.17 and 5.18. This in turn indicates that the important interaction potential that determines the behavior of p_0 is the H_2SO_4—H_2O interaction. In the present work, we adopted the *ab initio* results of Kurdi and Kochanski.[139] To see the sensitivity of the hydration state of the acid molecule to the molecular parameters, we tested a model of sulfuric acid molecule parameterized using the results by Morokuma and Muguruma[162] given in Table 5.6. The resulting acid molecule shows no significant hydration. This is a rather unrealistic result and implies that the H_2SO_4—H_2O interaction is stronger than the prediction of Morokuma and Muguruma, adding credibility to our original parameterization.

5.7 Summary and Implications for Classical Binary Nucleation Theory

We have developed a classical mechanical model representation of the H_2SO_4/H_2O binary system. The model has been used in Monte Carlo simulation to obtain a significant section of the free energy surface of binary cluster formation. To our knowledge, this is the first

time that such an extensive free energy calculation has been performed for clusters in a binary system. The mixed ensemble simulation is effective both in sampling very different configurations of clusters relevant in homogeneous nucleation and in evaluating the cluster free energy. When the method is used under the approximation discussed in Appendix I, the required computational effort is further reduced, perhaps even to the point less than that required in a canonical ensemble simulation on a single component system involving clusters of comparable size.

Our simulation yields considerable molecular level insight. Clusters observed are highly nonspherical. At conditions typical of H_2SO_4/H_2O binary nucleation, a cluster with a given number of acid molecules has several very different conformations, which are close in free energy and hence equally relevant in nucleation. Each conformation has fairly long Monte Carlo lifetime. Dissociation behavior of H_2SO_4 in a cluster differs markedly from that in bulk solution and depends sensitively on the assumed value of the free energy f_{hb} of the dissociation reaction $H_2SO_4+H_2O \rightarrow HSO_4^-\cdot H_3O^+$. In a small cluster, no dissociation is observed. As the cluster size becomes larger, the probability of having an $HSO_4^-\cdot H_3O^+$ ion pair increases. However, in the clusters relevant in nucleation, the resulting ion pairs remain in contact and about 240 water molecules are required to observe the behavior which resembles that in bulk solution. When the assumed value of f_{hb} is increased to reflect its uncertainty, the probability of having the ion pair becomes negligible.

The reversible work obtained from simulation shows quantitative agreement with classical theory for small clusters, in which dissociation of the acid molecules is unlikely. This is rather surprising since classical theory assumes the same dissociation behavior in a cluster as in bulk liquid solution. Difference in dissociation behavior, in part, will be corrected by the surface term in classical theory, since dissociation behavior near the bulk vapor-liquid interface also differs from that in bulk solution. Therefore, this agreement just mentioned is attributed, to large extent, to a cancellation of errors, as discussed in Sec. 5.6.5. For larger clusters, for which dissociation occurs, the status is different. When the $H_2SO_4\cdot H_2O$ neutral pair dissociates to form the $HSO_4^-\cdot H_3O^+$ ion pair, its dipole moment becomes nearly 4 times larger, thereby stabilizing clusters of large N_w^c, which in turn results in a reversible work surface quite different from the classical prediction, indicating that the rate-limiting step in stable particle formation is the binary collision of two acid molecules, both of which are likely hydrated. This result, however, changes qualitatively as the assumed value of f_{hb}

is increased, indicating a need for an accurate estimate of this free energy.

Acknowledgments[169]

The authors wish to express gratitude to Dr. Tsan H. Lay for helpful discussions regarding the free energy of the reaction Eq. (5.9) and performing *ab initio* calculation for us and to Dr. Markku Kulmala for providing them with the program to perform a calculation using classical theory. Z.-G. W. acknowledges support from the Camille and Henry Dreyfus Foundation and the Alfred P. Sloan Foundation. This work was supported by National Science Foundation grant ATM-9614105. Simulation is performed in large part using the parallel computer system operated by Caltech Center for Advanced Computing Research (CACR).

Chapter 6 Summary

Given the limitation of classical nucleation theory, arising from its macroscopic nature, we have attempted to establish the foundation of molecular level theory of vapor phase nucleation. In doing so, we have focused on evaluating the reversible work of cluster formation and followed two major trends in this direction, namely, statistical mechanical density functional theory and molecular level simulation.

At first sight, density functional theory appears quite approximate in its nature. For example, to reduce the computational effort, one must be content with an oversimplified model representation of molecules and the functional form of the pair distribution must be assumed as an input to the theory, net effect of which on the predicted reversible work cannot be assessed. However, the very fact that the theory requires only a minor computational effort allows one to derive classical predictions using the bulk thermodynamic quantities obtained from the same theoretical framework. When a comparison is made of the results of density functional theory with those of classical theory, the difference can be attributed mainly to the effect of the molecular level details that are captured by the model representations. Thus, the theory has been successful in addressing semi-quantitative behavior of various interesting systems.

Molecular simulation offers an alternative approach to molecular theory. In this method, one encounters two major drawbacks. First, from a fundamental point of view, the precise definition of a cluster has been a long-standing issue in nucleation theory. Secondly, the large scale computation involved in simulation has hitherto hindered a wide acceptance of this approach beyond a rather uninteresting case of Lennard-Jonesian clusters. Thus, we have challenged the problem of the precise definition of a cluster. The method is quite distinct in its simplicity and computational efficiency and simultaneously overcomes these difficulties.

The molecular level approaches require the intermolecular potentials as the fundamental information. The requirement is quite often too strong for a system of practical interest and predictions of the molecular theory must be regarded as at most semi-quantitative at the present. However, considerable molecular level insight can be obtained that is otherwise

unattainable, which adds to our understanding of the phenomenon of nucleation.

In this work, we have focused on evaluating the reversible work W^{rev} of cluster formation. As Eq. (1.1) suggests, however, any theory of nucleation would be incomplete without the accompanying rate theory. At least from a fundamental point of view, it appears quite unsatisfactory to simply borrow the expression from classical theory. Thus, development of the appropriate rate theory should be a next step in establishing the fully molecular level theory of nucleation.

Appendix A: Definitions of Multipole Moments

We start from the expression for the electrostatic energy $U(1)$ in the external electric field $F_\alpha(\mathbf{r})$ of a neutral molecule 1 in a fixed position and orientation:[78,79]

$$\begin{aligned} U(1) &= -\mu_\alpha^{(P)}(1)F_\alpha(\mathbf{r}_1) - \frac{1}{3}\Theta_{\alpha\beta}^{(P)}(1)F_{\alpha\beta}(\mathbf{r}_1) \\ &\quad -\frac{1}{15}\Omega_{\alpha\beta\gamma}^{(P)}(1)F_{\alpha\beta\gamma}(\mathbf{r}_1) - \frac{1}{105}\Phi_{\alpha\beta\gamma\delta}^{(P)}(1)F_{\alpha\beta\gamma\delta}(\mathbf{r}_1) \\ &\quad -\frac{1}{2}\alpha_{\alpha\beta}(1)F_\alpha(\mathbf{r}_1)F_\beta(\mathbf{r}_1) - \frac{1}{3}A_{\alpha,\beta\gamma}(1)F_\alpha(\mathbf{r}_1)F_{\beta\gamma}(\mathbf{r}_1) + h.o. \end{aligned} \tag{A1}$$

where $\mu_\alpha^{(P)}(1)$, $\Theta_{\alpha\beta}^{(P)}(1)$, $\Omega_{\alpha\beta\gamma}^{(P)}(1)$, and $\Phi_{\alpha\beta\gamma\delta}^{(P)}(1)$ are defined as follows:[170]

$$\begin{aligned} \mu_\alpha^{(P)}(1) &= \int d\mathbf{r}\varrho^{(1)}(\mathbf{r})\, x_\alpha \\ \Theta_{\alpha\beta}^{(P)}(1) &= \frac{1}{2}\int d\mathbf{r}\, \varrho^{(1)}(\mathbf{r})\,[\,3x_\alpha x_\beta - r^2\delta_{\alpha\beta}\,] \\ \Omega_{\alpha\beta\gamma}^{(P)}(1) &= \frac{1}{2}\int d\mathbf{r}\, \varrho^{(1)}(\mathbf{r})\,[\,5x_\alpha x_\beta x_\gamma - r^2(x_\alpha\delta_{\beta\gamma} + x_\beta\delta_{\gamma\alpha} + x_\gamma\delta_{\alpha\beta})\,] \\ \Phi_{\alpha\beta\gamma\delta}^{(P)}(1) &= \frac{1}{8}\int d\mathbf{r}\, \varrho^{(1)}(\mathbf{r})\,[\,35x_\alpha x_\beta x_\gamma x_\delta \\ &\qquad -5r^2(x_\alpha x_\beta\delta_{\gamma\delta} + x_\alpha x_\gamma\delta_{\beta\delta} + x_\alpha x_\delta\delta_{\beta\gamma} \\ &\qquad\quad +x_\beta x_\gamma\delta_{\alpha\delta} + x_\beta x_\delta\delta_{\alpha\gamma} + x_\gamma x_\delta\delta_{\alpha\beta}) \\ &\qquad +r^4(\delta_{\alpha\beta}\delta_{\gamma\delta} + \delta_{\alpha\gamma}\delta_{\beta\delta} + \delta_{\alpha\delta}\delta_{\beta\gamma})\,] \end{aligned} \tag{A2}$$

and respectively, the permanent electric dipole, quadrupole, octopole, and hexadecapole moments, of the molecule 1 expressed in a laboratory coordinate system $O - x_1x_2x_3$. (See Fig. 3.1.) Clearly, these quantities are all invariant with respect to any permutation of the indices and become zero when the sum is taken with respect to any two indices. $\varrho^{(1)}(\mathbf{r})$ is the charge density distribution in the molecule 1 in the absence of any external field. We introduce the total multipole moments by[78,79]

$$\begin{aligned} \mu_\alpha^{(T)}(1) &\equiv -\frac{\partial U}{\partial F_\alpha} \\ &= \mu_\alpha^{(P)}(1) + \alpha_{\alpha\beta}(1)F_\beta(\mathbf{r}_1) + \frac{1}{3}A_{\alpha,\beta\gamma}(1)F_{\beta\gamma}(\mathbf{r}_1) + h.o. \\ \Theta_{\alpha\beta}^{(T)}(1) &\equiv -3\frac{\partial U}{\partial F_{\alpha\beta}} \\ &= \Theta_{\alpha\beta}^{(P)}(1) + A_{\gamma,\alpha\beta}(1)F_\gamma(\mathbf{r}_1) + h.o. \end{aligned}$$

$$\begin{aligned}
\Omega^{(T)}_{\alpha\beta\gamma}(1) &\equiv -15\,\frac{\partial U}{\partial F_{\alpha\beta\gamma}} \\
&= \Omega^{(P)}_{\alpha\beta\gamma}(1) + h.o. \\
\Phi^{(T)}_{\alpha\beta\gamma\delta}(1) &\equiv -105\,\frac{\partial U}{\partial F_{\alpha\beta\gamma\delta}} \\
&= \Phi^{(P)}_{\alpha\beta\gamma\delta}(1) + h.o. \qquad \text{(A3)}
\end{aligned}$$

Since $A_{\gamma,\,\alpha\beta}$ is symmetric with respect to α and β and $A_{\gamma,\,\alpha\alpha} \equiv 0$,[78,79] it is clear that the total multipole moments possess the same properties as those of the permanent multipole moments mentioned above. In fact, we can define the total multipole moments through similar relations to those given in Eq. (A2) with the superscript (P) replaced by (T). Finally, we can rewrite Eq. (A1) to obtain Eq. (3.4) by means of Eq. (A3).

Appendix B: $U^{mp}(1,2)$

We start from Eq. (3.9). $F_\alpha^{(2)}(\mathbf{r}_1)$ is given in terms of the electrostatic potential $\Psi^{(2)}(\mathbf{r})$ created by the total multipole moments on the molecule 2:

$$F_\alpha^{(2)}(\mathbf{r}_1) = -\left.\frac{\partial \Psi^{(2)}(\mathbf{r})}{\partial x_\alpha}\right|_{\mathbf{r}=\mathbf{r}_1}. \tag{B4}$$

Denoting by $\varrho^{(2)}(\mathbf{r})$ the charge density distribution in the molecule 2 in the presence of the ion and the other molecules,

$$\Psi^{(2)}(\mathbf{r}) = \int d\mathbf{r}' \frac{\varrho^{(2)}(\mathbf{r}')}{|\mathbf{r}-\mathbf{r}'|}. \tag{B5}$$

We expand the denominator around $\mathbf{r}' = \mathbf{r}_2$ and use Eq. (A2) with the superscript (P) replaced by (T). Taking the spatial derivatives of the resulting expression with respect to $\mathbf{r}$ and setting $\mathbf{r} = \mathbf{r}_1$, as indicated by Eq. (3.6), we obtain for a neutral molecule

$$\begin{aligned}
F_\alpha^{(2)}(\mathbf{r}_1) &= T_{\alpha\beta}\,\mu_\beta^{(T)}(2) + \frac{1}{3}T_{\alpha\beta\gamma}\,\Theta_{\beta\gamma}^{(T)}(2) \\
&\quad + \frac{1}{15}T_{\alpha\beta\gamma\delta}\,\Omega_{\beta\gamma\delta}^{(T)}(2) + \frac{1}{105}T_{\alpha\beta\gamma\delta\varepsilon}\,\Phi_{\beta\gamma\delta\epsilon}^{(T)}(2) + O({r_{12}}^{-7}) \\
F_{\alpha\beta}^{(2)}(\mathbf{r}_1) &= -T_{\alpha\beta\gamma}\,\mu_\gamma^{(T)}(2) - \frac{1}{3}T_{\alpha\beta\gamma\delta}\,\Theta_{\gamma\delta}^{(T)}(2) - \frac{1}{15}T_{\alpha\beta\gamma\delta\varepsilon}\,\Omega_{\gamma\delta\epsilon}^{(T)}(2) + O({r_{12}}^{-7}) \\
F_{\alpha\beta\gamma}^{(2)}(\mathbf{r}_1) &= T_{\alpha\beta\gamma\delta}\,\mu_\delta^{(T)}(2) + \frac{1}{3}T_{\alpha\beta\gamma\delta\varepsilon}\,\Theta_{\delta\epsilon}^{(T)}(2) + O({r_{12}}^{-7}) \\
F_{\alpha\beta\gamma\delta}^{(2)}(\mathbf{r}_1) &= -T_{\alpha\beta\gamma\delta\varepsilon}\,\mu_\epsilon^{(T)}(2) + O({r_{12}}^{-7}),
\end{aligned} \tag{B6}$$

where

$$\begin{aligned}
T_{\alpha\beta} &\equiv \left.\frac{\partial^2 r^{-1}}{\partial x_\alpha \partial x_\beta}\right|_{\mathbf{r}=\mathbf{r}_{12}} \\
T_{\alpha\beta\gamma} &\equiv \left.\frac{\partial^3 r^{-1}}{\partial x_\alpha \partial x_\beta \partial x_\gamma}\right|_{\mathbf{r}=\mathbf{r}_{12}} \\
T_{\alpha\beta\gamma\delta} &\equiv \left.\frac{\partial^4 r^{-1}}{\partial x_\alpha \partial x_\beta \partial x_\gamma \partial x_\delta}\right|_{\mathbf{r}=\mathbf{r}_{12}} \\
T_{\alpha\beta\gamma\delta\varepsilon} &\equiv \left.\frac{\partial^5 r^{-1}}{\partial x_\alpha \partial x_\beta \partial x_\gamma \partial x_\delta \partial x_\varepsilon}\right|_{\mathbf{r}=\mathbf{r}_{12}}.
\end{aligned} \tag{B7}$$

Using Eq. (B6) in Eq. (3.9), we obtain

$$
\begin{aligned}
U^{mp}(1,2) \;=\; & -T_{\alpha\beta}\,\mu_\alpha^{(T)}(1)\,\mu_\beta^{(T)}(2) \\
& -\frac{1}{3}\,T_{\alpha\beta\gamma}\left\{\mu_\alpha^{(T)}(1)\,\Theta_{\beta\gamma}^{(T)}(2)-\Theta_{\alpha\beta}^{(T)}(1)\,\mu_\gamma^{(T)}(2)\right\} \\
& -T_{\alpha\beta\gamma\delta}\left\{\frac{1}{15}\,\mu_\alpha^{(T)}(1)\,\Omega_{\beta\gamma\delta}^{(T)}(2)-\frac{1}{9}\,\Theta_{\alpha\beta}^{(T)}(1)\,\Theta_{\gamma\delta}^{(T)}(2)\right. \\
& \qquad \left.+\frac{1}{15}\,\Omega_{\alpha\beta\gamma}^{(T)}(1)\,\mu_\delta^{(T)}(2)\right\} \\
& -T_{\alpha\beta\gamma\delta\varepsilon}\left\{\frac{1}{105}\,\mu_\alpha^{(T)}(1)\,\Phi_{\beta\gamma\delta\varepsilon}^{(T)}(2)-\frac{1}{45}\,\Theta_{\alpha\beta}^{(T)}(1)\,\Omega_{\gamma\delta\varepsilon}^{(T)}(2)\right. \\
& \qquad \left.+\frac{1}{45}\,\Omega_{\alpha\beta\gamma}^{(T)}(1)\,\Theta_{\delta\varepsilon}^{(T)}(2)-\frac{1}{105}\,\Phi_{\alpha\beta\gamma\delta}^{(T)}(1)\,\mu_\varepsilon^{(T)}(2)\right\}. \qquad \text{(B8)}
\end{aligned}
$$

When $\mathbf{r}_1$ and $\mathbf{r}_2$ are exchanged, $T_{\alpha\beta\gamma}$ and $T_{\alpha\beta\gamma\delta\varepsilon}$ change their signs while $T_{\alpha\beta}$ and $T_{\alpha\beta\gamma\delta}$ remain unaffected, since $\mathbf{r}_{12}=-\mathbf{r}_{21}$. Thus, $U^{mp}(1,2)$ is symmetric in 1 and 2, a property used in arriving at Eqs. (3.35) and (3.36) from Eq. (3.32).

Appendix C: The Ion-Molecule Interaction Energy

We choose the coordinate system in which the position vector $\mathbf{r}_1$ of the molecule 1 is parallel to the x_3-axis. (See Fig. 3.1.) The only non-zero components of the electric field and its spatial gradients at $\mathbf{r}_1$, resulting from a point charge q at the origin are

$$\begin{aligned}
F_3 &= \frac{q}{{r_1}^2} \\
F_{11} &= F_{22} = \frac{q}{{r_1}^3} \\
F_{33} &= -\frac{2q}{{r_1}^3} \\
F_{113} &= F_{223} = -\frac{3q}{{r_1}^4} \\
F_{333} &= \frac{6q}{{r_1}^4} \\
F_{1111} &= F_{2222} = -\frac{9q}{{r_1}^5} \\
F_{1122} &= -\frac{3q}{{r_1}^5} \\
F_{1133} &= F_{2233} = \frac{12q}{{r_1}^5} \\
F_{3333} &= -\frac{24q}{{r_1}^5}
\end{aligned} \tag{C9}$$

and those obtained by any permutation of their indices. Using the symmetry and traceless properties discussed in Appendix I of the multipole moments and the polarizabilities, we therefore obtain

$$\begin{aligned}
\mu_\alpha(1)F_\alpha(\mathbf{r}_1) &= \frac{q}{{r_1}^2}\,\mu_3(1) \\
\Theta_{\alpha\beta}(1)F_{\alpha\beta}(\mathbf{r}_1) &= -\frac{3q}{{r_1}^3}\,\Theta_{33}(1) \\
\Omega_{\alpha\beta\gamma}(1)F_{\alpha\beta\gamma}(\mathbf{r}_1) &= \frac{15q}{{r_1}^4}\,\Omega_{333}(1) \\
\Phi_{\alpha\beta\gamma\delta}(1)F_{\alpha\beta\gamma\delta}(\mathbf{r}_1) &= -\frac{105q}{{r_1}^5}\,\Phi_{3333}(1) \\
\alpha_{\alpha\beta}(1)F_\alpha(\mathbf{r}_1)F_\beta(\mathbf{r}_1) &= \frac{{q}^2}{{r_1}^4}\,\alpha_{33}(1) \\
A_{\alpha,\,\beta\gamma}(1)F_\alpha(\mathbf{r}_1)F_{\beta\gamma}(\mathbf{r}_1) &= -\frac{3{q}^2}{{r_1}^5}\,A_{3,\,33}(1).
\end{aligned} \tag{C10}$$

The first four equations are valid for both total and permanent multipole moments. Using

Eq. (C10) and setting $q = q^{ion}$, we rewrite Eq. (3.8) to obtain Eq. (3.14). Similar procedures are followed with $q = q^{eff}(r_1)$ to obtain Eq. (3.19) from Eq. (3.4) and Eq. (3.20) from Eq. (3.5).

Finally, using Eq. (C9) in Eq. (A3) with $q = q^{eff}(r_1)$, we obtain

$$\begin{aligned}
\mu_3^{(T)}(1) &= \mu_3^{(P)}(1) + q^{eff}(r_1)\left(\frac{1}{{r_1}^2}\,\alpha_{33}(1) - \frac{1}{{r_1}^3}\,A_{3,33}(1)\right) + h.o. \\
\Theta_{33}^{(T)}(1) &= \Theta_{33}^{(P)}(1) + \frac{q^{eff}(r_1)}{{r_1}^2} A_{3,33}(1) + h.o \\
\Omega_{333}^{(T)}(1) &= \Omega_{333}^{(P)}(1) + h.o. \\
\Phi_{3333}^{(T)}(1) &= \Phi_{3333}^{(P)}(1) + h.o.
\end{aligned} \tag{C11}$$

which is substituted into Eq. (3.14) to obtain Eq. (3.21).

Appendix D: Derivation of Eq. (3.36)

We start from Eq. (3.32), which is rewritten here as

$$\begin{aligned}\Omega[n, q^{eff}] &= \int d\mathbf{r}_1\, f^d(n(r_1)) - \int d\mathbf{r}_1\, n(r_1)\,\{\,\mu + k_BT \log[\,Z_R(r_1)\,]\,\} \\ &+ \int d1\, n(r_1) m(1) \left[\, q^{ion} - q^{eff}(r_1) \,\right]\, u^T(1) \\ &+ \frac{1}{2} \iint d\mathbf{r}_1\, d\mathbf{r}_2\, n(r_1) n(r_2) H(r_{12} - d) \phi^{att}(r_{12}) \\ &+ \frac{1}{2} \iint d1\, d2\, n(r_1) n(r_2) m(1) m(2) H(r_{12} - d) \phi^{mp}(1,2). \end{aligned} \tag{D12}$$

Consider an infinitesimal change in $q^{eff}(r_1)$ while $n(r_1)$ is fixed. Noting that $\phi^{mp}(1,2)$ is symmetric in 1 and 2,

$$\begin{aligned}\delta\Omega &= -k_BT \int d\mathbf{r}_1\, n(r_1) \frac{1}{Z_R(r_1)} \frac{\partial Z_R(r_1)}{\partial q^{eff}(r_1)}\, \delta q^{eff}(r_1) \\ &- \int d1\, n(r_1) m(1) u^T(1)\, \delta q^{eff}(r_1) \\ &+ \int d1\, n(r_1) \left[\, q^{ion} - q^{eff}(r_1) \,\right]\, u^T(1)\, \delta m(1) \\ &+ \int d1\, n(r_1) m(1) \left[\, q^{ion} - q^{eff}(r_1) \,\right]\, \frac{\partial u^T(1)}{\partial q^{eff}(r_1)}\, \delta q^{eff}(r_1) \\ &+ \iint d1\, d2\, n(r_1) n(r_2) m(2) H(r_{12} - d) \phi^{mp}(1,2)\, \delta m(1) \\ &+ \iint d1\, d2\, n(r_1) n(r_2) m(1) m(2) H(r_{12} - d) \frac{\partial \phi^{mp}(1,2)}{\partial q^{eff}(r_1)}\, \delta q^{eff}(r_1). \end{aligned} \tag{D13}$$

From Eqs. (3.19)-(3.21), (3.28), and (3.29)

$$\begin{aligned}\frac{\partial u^T(1)}{\partial q^{eff}(r_1)} &= -u^{pol}(1) \\ \frac{1}{Z_R(r_1)} \frac{\partial Z_R(r_1)}{\partial q^{eff}(r_1)} &= -\frac{1}{k_BT} \left\langle u^T(1) \right\rangle_{\hat{R}_1} \\ \delta m(1) &= \frac{1}{k_BT} m(1) \left[\left\langle u^T(1) \right\rangle_{\hat{R}_1} - u^T(1) \right] \delta q^{eff}(r_1). \end{aligned} \tag{D14}$$

Thus Eq. (D12) finally yields

$$\begin{aligned}\frac{\delta\Omega}{\delta q^{eff}} &= \frac{n(r_1)}{k_BT} \left[\left[\, q^{eff}(r_1) - q^{ion} \,\right] \left\{ \left[\left\langle u^T(1)^2 \right\rangle_{\hat{R}_1} - \left\langle u^T(1) \right\rangle_{\hat{R}_1}^2 \right] + k_BT \left\langle u^{pol}(1) \right\rangle_{\hat{R}_1} \right\} \right. \\ &\left. - \int d\mathbf{r}_2\, n(r_2) H(r_{12} - d) \right.\end{aligned}$$

$$\times \left\{ \left[\left\langle \phi^{mp}(1,2) u^T(1) \right\rangle_{\hat{R}_1 \hat{R}_2} - \langle \phi^{mp}(1,2) \rangle_{\hat{R}_1 \hat{R}_2} \left\langle u^T(1) \right\rangle_{\hat{R}_1} \right] \right.$$
$$\left. -k_B T \left\langle \frac{\partial \phi^{mp}(1,2)}{\partial q^{eff}(r_1)} \right\rangle_{\hat{R}_1 \hat{R}_2} \right\} \Bigg] . \tag{D15}$$

Assuming that $n(r_1)$ is non-zero everywhere in the system, we finally arrive at Eq. (3.36).

Appendix E: Analytical Integrations of Eqs. (3.32), (3.35), and (3.36)

When Eq. (3.28) is employed, it becomes convenient to introduce the local coordinate system $O^{(j)} - x_1^{(j)} x_2^{(j)} x_3^{(j)}$ at the center of the molecule j, in which the $x_3^{(j)}$-axis is parallel to $\mathbf{r}_j$. The orientation of the molecule j is determined by specifying the Euler angle $(\phi_j, \theta_j, \psi_j)$ of the body fixed coordinate system $O^{(Bj)} - x_1^{(Bj)} x_2^{(Bj)} x_3^{(Bj)}$ on the molecule j with respect to the local coordinate system. We have chosen $O - x_1 x_2 x_3$ so that the x_3-axis is parallel to the $x_3^{(1)}$-axis. (See Fig. 3.1.)

Since any tensor in the form of $G_{333\cdots3}(1)$ is invariant under a rotation around the $x_3^{(1)}$-axis specified by ϕ_1, it is readily seen from Eqs. (3.19)-(3.21) that $U(1)$, $u^{pol}(1)$, and $u^T(1)$ are all independent of ϕ_1. For clarity, we introduce new notations:

$$\begin{aligned} U_0(\xi_1) &= U(1) \\ u_0^{pol}(\xi_1) &= u^{pol}(1) \\ u_0^T(\xi_1) &= u^T(1). \end{aligned} \tag{E16}$$

We use the notation ξ_j to denote the position $\mathbf{r}_j$ and the orientation (θ_j, ψ_j) of the molecule j. The orientation alone is denoted by ω_j, which reduces to θ_j in the case of a linear molecule. Performing the integration with respect to ϕ_1 in $Z_R(r_1)$, we define $m_0(\xi_1)$ through

$$\begin{aligned} m(1) &= \frac{1}{2\pi\, Z_0(r_1)} \exp\left\{-\frac{U_0(\xi_1)}{k_B T}\right\} \\ &\equiv \frac{1}{2\pi} m_0(\xi_1), \end{aligned} \tag{E17}$$

where

$$\begin{aligned} Z_0(r_1) &\equiv \int d\omega_1 \exp\left\{-\frac{U_0(\xi_1)}{k_B T}\right\} \\ &= \frac{1}{2\pi} Z_R(r_1). \end{aligned} \tag{E18}$$

Using Eqs. (E16)-(E18) in Eqs. (3.32), (3.35), and (3.36), we obtain

$$\begin{aligned} \Omega[n, q^{eff}] &= \int d\mathbf{r}_1\, f^d(n(r_1)) - \int d\mathbf{r}_1\, n(r_1) \{\, \mu + k_B T \log[\, 2\pi\, Z_0(r_1)\,]\,\} \\ &\quad + \int d\mathbf{r}_1\, n(r_1) \left[\, q^{ion} - q^{eff}(r_1)\,\right] \left\langle u_0^T(\xi_1) \right\rangle_{\omega_1} \end{aligned}$$

$$+\frac{1}{2}\iint d\mathbf{r}_1\, d\mathbf{r}_2\, n(r_1)n(r_2)H(r_{12}-d)\phi^{att}(r_{12})$$
$$+\frac{1}{2}\iint d\mathbf{r}_1\, d\mathbf{r}_2\, n(r_1)n(r_2)H(r_{12}-d)\,\langle\phi_0^{mp}(\xi_1,\xi_2)\rangle_{\omega_1\omega_2} \qquad \text{(E19)}$$

$$\begin{aligned} 0 &= \mu^d(n(r_1)) - \{\,\mu + k_BT\log\,[\,2\pi Z_0(r_1)\,]\,\} \\ &\quad + \Big[\,q^{ion} - q^{eff}(r_1)\,\Big]\,\Big\langle u_0^T(\xi_1)\Big\rangle_{\omega_1} \\ &\quad + \int d\mathbf{r}_2\, n(r_2)H(r_{12}-d)\phi^{att}(r_{12}) \\ &\quad + \int d\mathbf{r}_2\, n(r_2)H(r_{12}-d)\,\langle\phi_0^{mp}(\xi_1,\xi_2)\rangle_{\omega_1\omega_2}\,, \end{aligned} \qquad \text{(E20)}$$

and

$$\begin{aligned} 0 &= \Big[\,q^{eff}(r_1) - q^{ion}\,\Big]\left\{\left[\,\Big\langle u_0^T(\xi_1)^2\Big\rangle_{\omega_1} - \Big\langle u_0^T(\xi_1)\Big\rangle_{\omega_1}^2\,\right] + k_BT\,\Big\langle u_0^{pol}(\xi_1)\Big\rangle_{\omega_1}\right\} \\ &\quad - \int d\mathbf{r}_2\, n(r_2)H(r_{12}-d)\left\{\left[\,\Big\langle\phi_0^{mp}(\xi_1,\xi_2)u_0^T(\xi_1)\Big\rangle_{\omega_1\omega_2} - \langle\phi_0^{mp}(\xi_1,\xi_2)\rangle_{\omega_1\omega_2}\,\Big\langle u_0^T(\xi_1)\Big\rangle_{\omega_1}\,\right]\right. \\ &\qquad \left. -k_BT\left\langle\frac{\partial\phi_0^{mp}(\xi_1,\xi_2)}{\partial q^{eff}(r_1)}\right\rangle_{\omega_1\omega_2}\right\}, \end{aligned} \qquad \text{(E21)}$$

respectively. For arbitrary functions $G_a(\xi_1)$ and $G_b(\xi_1,\xi_2)$, we have defined their angular average by

$$\langle G_a(\xi_1)\rangle_{\omega_1} \equiv \int d\omega_1\, m(\xi_1)\, G_a(\xi_1) \qquad \text{(E22)}$$

and

$$\langle G_b(\xi_1,\xi_2)\rangle_{\omega_1\omega_2} \equiv \iint d\omega_1\, d\omega_2\, m(\xi_1)m(\xi_2)\, G_b(\xi_1,\xi_2), \qquad \text{(E23)}$$

respectively. $\phi_0^{mp}(\xi_1,\xi_2)$ is defined by

$$\begin{aligned} \phi_0^{mp}(\xi_1,\xi_2) &\equiv \frac{1}{(2\pi)^2}\int_0^{2\pi} d\phi_1 \int_0^{2\pi} d\phi_2\, \phi^{mp}(1,2) \\ &= -T_{\alpha\beta}\,\mu_\alpha^{(T)}(\xi_1)\,\mu_\beta^{(T)}(\xi_2) \\ &\quad -\frac{1}{3}\,T_{\alpha\beta\gamma}\left\{\mu_\alpha^{(T)}(\xi_1)\,\theta_{\beta\gamma}^{(T)}(\xi_2) - \Theta_{\alpha\beta}^{(T)}(\xi_1)\,\mu_\gamma^{(T)}(\xi_2)\right\} \\ &\quad -T_{\alpha\beta\gamma\delta}\left\{\frac{1}{15}\,\mu_\alpha^{(T)}(\xi_1)\,\Omega_{\beta\gamma\delta}^{(T)}(\xi_2) - \frac{1}{9}\,\Theta_{\alpha\beta}^{(T)}(\xi_1)\,\Theta_{\gamma\delta}^{(T)}(\xi_2)\right. \\ &\qquad \left. +\frac{1}{15}\,\Omega_{\alpha\beta\gamma}^{(T)}(\xi_1)\,\mu_\delta^{(T)}(\xi_2)\right\} \\ &\quad -T_{\alpha\beta\gamma\delta\varepsilon}\left\{\frac{1}{105}\,\mu_\alpha^{(T)}(\xi_1)\,\Phi_{\beta\gamma\delta\varepsilon}^{(T)}(\xi_2) - \frac{1}{45}\,\Theta_{\alpha\beta}^{(T)}(\xi_1)\,\Omega_{\gamma\delta\varepsilon}^{(T)}(\xi_2)\right. \end{aligned}$$

$$+\frac{1}{45}\,\Omega^{(T)}_{\alpha\beta\gamma}(\xi_1)\,\Theta^{(T)}_{\delta\varepsilon}(\xi_2) - \frac{1}{105}\,\Phi^{(T)}_{\alpha\beta\gamma\delta}(\xi_1)\,\mu^{(T)}_{\varepsilon}(\xi_2)\Big\}, \quad \text{(E24)}$$

where the second equality follows from Eq. (B8) and the definitions

$$\begin{aligned}
\mu^{(T)}_{\alpha}(\xi_j) &\equiv \frac{1}{2\pi}\int_0^{2\pi} d\phi_j\,\mu^{(T)}_{\alpha}(j)\\
\Theta^{(T)}_{\alpha\beta}(\xi_j) &\equiv \frac{1}{2\pi}\int_0^{2\pi} d\phi_j\,\Theta^{(T)}_{\alpha\beta}(j)\\
\Omega^{(T)}_{\alpha\beta\gamma}(\xi_j) &\equiv \frac{1}{2\pi}\int_0^{2\pi} d\phi_j\,\Omega^{(T)}_{\alpha\beta\gamma}(j)\\
\Phi^{(T)}_{\alpha\beta\gamma\delta}(\xi_j) &\equiv \frac{1}{2\pi}\int_0^{2\pi} d\phi_j\,\Phi^{(T)}_{\alpha\beta\gamma\delta}(j). \qquad \text{(E25)}
\end{aligned}$$

We next rewrite $u^T_0(\xi_1)$ and $\phi^{mp}_0(\xi_1,\xi_2)$ in terms of the tensor components in the local coordinate system. When referred to the local coordinate system $O^{(j)} - x^{(j)}_1 x^{(j)}_2 x^{(j)}_3$, these tensors defined by Eq. (E25) are axially symmetric around the $x^{(j)}_3$-axis. Hence the only non-zero components are[79]

$$\begin{aligned}
&\mu^{(Tj)}_3(\xi_j)\\
\Theta^{(Tj)}_{11}(\xi_j) &= \Theta^{(Tj)}_{22}(\xi_j) = -\frac{1}{2}\,\Theta^{(Tj)}_{33}(\xi_j)\\
\Omega^{(Tj)}_{113}(\xi_j) &= \Omega^{(Tj)}_{223}(\xi_j) = -\frac{1}{2}\,\Omega^{(Tj)}_{333}(\xi_j)\\
\Phi^{(Tj)}_{1111}(\xi_j) &= \Phi^{(Tj)}_{2222}(\xi_j) = \frac{3}{8}\,\Phi^{(Tj)}_{3333}(\xi_j)\\
\Phi^{(Tj)}_{1122}(\xi_j) &= \frac{1}{8}\,\Phi^{(Tj)}_{3333}(\xi_j)\\
\Phi^{(Tj)}_{1133}(\xi_j) &= \Phi^{(Tj)}_{2233}(\xi_j) = -\frac{1}{2}\,\Phi^{(Tj)}_{3333}(\xi_j) \qquad \text{(E26)}
\end{aligned}$$

and those obtained by any permutation of the indices. We add the superscript j for the tensor components expressed in the local coordinate system $O^{(j)} - x^{(j)}_1 x^{(j)}_2 x^{(j)}_3$. For the particular choice of the coordinate system shown in Fig. 3.1, $O - x_1x_2x_3$ is related to $O^{(1)} - x^{(1)}_1 x^{(1)}_2 x^{(1)}_3$ by a linear translation. Thus, the tensor components expressed in the former are the same as those expressed in the latter. In particular,

$$\begin{aligned}
\mu^{(T)}_3(\xi_1) &= \mu^{(T1)}_3(\xi_1)\\
\Theta^{(T)}_{33}(\xi_1) &= \Theta^{(T1)}_{33}(\xi_1)\\
\Omega^{(T)}_{333}(\xi_1) &= \Omega^{(T1)}_{333}(\xi_1)
\end{aligned}$$

$$\Phi^{(T)}_{3333}(\xi_1) \;=\; \Phi^{(T1)}_{3333}(\xi_1). \tag{E27}$$

Other components are readily obtained from Eq. (E26). From Eqs. (3.14), (E16), (E25), and (E27)

$$u_0^T(\xi_1) = -\frac{1}{{r_1}^2}\,\mu_3^{(T1)}(\xi_1) + \frac{1}{{r_1}^3}\,\Theta_{33}^{(T1)}(\xi_1) - \frac{1}{{r_1}^4}\,\Omega_{333}^{(T1)}(\xi_1) + \frac{1}{{r_1}^5}\,\Phi_{3333}^{(T1)}(\xi_1). \tag{E28}$$

For the molecule 2,

$$\begin{aligned}
\mu_\alpha^{(T)}(\xi_2) &= a_{\beta\alpha}\mu_\beta^{(T2)}(\xi_2) \\
\Theta_{\alpha\beta}^{(T)}(\xi_2) &= a_{\gamma\alpha}a_{\delta\beta}\Theta_{\gamma\delta}^{(T2)}(\xi_2) \\
\Omega_{\alpha\beta\gamma}^{(T)}(\xi_2) &= a_{\delta\alpha}a_{\varepsilon\beta}a_{\mu\gamma}\Omega_{\delta\varepsilon\mu}^{(T2)}(\xi_2) \\
\Phi_{\alpha\beta\gamma\delta}^{(T)}(\xi_2) &= a_{\varepsilon\alpha}a_{\mu\beta}a_{\tau\gamma}a_{\rho\delta}\Phi_{\varepsilon\mu\tau\rho}^{(T2)}(\xi_2),
\end{aligned} \tag{E29}$$

where $a_{\alpha\beta}$ is the orthogonal transformation matrix from $O - x_1x_2x_3$ to $O^{(2)} - x_1^{(2)}x_2^{(2)}x_3^{(2)}$. Due to the axial symmetry of the system around the x_3-axis, we may set

$$\underline{\underline{a}} = \begin{pmatrix} \cos\theta & 0 & -\sin\theta \\ 0 & 1 & 0 \\ \sin\theta & 0 & \cos\theta \end{pmatrix}, \tag{E30}$$

where θ is the angle between the x_3-axis and the $x_3^{(2)}$-axis. Using Eqs. (E26), (E27), (E29), and (E30), we may integrate Eq. (E24) with respect to $\cos\theta$ to obtain

$$\begin{aligned}
\phi_0^{mp}(\xi_1,\xi_2) \;=\; & -\;\mu_3^{(T1)}(\xi_1)\mu_3^{(T2)}(\xi_2)\frac{\partial}{\partial(\cos\theta)}A_{\mu-\mu}(r_1,r_2,\cos\theta) \\
& -\frac{3}{2}\,\Theta_{33}^{(T1)}(\xi_1)\mu_3^{(T2)}(\xi_2)\frac{\partial}{\partial(\cos\theta)}A_{\Theta-\mu}(r_1,r_2,\cos\theta) \\
& -\frac{3}{2}\,\mu_3^{(T1)}(\xi_1)\Theta_{33}^{(T2)}(\xi_2)\frac{\partial}{\partial(\cos\theta)}A_{\Theta-\mu}(r_2,r_1,\cos\theta) \\
& +\frac{1}{2}\,\Omega_{333}^{(T1)}(\xi_1)\mu_3^{(T2)}(\xi_2)\frac{\partial}{\partial(\cos\theta)}A_{\Omega-\mu}(r_1,r_2,\cos\theta) \\
& +\frac{3}{4}\,\Theta_{33}^{(T1)}(\xi_1)\Theta_{33}^{(T2)}(\xi_2)\frac{\partial}{\partial(\cos\theta)}A_{\Theta-\Theta}(r_1,r_2,\cos\theta) \\
& +\frac{1}{2}\,\mu_3^{(T1)}(\xi_1)\Omega_{333}^{(T2)}(\xi_2)\frac{\partial}{\partial(\cos\theta)}A_{\Omega-\mu}(r_2,r_1,\cos\theta)
\end{aligned}$$

$$
\begin{aligned}
&+\frac{5}{8}\,\Phi^{(T1)}_{3333}(\xi_1)\mu^{(T2)}_{3}(\xi_2)\frac{\partial}{\partial(\cos\theta)}A_{\Phi-\mu}(r_1,r_2,\cos\theta)\\
&-\frac{5}{4}\,\Omega^{(T1)}_{333}(\xi_1)\Theta^{(T2)}_{33}(\xi_2)\frac{\partial}{\partial(\cos\theta)}A_{\Omega-\Theta}(r_1,r_2,\cos\theta)\\
&-\frac{5}{4}\,\Theta^{(T1)}_{33}(\xi_1)\Omega^{(T2)}_{333}(\xi_2)\frac{\partial}{\partial(\cos\theta)}A_{\Omega-\Theta}(r_2,r_1,\cos\theta)\\
&+\frac{5}{8}\,\mu^{(T1)}_{3}(\xi_1)\Phi^{(T2)}_{3333}(\xi_2)\frac{\partial}{\partial(\cos\theta)}A_{\Phi-\mu}(r_2,r_1,\cos\theta), \qquad \text{(E31)}
\end{aligned}
$$

where

$$
\begin{aligned}
A_{\mu-\mu}(r_1,r_2,\cos\theta) &= \frac{1}{{r_{12}}^3}\,(\cos^2\theta-1)\\
A_{\Theta-\mu}(r_1,r_2,\cos\theta) &= \frac{1}{{r_{12}}^5}\,(r_2\cos\theta-r_1)(\cos^2\theta-1)\\
A_{\Omega-\mu}(r_1,r_2,\cos\theta) &= \left[\frac{1}{{r_{12}}^5}-\frac{5}{{r_{12}}^7}\,(r_2\cos\theta-r_1)^2\right](\cos^2\theta-1)\\
A_{\Phi-\mu}(r_1,r_2,\cos\theta) &= \left[\frac{3}{{r_{12}}^7}-\frac{7}{{r_{12}}^9}\,(r_2\cos\theta-r_1)^2\right](r_2\cos\theta-r_1)(\cos^2\theta-1)\\
A_{\Theta-\Theta}(r_1,r_2,\cos\theta) &= \left[\frac{4}{{r_{12}}^5}\,\cos\theta+\frac{5}{{r_{12}}^7}\,r_1r_2(\cos^2\theta-1)\right](\cos^2\theta-1)\\
A_{\Omega-\Theta}(r_1,r_2,\cos\theta) &= \left[\frac{1}{{r_{12}}^7}\,(r_2-r_1\cos\theta)+\frac{2}{{r_{12}}^7}\,(r_2\cos\theta-r_1)\cos\theta\right.\\
&\quad\left.-\frac{7}{{r_{12}}^9}\,(r_2\cos\theta-r_1)^2(r_2-r_1\cos\theta)\right](\cos^2\theta-1). \qquad \text{(E32)}
\end{aligned}
$$

Recall that Eq. (C11) is obtained for the coordinate system in which the x_3-axis is parallel to $\mathbf{r}_1$. Since the $x^{(j)}_3$-axis in the local coordinate system of the molecule j is parallel to $\mathbf{r}_j$, we have similar relations:

$$
\begin{aligned}
\mu^{(Tj)}_{3}(\xi_j) &= \mu^{(Pj)}_{3}(\xi_j)+q^{eff}(r_j)\left(\frac{1}{{r_j}^2}\,\alpha^{(j)}_{33}(\xi_j)-\frac{1}{{r_j}^3}\,A^{(j)}_{3,33}(\xi_j)\right)+h.o.\\
\Theta^{(Tj)}_{33}(\xi_j) &= \Theta^{(Pj)}_{33}(\xi_j)+\frac{q^{eff}(r_j)}{{r_j}^2}A^{(j)}_{3,33}(\xi_j)+h.o\\
\Omega^{(Tj)}_{333}(\xi_j) &= \Omega^{(Pj)}_{333}(\xi_j)+h.o.\\
\Phi^{(Tj)}_{3333}(\xi_j) &= \Phi^{(Pj)}_{3333}(\xi_j)+h.o. \qquad \text{(E33)}
\end{aligned}
$$

where the superscript j has the same significance as before. The functional form of each tensor given by Eq. (E33) is identical for every molecule, as a result of the spherical symmetry of the system. Note that the tensor components on the R.H.S. of Eq. (E33) are expressed in the local coordinate system $O^{(j)}-x^{(j)}_1x^{(j)}_2x^{(j)}_3$ and can be expressed in terms

of those in the body fixed coordinate system $O^{(Bj)} - x_1^{(Bj)} x_2^{(Bj)} x_3^{(Bj)}$ and the Euler angle $(\phi_j = 0, \theta_j, \psi_j)$ of the latter with respect to the former. Although a molecule is supposed to be a sphere in our model representation, part of the molecular symmetry is captured in the model through the symmetry of these tensors.

For arbitrary function $G_c(r_1, r_2, \cos\theta)$, we have

$$\begin{aligned} & \int d\mathbf{r}_2 \, H(r_{12} - d) \, G_c(r_1, r_2, \cos\theta) \\ = \; & 2\pi \int_{r^{ion}+\frac{d}{2}}^{\infty} {r_2}^2 dr_2 \int_{-1}^{c(r_1,r_2)} d(\cos\theta) \, G_c(r_1, r_2, \cos\theta) \end{aligned} \tag{E34}$$

and

$$\begin{aligned} & \iint d\mathbf{r}_1 \, d\mathbf{r}_2 \, H(r_{12} - d) \, G_c(r_1, r_2, \cos\theta) \\ = \; & 8\pi^2 \int_{r^{ion}+\frac{d}{2}}^{r_0} {r_1}^2 dr_1 \int_{r^{ion}+\frac{d}{2}}^{\infty} {r_2}^2 dr_2 \int_{-1}^{c(r_1,r_2)} d(\cos\theta) \, G_c(r_1, r_2, \cos\theta), \end{aligned} \tag{E35}$$

where r_0 is the radius of the system boundary. $c(r_1, r_2)$ is unity except when the molecule 2 stays inside the spherical shell $r_L < r < r_1 + d$, where r_L is the larger of $r^{ion} + \frac{d}{2}$ and $r_1 - d$. In this case,

$$c(r_1, r_2) = \frac{{r_1}^2 + {r_2}^2 - d^2}{2 r_1 r_2}, \tag{E36}$$

which is the cosine of the angle between $\mathbf{r}_1$ and $\mathbf{r}_2$ when the molecule 2 is in contact with the molecule 1. This is the consequence of the hard sphere exclusion represented by $H(r_{12} - d)$. When Eq. (E36) is used along with Eq. (E31) and the relation

$$\phi^{att}(r_{12}) = \frac{\partial}{\partial(\cos\theta)} \left[-\frac{\epsilon^{att} \, d^6}{4 r_1 r_2 \, ({r_1}^2 + {r_2}^2 - 2 r_1 r_2 \cos\theta)^2} \right], \tag{E37}$$

which follows from Eq. (3.3), integrals with respect to $\cos\theta$ in Eqs. (E19)-(E21) become analytically tractable, reducing the dimensionality of the integrals in Eq. (E19) to at most four: two over ω_1 in calculating the angular average of the total multipole moments on the molecule 1, and the other two over r_1 and r_2. It is not necessary to calculate the angular average of the total multipole moments on the molecule 2, for they are identical as functions of the ion-molecule distance to those for the molecule 1. Similarly, integrations in Eqs. (E20) and (E21) are at most three dimensional.

Finally, the quantities defined in Eq. (E32) become zero at $\cos\theta = \pm 1$. Thus, the integration of $\phi_0^{mp}(\xi_1, \xi_2)$ with respect to $\cos\theta$ vanishes unless r_2 is in the spherical shell described above. Hence the contribution to the free energy density or the local dielectric constant at r_1 through $\phi^{mp}(1,2)$ comes from only those molecules within this spherical shell. Also, $c(r_1, r_2)$ approaches unity as $r_1 \longrightarrow \infty$, hence this contribution tends to cancel at this limit, the fact used in the discussion of Fig. 3.8 in Sec. 3.4.1. These are the results of our mean field approximation.

Appendix F: Derivation of Eq. (5.5)

Let N_a denote the total number of sulfuric acid molecules in the system of volume V. Although no dissociation is allowed in the vapor in accordance with the choice of the reference state, we take account of the possible dissociation in the cluster. Thus, it is most convenient to start from a classical mechanical partition function of a dissociative model. In view of the fact that the second dissociation of sulfuric acid is negligible compared to the first, we can introduce a model composed of water molecules, bisulfate ions, and protons. The partition function for the system is

$$\begin{aligned}\Phi^c(\beta, V, \mu_w, N_a; N_a^c) &= \frac{1}{N_a!}\left(\frac{q_p}{\Lambda_p^3}\right)^{N_a}\frac{1}{N_a!}\left(\frac{q_b}{\Lambda_b^3}\right)^{N_a} \\ &\quad\times\sum_{N_w'=0}^{\infty}\frac{1}{N_w'!}\left(\frac{q_w e^{\beta\mu_w}}{\Lambda_w^3}\right)^{N_w'}\int d\{N'\}e^{-\beta U_{N'}'}, \qquad \text{(F38)}\end{aligned}$$

where the total number of bisulfate ions and that of the protons are both denoted by N_a in accordance with the charge neutrality condition, $N' \equiv 2N_a + N_w'$ is the total number of molecules, and $U_{N'}'$ is the interaction potential in this dissociative model description, whose explicit form is irrelevant here. The subscripts b and p stand for bisulfate ion and proton, respectively. The translational and orientational degrees of freedom of all molecules are collectively denoted by $\{N'\}$ in the configurational integral. As discussed in Sec. 5.2, an accurate representation of $U_{N'}$ is difficult to achieve. Instead, we rewrite Eq. (F38) to reflect the fact that the main contribution to Φ^c comes from the configurations in which protons are chemically bonded to either bisulfate ion or water. Let N_i be the number of protons bonding to water molecules to form hydronium ions. The remaining $N_a - N_i$ protons bond to bisulfate ions to form sulfuric acid molecules. We assume that N_a acid molecules can be divided into N_a^v vapor molecules, for which no dissociation is allowed in accord with the definition of the reference state, and N_a^c molecules belonging to the cluster. The assumption is reasonable since n_s is many orders of magnitude smaller than the corresponding value in the cluster. Then Eq. (F38) can be approximated by

$$\begin{aligned}&\Phi^c(\beta, V, \mu_w, N_a; N_a^c) \\ &\approx \sum_{N_i=0}^{N_a^c}\sum_{N_w'=N_i}^{\infty}\frac{1}{N_a!}\left(\frac{q_p}{\Lambda_p^3}\right)^{N_a}\frac{1}{N_a!}\left(\frac{q_b}{\Lambda_b^3}\right)^{N_a}\frac{1}{N_w'!}\left(\frac{q_w e^{\beta\mu_w}}{\Lambda_w^3}\right)^{N_w'}\end{aligned}$$

$$\times N_a! \begin{pmatrix} N_a \\ N_a^v \end{pmatrix} \begin{pmatrix} N_a^c \\ N_a^c - N_i \end{pmatrix} \begin{pmatrix} N_w' \\ N_i \end{pmatrix}$$
$$\times \left[\int d1 e^{-\beta u_{pb}(1)} \right]^{N_a - N_i} \left[\int d1 e^{-\beta u_{pw}(1)} \right]^{N_i} \int d\{N\} e^{-\beta U_N}, \tag{F39}$$

where $N \equiv N_a + N_i + N_w$ with N_w denoting the number of water molecules excluding the protonated ones, and U_N is the total intermolecular interaction potential excluding the intramolecular interaction denoted by u_{pb} and u_{pw}. The upper limit of the first summation arises from the fact that dissociation of the sulfuric acid molecules is allowed only for those molecules inside the cluster and hence the number N_i of hydronium ions formed by the accompanying protonation of water cannot exceed N_a^c. The lower limit of the second summation reflects the fact that the hydronium ions thus formed have to remain in the system as a result of the charge neutrality condition. The factor

$$N_a! \begin{pmatrix} N_a \\ N_a^v \end{pmatrix} \begin{pmatrix} N_a^c \\ N_a^c - N_i \end{pmatrix} \begin{pmatrix} N_w' \\ N_i \end{pmatrix} \tag{F40}$$

is introduced here since the molecules must be regarded as distinguishable in the configurational integral. In Eq. (F40), the factors $\begin{pmatrix} N_a \\ N_a^v \end{pmatrix}$, $\begin{pmatrix} N_a^c \\ N_a^c - N_i \end{pmatrix}$, and $\begin{pmatrix} N_w' \\ N_i \end{pmatrix}$ respectively denote the number of ways of choosing N_a^v bisulfate ions out of N_a to be protonated and placed in the vapor phase, $N_a^c - N_i$ bisulfate ions to be protonated in the cluster, and N_i water molecules to be protonated in the system. Then, $N_a!$ takes care of all possible permutations of protons among all protonated species. Defining the molecular partition functions by

$$\frac{q_s}{\Lambda_s^3} \equiv \frac{q_p q_b}{\Lambda_p^3 \Lambda_b^3} \int d1 e^{-\beta u_{pb}(1)} \tag{F41}$$

and

$$\frac{q_h}{\Lambda_h^3} \equiv \frac{q_p q_w}{\Lambda_p^3 \Lambda_w^3} \int d1 e^{-\beta u_{pw}(1)}, \tag{F42}$$

we obtain Eq. (5.5).

Appendix G: Evaluation of Ξ^c by a Thermodynamic Integration

A common procedure[47] to evaluate Eq. (5.10) relies on the identity

$$\Xi_w^c(\beta, V, \mu_w, N_a^c, N_i) = \Xi_w(\beta_0, V, \mu_w, N_a^c, N_i) \exp\left[-\int_{\beta_0}^{\beta} < U_N >_{z_w} d\beta\right], \tag{G43}$$

where β_0 is chosen to be sufficiently small that the system can be regarded as an ideal gas composed of water, sulfuric acid, and bisulfate-hydronium ion pairs. The subscript x for $< \cdots >_x$ reminds us that the quantity x is held constant in evaluating the integration. The procedure implied in Eq. (G43) is not particularly attractive since, if we are to obtain the free energy of a cluster under various values of relative humidity, the integration has to be performed at each value of z_w. Each integration involves quite a few number of simulations at high temperatures, where the properties of clusters are not of direct interest. The disadvantage is prominent when $N_i = N_a^c$, where the bisulfate-hydronium ion pairs form a cluster even above 2000 K. These unphysical states, nonetheless, have to be simulated if one uses Eq. (G43). It is more convenient to take an alternative integration path:

$$\begin{aligned} & \Xi_w^c(\beta, V, \mu_w, N_a^c, N_i) \\ = \; & \Xi_w(\beta_0, V, \mu_{w0}, N_a^c, N_i) \\ \times \; & \exp\left[-\int_{\beta_0}^{\beta} < U_N >_{z_{w0}} d\beta + \int_{\log z_{w0}}^{\log z_w} < N_w >_{\beta} d\log z_w\right], \end{aligned} \tag{G44}$$

where, for an appropriate choice of β_0 in accordance with the ideal gas state just mentioned, $\Xi_w(\beta_0, V, \mu_{w0}, N_a^c, N_i)$ is given by

$$\Xi_w(\beta_0, V, \mu_{w0}, N_a^c, N_i) = N_i!(V\Omega)^{N_a^c} e^{z_{w0} V\Omega} \left[\int d1 e^{-\beta_0 u_{hb}(1)}\right]^{N_i}, \tag{G45}$$

where $N_i!$ accounts for the possible number of ways of forming the ion pairs from the ions which are regarded as distinguishable in $\Xi_w(\beta_0, V, z_{w0}, N_a^c, N_i)$. In applying Eq. (G44), the temperature integration involving unphysical high temperature states has to be performed only once at fugacity z_{w0}. Unlike Eq. (G43), all the intermediate states between z_{w0} and z_w, as implied in the second integration in Eq. (G44), are of direct interest to us. In Appendix I, we introduce an approximation that further reduces the computational effort.

It is convenient to rewrite Eq. (G44) in terms of excess quantities. For this purpose, we

rewrite the factors involving z_{w0} and β_0 in Eq. (G45) by means of the following identities:

$$\begin{aligned} e^{z_{w0}\Omega V} &= e^{n_{w0}V} \\ &= \exp\left[n_w V - \int_{\log n_{w0}}^{\log n_w} n_w V d\log n_w\right] \end{aligned} \tag{G46}$$

and

$$\int d1 e^{-\beta u_{hb}(1)} = \exp\left[-\int_{\beta_0}^{\beta} < u_{hb} > d\beta\right] \int d1 e^{-\beta_0 u_{hb}(1)}, \tag{G47}$$

where the thermal average is taken in the canonical ensemble of a single bisulfate-hydronium ion pair. Using Eqs. (G46) and (G47) in Eq. (G45) and substituting the resulting expression in Eq. (G44), we obtain

$$\begin{aligned} & \Xi_w^c(\beta, V, \mu_w, N_a^c, N_i) \\ = \; & N_i!(V\Omega)^{N_a^c} e^{n_w V} \left[\int d1 e^{-\beta u_{hb}(1)}\right]^{N_i} \\ & \times \exp\left\{-\int_{\beta_0}^{\beta} [< U_N >_{n_{w0}} - N_i < u_{hb} >] d\beta \right. \\ & \qquad \left. + \int_{\log n_{w0}}^{\log n_w} [< N_w >_\beta - n_w V] d\log n_w \right\}. \end{aligned} \tag{G48}$$

At β_0, non-negligible interaction energies arises only from the ionic interaction in each of the ion pairs. Thus, the first integral in the exponential is independent of β_0 as long as it is chosen sufficiently small. The integrand in the second integral is the excess number of water molecules over the ideal gas value. Hence the integral is independent of V, provided that the system boundary is far from the molecules in the cluster. The volume dependence of the first integral is addressed in Appendix H.

For an accurate estimate of the free energy, each thermal average in Eq. (G48) has to be evaluated at a sufficient number of points along the integration path. One way to verify if this condition is met is through the identity:

$$\begin{aligned} \int_{\beta_0}^{\beta} [< U_N >_{n_w} - N_i < u_{hb} >] d\beta \;\; &= \;\; \int_{\beta_0}^{\beta} [< U_N >_{n_{w0}} - N_i < u_{hb} >] d\beta \\ & \quad - \int_{\log n_{w0}}^{\log n_w} [< N_w >_\beta - n_w V] d\log n_w, \end{aligned} \tag{G49}$$

which follows from Eqs. (G43), (G44), and (G45). The identity Eq. (G49) is checked for a

Table 6.1: Consistency check by means of Eq. (G49).

N_a^c	N_i	L.H.S. of Eq. (G49)[a]	R.H.S. of Eq. (G49)[a,b]
1	0	-15.96 ± 0.47	-15.58 ± 0.53
0	1	-61.21 ± 1.01	-60.42 ± 1.24
2	0	-39.91 ± 0.74	-39.79 ± 0.88

[a]Evaluated at $T = 298.15$ K and $n_w = 0.6 \times 10^{-6}$ Å^{-3}. In k_BT unit.
[b]$n_{w0} = 0.1048 \times 10^{-6}$ Å^{-3}.

few cases and the results are shown in Table 6.1. Within the range of the error bars, the agreement is excellent, indicating that the numbers of the intermediate temperatures, n_w, and the Monte Carlo steps in each simulation are sufficient.

Appendix H: Choice of V

Eq. (5.2) shows that $e^{-\beta W^{rev}}$ is the probability of finding a cluster in the system of volume V relative to the probability of finding no cluster. Since the cluster can be found anywhere in the system and the event of finding it at one place or another is mutually exclusive by our choice of V as discussed in Sec. 5.3, we have

$$e^{-\beta W^{rev}} \sim V, \tag{H50}$$

provided that care is taken to avoid the surface effect of the system boundary. One way to achieve this is to fix one of the acid molecules at the center of the system and take the system boundary far from the molecules forming the cluster, which imposes a lower limit on V. Analytically integrating over the coordinates of the acid molecule thus fixed by ignoring the surface effect, we obtain Eq. (H50).

The upper limit on V arises from the condition Eq. (5.16) and the requirement that Ξ_w^c be evaluated accurately by simulation of a finite length of time. Combining Eqs. (5.2), (5.3), (5.7), (5.10), and (H50), we obtain

$$\Xi_w^c \sim V e^{n_w V}. \tag{H51}$$

Using Eq. (H51) in Eq. (G48), we find that

$$-\int_{\beta_0}^{\beta} [< U_N >_{n_{w0}} - N_i < u_{hb} >] \, d\beta = (1 - N_a^c) \log V + \text{const.} \tag{H52}$$

When the L.H.S. of Eq. (H52) is evaluated from a simulation, one can address its accuracy by examining if Eq. (H52) is satisfied. Note that, at β, the probability for N_a^c acid molecules to form a single cluster with water molecules must be dominant, namely, the cluster is stable with respect to evaporation of acid molecules. On the other hand, at β_0, the probability that they form an ideal gas is dominant. Around the temperature range where the acid molecules start to evaporate, both ideal gas vapor and the cluster have comparable probabilities. Thus, for the thermal averages to be estimated correctly in this temperature range, the probability for molecules to collide has to be non-negligible even after an evaporation event. Since simulation can be performed only for a finite period of time, V must be chosen to be

Table 6.2: Proportionality constant of $\log V$ in Eq. (H52)

N_a^c	N_i	simulation	Eq. (H52)
2	1	-1.04 ± 0.14	-1
2	0	-0.93 ± 0.03	-1
3	0	-1.94 ± 0.07	-2

sufficiently small, which imposes an upper limit on V. In particular, we choose V so that Eq. (H52) holds for a certain range of V including the one employed in simulation.

Note that the last integrand in Eq. (G48) is the excess number of water molecules over the ideal gas value resulting from the presence of the cluster and is independent of V if it is larger than its lower limit mentioned above. Thus, its integral is absorbed in the constant term. The particular form of V dependence shown in Eq. (H52) is not surprising since the integral in the equation is the reversible work required to form a cluster from the ideal gas state by gradually turning on the interaction among water and acid molecules and hence reflects the change in the entropic contributions of the acid molecules. Such terms as $< N_w > \log V$ do not arise in Eq. (H52), since the system is open to water molecules.

To verify that our choice of V satisfies Eq. (H52), we calculated the L.H.S. of the equation for four different values of V corresponding to the container radius of 25, 37.5, 50, and 64 Å. Since Eq. (H52) is concerned with the change in entropic contributions of acid molecules, simulation was performed in the canonical ensemble in the absence of water molecules for 3×10^8 MC steps. The temperature corresponding to the upper limit of the integral in Eq. (H52) is 400 K since, as the acid molecules form a cluster below this temperature, the integrand in Eq. (H52) becomes independent of V, thereby contributing to the constant term in Eq. (H52). Also, in the temperature range involved, $< N_w >$ is negligible, again verifying the use of the canonical ensemble. The resulting values of the L.H.S of Eq. (H52) were least-squares fitted to a linear equation. The value of the proportionality constant of $\log V$ is compared with the theoretical one, $1 - N_a^c$, in Table 6.2, revealing nearly exact agreement. Thus, our choice of V, corresponding to the container radius of 50Å, are appropriate in view of the number of MC steps involved in simulation.

In cluster simulation in a canonical ensemble, a system is commonly taken as a spherical container concentric with the center of mass of molecules forming a cluster. Then, one chooses V so that thermodynamic properties of a cluster is insensitive to the exact choice

of V. Since the center of mass of the cluster is fixed in this case, thermodynamic properties of the cluster evaluated from simulation reflects only the internal degrees of freedom of the cluster. It follows that if such choice of V is in fact possible, the cluster possesses a well-defined translational degrees of freedom as a whole when it is placed in the vapor phase, and *vice versa*. This, in turn, is necessary for nucleation theory to be formulated in terms of the concept of cluster as in classical theory. Under an idealized circumstance where simulation can be performed indefinite period of time, Eq. (H52) can be interpreted as a necessary and sufficient condition for a cluster to possess a well-defined translational degrees of freedom as a whole. This indicates that Eq. (H52), when applied to canonical ensemble cluster simulation, is an explicit implementation of the criterion by Lee *et al.*[91] in choosing V.

Appendix I: The Fugacity Dependence of W^{rev}

In this work, independent simulations were performed at several values of the fugacity z_w of water. Under a certain reasonable approximation, however, the results obtained at fugacity z_w can be used to estimate W^{rev} at different fugacity z'_w. Since this offers an improvement of the computational efficiency by a factor of several, we shall briefly describe the method here.

The time scale for a cluster to reach the internal mechanical equilibrium is many orders of magnitude shorter than that for the cluster to exchange a molecule with the vapor phase. Therefore, it is a common practice to assume that the configurational integral of an (N_a^c, N_w^c)-cluster is independent of the fugacity. Under this assumption, the first equality of Eq. (5.19) yields

$$\begin{aligned}
\Xi^c(\beta, V, \mu'_w, \mu_s; N_a^c, N_w^c) &= e^{n_s V}\left(\frac{q_s e^{\beta\mu_s}}{\Lambda_s^3}\right)^{N_a^c} \sum_{N_i=0}^{N_a^c} \frac{\chi^{N_i}}{(N_a^c - N_i)!N_i!} \frac{{z'_w}^{N_i}}{N_i!} \\
&\quad \times \frac{{z'_w}^{N_w}}{N_w!} \int d\{N\} e^{-\beta U_N} \\
&= e^{n_s V}\left(\frac{q_s e^{\beta\mu_s}}{\Lambda_s^3}\right)^{N_a^c} \sum_{N_i=0}^{N_a^c} \frac{\chi^{N_i}}{(N_a^c - N_i)!N_i!} \left(\frac{z'_w}{z_w}\right)^{N_w^c} \frac{z_w^{N_i}}{N_i!} \\
&\quad \times \frac{z_w^{N_w}}{N_w!} \int d\{N\} e^{-\beta U_N}. \qquad \text{(I53)}
\end{aligned}$$

Since Eq. (I53) differs from Eq. (5.19) only by the factor of $(z'_w/z_w)^{N_w^c}$, the desired expression for the reversible work follows from Eq. (5.21):

$$\begin{aligned}
& e^{-\beta W^{rev}(\beta, V, \mu'_w, \mu_s; N_a^c, N_w^c)} \\
&= (n_s V)^{N_a^c} \sum_{N_i=0}^{N_a^c} \left(\frac{z'_w}{z_w}\right)^{N_w^c} e^{-\beta\phi(\beta, V, \mu_w, N_a^c, N_i)} p(\beta, V, \mu_w, N_a^c, N_i, N_w^c - N_i). \qquad \text{(I54)}
\end{aligned}$$

The reversible work of the N_a^c-cluster is obtained by taking a summation of Eq. (I54) with respect to N_w^c. For a direct application of Eq. (I54) to yield the reversible work of cluster formation at z'_w of interest, it is necessary that the range over which $p(\mu_w, N_w)$ is non-negligible and that for $p(\mu'_w, N_w)$ overlap in a wide range of N_w. One can easily circumvent this condition by means of the umbrella sampling, which was employed in the free energy evaluation for a homogeneous nucleation in a single component system.[99]

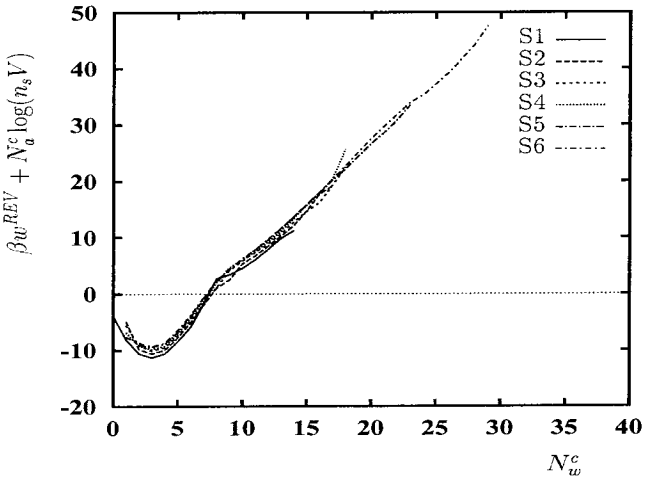

Figure 6.1: Comparison of the reversible work of cluster formation for $N_a^c = 1$ at $T = 298.15$K and $n_w = 0.1 \times 10^{-6}$ Å^{-3} obtained through Eq. (I54) by using other values of n_w. The conditions of simulation for S1, ..., S6 are given in Table 4.1. $f_{hb} = 20$ kcal/mol.

To demonstrate the utility of Eq. (I54), we calculated W^{rev} at $n'_w = 0.1 \times 10^{-6}$ Å, using the result of the simulations performed at the other values of n_w as summarized in Table 4.1. The result is shown in Fig. 6.1, which indicates a remarkable agreement of the calculated values of W^{rev}. The slight discrepancy arises because of the vapor contribution[99] to N_w^c and the change in the dominant part of p as n_w changes.

Bibliography

[1] A. C. Zettlemoyer, ed., *Nucleation.* New York: Marcel Dekker, Inc., 1969.

[2] G. S. Springer, "Homogeneous Nucleation," *Adv. Heat Transfer*, vol. 14, pp. 281–346, 1978.

[3] D. W. Oxtoby, "Homogeneous Nucleation: Theory and Experiment," *J. Phys. Condens. Matter*, vol. 4, pp. 7627–7650, 1992.

[4] H. Reiss, "The Kinetics of Phase Transitions in Binary Systems," *J. Chem. Phys.*, vol. 18, pp. 840–848, 1950.

[5] J. W. Gibbs, *The Scientific Papers of J. Willard Gibbs*, vol. I. Thermodynamics. New York: Dover, 1961.

[6] K. Nishioka, "Thermodynamic Formalism for a Liquid Microcluster in Vapor," *Phys. Rev. A*, vol. 36, pp. 4845–4851, 1987.

[7] R. C. Tolman, "Consideration of the Gibbs Theory of Surface Tension," *J. Chem. Phys.*, vol. 16, pp. 758–774, 1948.

[8] R. C. Tolman, "The Superficial Density of Matter at a Liquid-Vapor Boundary," *J. Chem. Phys.*, vol. 17, pp. 118–127, 1949.

[9] R. C. Tolman, "The Effect of Droplet Size on Surface Tension," *J. Chem. Phys.*, vol. 17, pp. 333–337, 1949.

[10] F. O. Koenig, "On the Thermodynamic Relation between Surface Tension and Curvature," *J. Chem. Phys.*, vol. 18, pp. 449–459, 1950.

[11] J. Frenkel, "Statistical Theory of Condensation Phenomena," *J. Chem. Phys.*, vol. 7, pp. 200–201, 1939.

[12] J. Frenkel, "A General Theory of Heterophase Fluctuations and Pretransition Phenomena," *J. Chem. Phys.*, vol. 7, pp. 538–547, 1939.

[13] W. Band, "Dissociation Treatment of Condensing Systems," *J. Chem. Phys*, vol. 7, pp. 324–326, 1939.

[14] W. Band, "Dissociation Treatment of Condensing Systems. II," *J. Chem. Phys*, vol. 7, pp. 927–931, 1939.

[15] J. L. Katz, H. Saltsburg, and H. Reiss, "Nucleation in Associated Vapors," *J. Colloid and Interface Sci.*, vol. 21, pp. 560–568, 1966.

[16] K. Nishioka and I. Kusaka, "Thermodynamic Formulas of Liquid Phase Nucleation from Vapor in Multicomponent Systems," *J. Chem. Phys.*, vol. 96, pp. 5370–5376, 1992.

[17] K. Nishioka, I. Kusaka, and A. Mori, "Interfacial Thermodynamics of Noncritical Clusters and Homogeneous Nucleation in Multicomponent Systems," *J. Cryst. Growth*, vol. 128, pp. 1157–1161, 1993.

[18] R. G. Renninger, F. C. Hiller, and R. C. Bone, "Comment on 'Self-Nucleation in the Sulfuric Acid-Water System'," *J. Chem. Phys.*, vol. 75, pp. 1584–1585, 1981.

[19] G. J. Doyle, "Response to the Comment on 'Self-Nucleation in the Sulfuric Acid-Water System'," *J. Chem. Phys.*, vol. 75, pp. 1585–1586, 1981.

[20] G. Wilemski, "Composition of the Critical Nucleus in Multicomponent Vapor Nucleation," *J. Chem. Phys.*, vol. 80, pp. 1370–1372, 1984.

[21] G. Wilemski, "Some Issues of Thermodynamic Consistency in Binary Nucleation Theory," *J. Chem. Phys.*, vol. 88, pp. 5134–5136, 1988.

[22] J. Lothe and G. M. Pound, "Reconsiderations of Nucleation Theory," *J. Chem. Phys.*, vol. 36, pp. 2080–2085, 1962.

[23] J. Lothe and G. M. Pound, "On the Statistical Mechanics of Nucleation Theory," *J. Chem. Phys.*, vol. 45, pp. 630–634, 1966.

[24] J. Lothe and G. M. Pound, "Concentration of Clusters in Nucleation and the Classical Phase Integral," *J. Chem. Phys.*, vol. 48, pp. 1849–1852, 1968.

[25] J. Lothe and G. M. Pound, "Statistical Mechanics of Nucleation," in *Nucleation* (A. C. Zettlemoyer, ed.), (New York), pp. 109–149, Marcel Dekker, 1969.

[26] K. Nishioka and G. M. Pound, "Statistical Mechanics of Homogeneous Nucleation in Vapor," *Adv. Colloid and Interface Sci.*, vol. 7, pp. 205–278, 1977.

[27] H. Reiss and J. L. Katz, "Resolution of the Translation—Rotation Paradox in the Theory of Irreversible Condensation," *J. Chem. Phys.*, vol. 46, pp. 2496–2499, 1967.

[28] H. Reiss, J. L. Katz, and E. R. Cohen, "Translation—Rotation Paradox in the Theory of Nucleation," *J. Chem. Phys.*, vol. 48, pp. 5553–5560, 1968.

[29] R. Kikuchi, "Statistical Mechanics of a Liquid Droplet," *Adv. Colloid and Interface Sci.*, vol. 7, pp. 67–102, 1977.

[30] H. Reiss, "The Replacement Free Energy in Nucleation Theory," *Adv. Colloid and Interface Sci.*, vol. 7, pp. 1–66, 1977.

[31] H. Reiss, W. K. Kegel, and J. L. Katz, "Resolution of the Problems of Replacement Free Energy, $1/S$, and Internal Consistency in Nucleation Theory by Consideration of the Length Scale for Mixing Entropy," *Phys. Rev. Lett.*, vol. 78, pp. 4506–4509, 1997.

[32] R. Evans, "The Nature of the Liquid-Vapor Interface and Other Topics in the Statistical Mechanics of Non-Uniform, Classical Fluids," *Adv. Phys*, vol. 28, pp. 143–200, 1979.

[33] D. W. Oxtoby and R. Evans, "Nonclassical Nucleation Theory for the Gas-Liquid Transition," *J. Chem. Phys*, vol. 89, pp. 7521–7530, 1988.

[34] X. C. Zeng and D. W. Oxtoby, "Gas-Liquid Nucleation in Lennard-Jones Fluids," *J. Chem. Phys.*, vol. 94, pp. 4472–4478, 1991.

[35] X. C. Zeng and D. W. Oxtoby, "Binary Homogeneous Nucleation Theory for the Gas-Liquid Transition: A Nonclassical Approach," *J. Chem. Phys.*, vol. 95, pp. 5940–5947, 1991.

[36] V. Talanquer and D. W. Oxtoby, "Nucleation in Dipolar Fluids: Stockmayer Fluids," *J. Chem. Phys.*, vol. 99, pp. 4670–4679, 1993.

[37] V. Talanquer and D. W. Oxtoby, "Nucleation of Bubbles in binary fluids," *J. Chem. Phys.*, vol. 102, pp. 2156–2164, 1995.

[38] V. Talanquer and D. W. Oxtoby, "Nucleation in Molecular and Dipolar fluids: Interaction Site Model," *J. Chem. Phys.*, vol. 103, pp. 3686–3695, 1995.

[39] V. Talanquer and D. W. Oxtoby, "Density Functional Analysis of Phenomenological Theories of Gas-Liquid Nucleation," *J. Phys. Chem.*, vol. 99, pp. 2865–2874, 1995.

[40] D. W. Oxtoby, V. Talanquer, and A. Laaksonen, "Density Functional Theory for Binary Nucleation," in *Nucleation and Atmospheric Aerosols, Proceedings of the Fourteenth International Conference on Nucleation and Atmosheric Aerosols* (M. Kulmala and P. E. Wagner, eds.), (New York), pp. 21–29, Pergamon, 1996.

[41] I. Kusaka, Z.-G. Wang, and J. H. Seinfeld, "Ion-Induced Nucleation: A Density Functional Approach," *J. Chem. Phys.*, vol. 102, pp. 913–924, 1995.

[42] I. Kusaka, Z.-G. Wang, and J. H. Seinfeld, "Ion-Induced Nucleation. II. Polarizable multipolar molecules," *J. Chem. Phys.*, vol. 103, pp. 8993–9009, 1995.

[43] V. Talanquer and D. W. Oxtoby, "Nucleation in the Presence of an Amphiphile - A Density-Functional Approach," *J. Chem. Phys.*, vol. 106, pp. 3673–3680, 1997.

[44] D. Kane, G. M. Daly, and M. S. El-Shall, "Condensation of Supersaturated Vapors on Benzene Ions Generated by Resonant Two-Photon Ionization: A New Technique for Ion Nucleation," *J. Phys. Chem.*, vol. 99, pp. 7867–7870, 1995.

[45] D. Kane and M. S. El-Shall, "Ion Nucleation as a Detector: Application of REMPI to Generate Selected Ions in Supersaturated Vapors," *Chem. Phys. Lett.*, vol. 259, pp. 482–487, 1996.

[46] T. Seto, K. Okuyama, L. de Juan, and J. F. de la Mora, "Condensation of Supersaturated Vapors on Monovalent and Divalent Ions of Varying Size," *J. Chem. Phys.*, vol. 107, pp. 1576–1585, 1997.

[47] M. P. Allen and D. J. Tildesley, *Computer Simulation of Liquids.* New York: Oxford University Press, 1987.

[48] H. Reiss, A. Tabazadeh, and J. Talbot, "Molecular theory of Vapor Phase Nucleation: The Physically Consistent Cluster," *J. Chem. Phys.*, vol. 92, pp. 1266–1274, 1990.

[49] H. M. Ellerby, C. L. Weakliem, and H. Reiss, "Toward a Molecular Theory of Vapor-Phase Nucleation. I. Identification of the Average Embryo," *J. Chem. Phys.*, vol. 95, pp. 9209–9218, 1991.

[50] H. M. Ellerby and H. Reiss, "Toward a Molecular Theory of Vapor-Phase Nucleation. II. Fundamental Treatment of the Cluster Distribution," *J. Chem. Phys.*, vol. 97, pp. 5766–5772, 1992.

[51] C. L. Weakliem and H. Reiss, "Toward a Molecular Theory of Vapor-Phase Nucleation. III. Thermodynamic Properties of Argon Clusters from Monte Carlo Simulations and a Modified Liquid Drop Theory," *J. Chem. Phys.*, vol. 99, pp. 5374–5383, 1993.

[52] C. L. Weakliem and H. Reiss, "Toward a Molecular Theory of Vapor Phase Nucleation. IV. Rate Theory Using the Modified Liquid Drop Model," *J. Chem. Phys.*, vol. 101, pp. 2398–2406, 1994.

[53] K. J. Oh, X. C. Zeng, and H. Reiss, "Toward a Molecular Theory of Vapor-Phase Nucleation. V. Self-Consistency in the Decoupled Dimer Limit," *J. Chem. Phys.*, vol. 107, pp. 1242–1246, 1997.

[54] J. W. Gibbs, *Elementary Principles in Statistical Mechanics.* Woodbridge, Connecticut: Ox Bow Press, 1981.

[55] W. Heisenberg, *Physics and Beyond.* New York: Harper & Row, 1971. Translated by A. J. Pomerans.

[56] C. T. R. Wilson *Phil. Trans. R. Soc. London Ser. A*, vol. 189, p. 265, 1897.

[57] L. Loeb, A. Kip, and A. W. Einarsson, "On the Nature of Ionic Sign Preference in C.T.R. Wilson Cloud Chamber Condensation Experiments," *J. Chem. Phys.*, vol. 6, pp. 264–273, 1938.

[58] L. Scharrer *Ann. Physik.*, vol. 35, p. 619, 1939.

[59] D. R. White and J. L. Kassner, Jr., "Experimental and Theoretical Study of the Sign Preference in the Nucleation of Water Vapor," *Aerosol. Sci.*, vol. 2, pp. 201–206, 1971.

[60] H. Rabeony and P. Mirabel, "Experimental Study of Vapor Nucleation of Ions," *J. Phys. Chem.*, vol. 91, pp. 1815–1818, 1987.

[61] K. Okuyama, M. Adachi, H. Shinagawa, G. Shi, and J. H. Seinfeld, "Experimental Study of Nucleation in Ions with DBP Vapor," *J. Aerosol Sci.*, vol. 22, Suppl. 1, pp. S85–S88, 1991.

[62] M. Adachi, K. Okuyama, and J. H. Seinfeld, "Experimental Studies of Ion-Induced Nucleation," *J. Aerosol Sci.*, vol. 23, pp. 327–337, 1992.

[63] J. J. Thomson, *Conduction of Electricity through Gases.* Cambridge: Cambridge University Press, 1906.

[64] L. Y. Chan and V. A. Mohnen, "Ion Nucleation Theory," *J. Atmos. Sci.*, vol. 37, pp. 2323–2331, 1980.

[65] S. H. Suck, "Change of Free Energy in Heteromolecular Nucleation: Electrostatic Energy Contribution," *J. Chem. Phys.*, vol. 75, pp. 5090–5096, 1981.

[66] A. I. Rusanov, "Thermodynamic Theory of Nucleation on Charged Particles," *J. Colloid and Interface Sci.*, vol. 68, pp. 32–47, 1979.

[67] A. I. Rusanov and F. M. Kuni, "Reformulation of the Thermodynamic Theory of Nucleation on Charged Particles," *J. Colloid and Interface Sci.*, vol. 100, pp. 264–277, 1984.

[68] A. K. Shchĕkin, A. I. Rusanov, and F. M. Kuni, "Theory of Nucleation on Charged Nuclei," *Kolloidn. Zh.*, vol. 46, pp. 535–543, 1984.

[69] H. Rabeony and P. Mirabel, "Vapor Nucleations on Ions," *J. Chim. Phys.*, vol. 83, pp. 219–224, 1986.

[70] N. F. Carnahan and K. E. Starling *J. Chem. Phys.*, vol. 51, p. 635, 1969.

[71] N. F. Carnahan and K. E. Starling *J. Chem. Phys.*, vol. 53, p. 600, 1970.

[72] A. W. Castleman, Jr., P. M. Holland, and R. G. Keesee, "The Properties of Ion Clusters and Their Relationship to Heteromolecular Nucleation," *J. Chem. Phys.*, vol. 68, pp. 1760–1767, 1978.

[73] J. L. Katz, J. A. Fisk, and V. M. Chakarov, "Condensation of a Supersaturated Vapor IX. Nucleation on Ions," *J. Chem. Phys.*, vol. 101, pp. 2309–2318, 1994.

[74] F. He and P. K. Hopke, "Experimental Study of Ion-Induced Nucleation by Radon Decay," *J. Chem. Phys*, vol. 99, pp. 9972–9978, 1993.

[75] I. N. Tang, H. R. Muckelwitz, and A. W. Castleman, Jr. *Nature*, vol. 230, p. 175, 1971.

[76] K. G. Spears, "Ion-Neutral Bonding," *J. Chem. Phys.*, vol. 57, pp. 1850–1858, 1972.

[77] A. W. Castleman, Jr., "Nucleation and Molecular Clustering About Ions," *Adv. Colloid and Interface Sci.*, vol. 10, pp. 73–128, 1979.

[78] A. D. Buchingham, "2. Permanent and Induced Molecular Moments and Long-Range Intermolecular Forces," *Adv. Chem. Phys.*, vol. 12, pp. 107–142, 1967.

[79] A. D. McLean and M. Yoshimine, "Theory of Molecular Polarizabilities," *J. Chem. Phys.*, vol. 47, pp. 1927–1935, 1967.

[80] D. R. Lide, ed., *CRC Handbook of Chemistry and Physics.* Boca Raton FL: CRC Press, 74 ed., 1993.

[81] C. Huiszoon, "*Ab Initio* Calculations of Multipole Moments, Polarizabilities and Isotropic Long Range Interaction Coefficients for Dimethylether, Methanol, Methane, and Water," *Mol. Phys.*, vol. 58, pp. 865–885, 1986.

[82] K. Woliński, A. J. Sadlej, and G. Karlström, "Molecular Quadrupole Moments," *Mol. Phys.*, vol. 72, pp. 425–432, 1991.

[83] G. Maroulis, "Electric Moments, Polarizabilities and Hyperpolarizabilities for Carboon Disulfide (S=C=S) from Accurate SCF Calculations," *Chem. Phys. Lett.*, vol. 199, pp. 250–256, 1992.

[84] G. Maroulis, "A Complete Description of the Electric Dipole Moment, Polarizability and Hyperpolarizability tensors of Hydrogen Peroxide," *J. Chem. Phys.*, vol. 96, pp. 6048–6052, 1992.

[85] G. Maroulis, "Electric Quadrupole Moment and Quadrupole Polarizability of Hydrogen Bromide," *J. Phys. B: At. Mol. Opt. Phys.*, vol. 26, pp. 2957–2964, 1993.

[86] G. Maroulis, "Electric Dipole Hyperpolarizability and Quadrupole Polarizability of Methane from Finite-Field Coupled Cluster and Fourth-Order Many-Body Perturbation Theory Calculations," *Chem. Phys. Lett.*, vol. 226, pp. 420–426, 1994.

[87] L. Pauling, *General Chemistry.* New York: Dover, 1988.

[88] A. J. Stone, "Distributed Multipole Analysis, Or How to Describe a Molecular Charge Distribution," *Chem. Phys. lett.*, vol. 83, pp. 233–239, 1981.

[89] A. J. Stone and M. Alderton, "Distributed Multipole Analysis. Methods and Applications," *Mol. Phys.*, vol. 56, pp. 1047–1064, 1985.

[90] A. J. Stone, "Distributed Polarizabilities," *Mol. Phys.*, vol. 56, pp. 1065–1082, 1985.

[91] J. K. Lee, J. A. Barker, and F. F. Abraham, "Theory and Monte Carlo Simulation of Physical Clusters in the Imperfect Vapor," *J. Chem. Phys.*, vol. 58, pp. 3166–3180, 1973.

[92] V. Talanquer and D. W. Oxtoby, "Dynamical Density Functional Theory of Gas-Liquid Nucleation," *J. Chem. Phys.*, vol. 100, pp. 5190–5200, 1994.

[93] H. J. C. Berendsen, J. R. Grigera, and T. P. Straatsma, "The Missing Term in Effective Pair Potentials," *J. Phys. Chem.*, vol. 91, pp. 6269–6271, 1987.

[94] R. Kubo, *Statistical Mechanics.* Amsterdam: Elsevier Science Publishers, 1965.

[95] F. H. Stillinger, Jr., "Rigorous Basis of the Frenkel-Band Theory of Association Equilibrium," *J. Chem. Phys.*, vol. 38, pp. 1486–1494, 1963.

[96] D. Chandler, *Introduction to Modern Statistical Mechanics.* New York: Oxford University Press, 1987.

[97] R. Kelterbaum, N. Turki, A. Rahmouni, and E. Kochanski, "Traps in Modelling Intermolecular Three-Body Forces: Example of the Water System and Protonated Hydrates," *J. Mol. Struct. (THEOCHEM)*, vol. 314, pp. 191–210, 1994.

[98] Pictures of clusters were produced by a program RasMol developed by Dr. R. Sayle.

[99] I. Kusaka, Z.-G. Wang, and J. H. Seinfeld, "Direct Evaluation of the Equilibrium Distribution of Physical Clusters by a Grand Canonical Monte Carlo Simulation." To be published.

[100] D. Stauffer, "Kinetic Theory of Two-Component ("Heteromolecular") Nucleation and Condensation," *J. Aerosol Sci.*, vol. 7, pp. 319–333, 1976.

[101] V. A. Shneidman and M. C. Weinberg, "Induction Time in Transient Nucleation Theory," *J. Chem. Phys.*, vol. 97, pp. 3621–3628, 1992.

[102] V. A. Shneidman and M. C. Weinberg, "Transient Nucleation Induction Time from the Birth-Death Equations," *J. Chem. Phys.*, vol. 97, pp. 3629–3638, 1992.

[103] L. M. Berezhkovskii and V. Yu. Zitserman, "Direction of the Nucleation Current through the Saddle Point in the Binary Nucleation Theory and the Saddle Point Avoidance," *J. Chem. Phys.*, vol. 102, pp. 3331–3336, 1995.

[104] Z. Kožíšek and P. Demo, "Transient Nucleation in Binary Ideal Solution," *J. Chem. Phys.*, vol. 102, pp. 7595–7601, 1995.

[105] B. E. Wyslouzil and G. Wilemski, "Binary Nucleation Kinetics. II. Numerical Solution of the Birth-Death Equations," *J. Chem. Phys.*, vol. 103, pp. 1137–1151, 1995.

[106] G. J. Doyle, "Self-Nucleation in the Sulfuric Acid-Water System," *J. Chem. Phys*, vol. 35, pp. 795–799, 1961.

[107] P. Mirabel and J. L. Katz, "Binary Homogeneous Nucleation as a Mechanism for the Formation of Aerosols," *J. Chem. Phys.*, vol. 60, pp. 1138–1144, 1974.

[108] P. Mirabel and J. L. Ponche, "Studies of Gas-Phase Clustering of Water on Sulphuric Acid Molecules," *Chem. Phys. Lett.*, vol. 183, pp. 21–24, 1991.

[109] R. H. Heist and H. Reiss, "Hydrates in Supersaturated Binary Sulfuric Acid-Water Vapor," *J. Chem. Phys.*, vol. 61, pp. 573–581, 1974.

[110] W. J. Shugard, R. H. Heist, and H. Reiss, "Theory of Vapor Phase Nucleation in Binary Mixtures of Water and Sulfuric Acid," *J. Chem. Phys.*, vol. 61, pp. 5298–5305, 1974.

[111] W. J. Shugard and H. Reiss, "Transient Nucleation in H_2O-H_2SO_4 Mixtures: A Stochastic Approach," *J. Chem. Phys.*, vol. 65, pp. 2827–2840, 1976.

[112] F. J. Schelling and H. Reiss, "Time Lag in Nucleation: A Variational Treatment of Relaxation Time in the Binary Sulfuric Acid-Water System," *J. Chem. Phys.*, vol. 74, pp. 3527–3531, 1981.

[113] A. Jaecker-Voirol, P. Mirabel, and H. Reiss, "Hydrates in Supersaturated Binary Sulfuric Acid-Water Vapor: A Reexamination," *J. Chem. Phys.*, vol. 87, pp. 4849–4852, 1987.

[114] A. Jaecker-Voirol and P. Mirabel, "Nucleation Rate in a Binary Mixture of Sulfuric Acid and Water Vapor," *J. Phys. Chem.*, vol. 92, pp. 3518–3521, 1988.

[115] A. Jaecker-Voirol and P. Mirabel, "Heteromolecular Nucleation in the Sulfuric Acid-Water System," *Atmos. Env.*, vol. 23, pp. 2053–2057, 1989.

[116] M. Kulmala and A. Laaksonen, "Binary Nucleation of Water-Sulfuric Acid System: Comparison of Classical theories with Different H_2SO_4 Saturation Vapor Pressures," *J. Chem. Phys.*, vol. 93, pp. 696–701, 1990.

[117] M. Kulmala, M. Lazaridis, A. Laaksonen, and T. Vesala, "Extended Hydrates Interaction Model: Hydrate Formation and the Energetics of Binary Homogeneous Nucleation," *J. Chem. Phys.*, vol. 94, pp. 7411–7413, 1991.

[118] A. Laaksonen and M. Kulmala, "Homogeneous Heteromolecular Nucleation of Sulphuric Acid and Water Vapours in Stratospheric Conditions: A Theoretical Study of the Effect of Hydrate Interaction," *J. Aerosol Sci.*, vol. 22, pp. 779–787, 1991.

[119] M. Lazaridis, M. Kulmala, and A. Laaksonen, "Binary Heterogeneous Nucleation of a Water-Sulphuric Acid System: The Effect of Hydrate Interaction," *J. Aerosol Sci.*, vol. 22, pp. 823–830, 1991.

[120] K. Nishioka and K. Fujita, "Transient Nucleation in Binary Vapor of Water and Sulfuric Acid," *J. Chem. Phys.*, vol. 100, pp. 532–540, 1994.

[121] R. McGraw, "Two-Dimensional Kinetics of Binary Nucleation in Sulfuric Acid-Water Mixtures," *J. Chem. Phys.*, vol. 102, pp. 2098–2108, 1995.

[122] H. Reiss, D. I. Margolese, and F. J. Schelling, "Experimental Study of Nucleation in Vapor Mixtures of Surfuric Acid and Water," *J. Colloid and Interface Sci.*, vol. 56, pp. 511–526, 1976.

[123] D. Boulaud, G. Madelaine, D. Vigla, and J. Bricard, "Experimental Study on the Nucleation of Water Vapor Sulfuric Acid Binary System," *J. Chem. Phys.*, vol. 66, pp. 4854–4860, 1977.

[124] P. Mirabel and J. L. Clavelin, "Experimental Study of Nucleation in Binary Mixtures: The Nitric Acid-Water and Sulfuric Acid-Water Systems," *J. Chem. Phys.*, vol. 68, pp. 5020–5027, 1978.

[125] F. J. Schelling and H. Reiss, "Expansion Cloud Chamber Observations on the Nucleation and Growth of Sulfuric Acid-Water Droplets," *J. Colloid and Interface Sci.*, vol. 83, pp. 246–264, 1981.

[126] B. E. Wyslouzil, J. H. Seinfeld, R. C. Flagan, and K. Okuyama, "Binary Nucleation in Acid-Water Systems. II. Sulfuric Acid-Water and a Comparison with Methanesulfonic Acid-Water," *J. Chem. Phys.*, vol. 94, pp. 6842–6850, 1991.

[127] Y. Viisanen, M. Kulmala, and A. Laaksonen, "Experiments on Gas-Liquid Nucleation of Sulfuric Acid and Water," *J. Chem. Phys.*, vol. 107, pp. 920–926, 1997.

[128] D. I. Zhukhovitskii, "Molecular Dynamics Study of Cluster Evolution in Supersaturated Vapor," *J. Chem. Phys.*, vol. 103, pp. 9401–9407, 1995.

[129] E. Kochanski, A. Rahmouni, R. Kelterbaum, R. Wiest, P. E. S. Wormer, and J. Langlet, "Are Clusters a Step Towards Our Knowledge of Liquids? The Case of Protonated Hydrates," *J. Chim. Phys*, vol. 88, pp. 2451–2456, 1991.

[130] R. L. Kuczkowski, R. D. Suenram, and F. J. Lovas, "Microwave Spectrum, Structure, and Dipole Moment of Sulfuric Acid," *J. Am. Chem. Soc.*, vol. 103, pp. 2561–2566, 1981.

[131] I. Kusaka, Z.-G. Wang, and J. H. Seinfeld. Presented at the 14-th International Conference on Nucleation and Atmospheric Aerosols in Helsinki, 1996.

[132] W. R. Cannon, B. M. Pettitt, and J. A. McCammon, "Sulfate Anion in Water: Model Structural, Thermodynamic, and Dynamic Properties," *J. Phys. Chem.*, vol. 98, pp. 6225–6230, 1994.

[133] A. Loewenstein and A. Szöke, "The Activation Energies of Proton Transfer Reactions in Water," *J. Am. Chem. Soc.*, vol. 84, pp. 1151–1154, 1962.

[134] Z. Luz and S. Meiboom, "The Activation Energies of Proton Transfer Reactions in Water," *J. Am. Chem. Soc.*, vol. 86, pp. 4768–4769, 1964.

[135] B. N. Hale and S. M. Kathmann, "Monte Carlo Simulation of Small H_2SO_4-H_2O Clusters," in *Nucleation and Atmospheric Aerosols, Proceedings of the Fourteenth International Conference on Nucleation and Atmospheric Aerosols* (M. Kulmala and P. E. Wagner, eds.), (New York), pp. 30–33, Pergamon, 1996.

[136] T. H. Lay. Private communication.

[137] F. H. Stillinger and C. W. David, "Polarization Model for Water and Its Ionic Dissociation Products," *J. Chem. Phys.*, vol. 69, pp. 1473–1484, 1978.

[138] J. W. Halley, J. R. Rustad, and A. Rahman, "A Polarizable, Dissociating Molecular Dynamics Model for Liquid Water," *J. Chem. Phys.*, vol. 98, pp. 4110–4119, 1993.

[139] L. Kurdi and E. Kochanski, "Theoretical Studies of Sulfuric Acid Monohydrate: Neutral or Ionic Complex?" *Chem. Phys. Lett.*, vol. 158, pp. 111–115, 1989.

[140] D. K. Remler and P. A. Madden, "Molecular Dynamics without Effective Potentials via the Car-Parrinello Approach," *Mol. Phys.*, vol. 70, pp. 921–966, 1990.

[141] K. Laasonen, M. Sprik, M. Parrinello, and R. Car, "'*Ab Initio*' Liquid Water," *J. Chem. Phys*, vol. 99, pp. 9080–9089, 1993.

[142] M. Tuckerman, K. Laasonen, M. Sprik, and M. Parrinello, "*Ab Initio* Molecular Dynamics Simulation of the Solvation and Transport of H_3O^+ and OH^- Ions in Water," *J. Phys. Chem.*, vol. 99, pp. 5749–5752, 1995.

[143] M. Tuckerman, K. Laasonen, M. Sprik, and M. Parrinello, "*Ab Initio* Molecular Dynamics Simulation of the Solvation and Transport of Hydronium and Hydroxyl Ions in Water," *J. Chem. Phys.*, vol. 103, pp. 150–161, 1995.

[144] R. G. Parr and W. Yang, *Density-Functional Theory of Atoms and Molecules.* New York: Oxford University Press, 1989.

[145] Y. K. Lau, S. Ikuta, and P. Kebarle, "Thermodynamics and Kinetics of the Gas-Phase Reactions: $H_3O^+(H_2O)_{n-1} + H_2O = H_3O^+(H_2O)_n$," *J. Am. Chem. Soc.*, vol. 104, pp. 1462–1469, 1982.

[146] X. Yang and A. W. Castleman, Jr., "Large Protonated Water Clusters $H^+(H_2O)_n$ $(1 \leq n < 60)$: The Production and Reactivity of Clathrate-like Structures Under Thermal Conditions," *J. Am. Chem. Soc.*, vol. 111, pp. 6845–6846, 1989.

[147] X. Yang and A. W. Castleman, Jr., "Laboratory Studies of Large Protonated Water Clusters Under the Conditions of Formation of Noctilucent Clouds in the Summer Mesopause," *J. Geophys. Res.*, vol. 96, pp. 22573–22578, 1991.

[148] Z. Shi, J. V. Ford, S. Wei, and A. W. Castleman, Jr., "Water Clusters: Contributions of Binding Energy and Entropy to Stability," *J. Chem. Phys.*, vol. 99, pp. 8009–8015, 1993.

[149] M. D. Newton, "*Ab Initio* Studies of the Hydrated H_3O^+ Ion. II. The Energetics of Proton Motion in Higher Hydrates $(n = 3 - 5)$," *J. Chem. Phys.*, vol. 67, pp. 5535–5546, 1977.

[150] C. K. Lutrus, D. E. Hagen, and S. H. S. Salk, "Calculation of Properties of Ionic Water Clusters by the MNDO Method," *Atmos. Env.*, vol. 24A, pp. 1397–1399, 1990.

[151] M. W. Jurema, K. N. Kirschner, and G. C. Shields, "Modeling of Magic Water Clusters $(H_2O)_{20}$ and $(H_2O)_{21}H^+$ with the PM3 Quantum-Mechanical Method," *J. Compt. Chem.*, vol. 14, pp. 1326–1332, 1993.

[152] A. Khan, "Theoretical Studies of the Clathrate Structures of $(H_2O)_{20}$, $H^+(H_2O)_{20}$ and $H^+(H_2O)_{21}$," *Chem. Phys. Lett.*, vol. 217, pp. 443–450, 1994.

[153] R. Kelterbaum and E. Kochanski, "Behavior and Evolution of the First 28 Protonated Hydrates from Monte Carlo Studies," *J. Phys. Chem.*, vol. 99, pp. 12493–12500, 1995.

[154] Y. Guissani and B. Guillot, "A Computer Simulation Study of the Liquid-Vapor Coexistence Curve of Water," *J. Chem. Phys.*, vol. 98, pp. 8221–8235, 1993.

[155] J. Alejandre, D. J. Tildesley, and G. A. Chapela, "Molecular Dynamics Simulation of the Orthobaric Densities and Surface Tension of Water," *J. Chem. Phys.*, vol. 102, pp. 4574–4583, 1995.

[156] R. S. Taylor, L. X. Dang, and B. C. Garrett, "Molecular Dynamics Simulations of the Liquid/Vapor Interface of SPC/E Water," *J. Phys. Chem.*, vol. 100, pp. 11720–11725, 1996.

[157] E. Kochanski, "Theoretical Determination of the Potential Surface for the System $H_3O^+ \ldots H_2O$ at Intermediate and Large Intermolecular Distances," *Nouv. J. Chim.*, vol. 8, pp. 605–610, 1984.

[158] S. L. Fornili, M. Migliore, and M. A. Palazzo, "Hydration of the Hydronium Ion. *Ab Initio* Calculations and Monte Carlo Simulation," *Chem. Phys. Lett.*, vol. 125, pp. 419–424, 1986.

[159] Y. Guissani, B. Guillot, and S. Bratos, "The Statistical Mechanics of the Ionic Equilibrium of Water: A Computer Simulation Study," *J. Chem. Phys.*, vol. 88, pp. 5850–5856, 1988.

[160] R. E. Kozack and P. C. Jordan, "Empirical Models for the Hydration of Protons," *J. Chem. Phys.*, vol. 96, pp. 3131–3136, 1992.

[161] W. R. Rodwell and L. Radom, "Definitive Theoretical Evidence for the Nonplanarity of the Hydronium Ion (H_3O^+)," *J. Am. Chem. Soc.*, vol. 103, pp. 2865–2866, 1981.

[162] K. Morokuma and C. Muguruma, "*Ab Initio* Molecular Orbital Study of the Mechanism of the Gas Phase Reaction SO_3+H_2O: Importance of the Second Water Molecule," *J. Am. Chem. Soc.*, vol. 116, pp. 10316–10317, 1994.

[163] W. Studziński, G. H. Spiegel, and R. A. Zahoransky, "Binary Nucleation and Condensation in Associated Vapors," *J. Chem. Phys.*, vol. 84, pp. 4008–4014, 1986.

[164] S. Tabata, "A Simple but Accurate Formula for the Saturation Vapor Pressure Over Liquid Water," *J. Appl. Meteor.*, vol. 12, pp. 1410–1411, 1973.

[165] H. Resat and M. Mezei, "Grand Canonical Ensemble Monte Carlo Simulation of the dCpG/Proflavine Crystal Hydrate," *Biophys. J.*, vol. 71, pp. 1179–1190, 1996.

[166] I. Prigogine and R. Defay, *Chemical Thermodynamics.* London: Longmans, 1954. Translated by D. H. Everett.

[167] S. G. Lias, J. E. Bartmess, J. F. Liebman, J. L. Holmes, R. D. Levin, and W. G. Mallard, "Gas-Phase Ion and Neutral Thermochemistry," *J. Phys. Chem. Ref. Data*, vol. 17, Suppl. 1, p. 1, 1988.

[168] Thermodynamic data necessary in classical theory are obtained from the program kindly provided to us by Dr. Markku Kulmala.

[169] I. Kusaka, Z.-G. Wang, and J. H. Seinfeld, "Binary Nucleation of Sulfuric Acid-Water: Monte Carlo Simulation." Submitted to J. Chem. Phys.

[170] D. E. Stogryn and A. P. Stogryn, "Molecular Multipole Moments," *Mol. Phys.*, vol. 11, pp. 371–393, 1966.